Chem Soc Rev

RSC Publishing

REVIEW ARTICLE

View Article Online
View Journal | View Issue

Luminescent probes and sensors for temperature

Cite this: *Chem. Soc. Rev.*, 2013, **42**, 7834

Xu-dong Wang,* Otto S. Wolfbeis and Robert J. Meier*

Received 15th March 2013

DOI: 10.1039/c3cs60102a

www.rsc.org/csr

Temperature (*T*) is probably the most fundamental parameter in all kinds of science. Respective sensors are widely used in daily life. Besides conventional thermometers, optical sensors are considered to be attractive alternatives for sensing and on-line monitoring of *T*. This *Review article* focuses on all kinds of luminescent probes and sensors for measurement of *T*, and summarizes the recent progress in their design and application formats. The introduction covers the importance of optical probes for *T*, the origin of their *T*-dependent spectra, and the various detection modes. This is followed by a survey on (a) molecular probes, (b) nanomaterials, and (c) bulk materials for sensing *T*. This section will be completed by a discussion of (d) polymeric matrices for immobilizing *T*-sensitive probes and (e) an overview of the various application formats of *T*-sensors. The review ends with a discussion on the prospects, challenges, and new directions in the design of optical *T*-sensitive probes and sensors.

1. Introduction

1.1. Lead-in

Temperature (*T*) is probably the most fundamental parameter in all kinds of science. Respective sensors[1,2] are widely used in daily life, in metrology, aerodynamics, climate and marine research, in chemistry, medicine, biology, military technology, air conditioning, in practically all devices for heating and cooling, in production plants and the storage of food and other goods, to mention some of the larger areas. It is estimated that the share of sensors for *T* amounts to as much as 75–80% of the world's sensor market.[3] Types of thermometers include (1) liquid-filled glass thermometers based on the thermal expansion of materials;[4] (2) thermocouples based on the Seebeck effect;[5,6]

Institute of Analytical Chemistry, Chemo- and Biosensors, University of Regensburg, 93040 Regensburg, Germany. E-mail: robert.meier@ur.de, xmuwxd@gmail.com; Fax: +49 941 943 4064; Tel: +49 941 943 4065

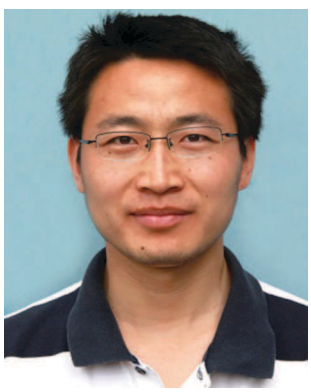

Xu-dong Wang

Xu-dong Wang, born in 1985, received his PhD degree in Chemistry from Xiamen University (Xiamen, China) in 2011. Since then, he has worked as a postdoctoral fellow in the group of Prof. Otto S. Wolfbeis at the University of Regensburg within an Alexander von Humboldt fellowship. His research interests are in the design of optical chemical and biosensors, nanosensors and molecular probes, developing novel (bio)sensing schemes, (nano)-materials and methods, and their applications to biological and chemical analysis. He has authored or coauthored more than 20 articles over the past five years, and his current h-index is 10 (May 2013).

Otto S. Wolfbeis

Otto S. Wolfbeis was a Full Professor of Analytical and Interface Chemistry at the University of Regensburg, Germany, from 1995–2012. He has authored numerous papers and reviews on optical (fiber) chemical sensors, fluorescent probes, labels and bioassays, on advanced (nano)materials for use in sensing schemes, and in spectroscopic methods including fluorescence (lifetime) imaging. He has (co)edited several books, and has acted as the (co)organizer of several conferences related to fluorescence spectroscopy (MAF) and to chemical sensors and biosensors (Europtrode). His h-index is 69 (May 2013). He is one of the 10 curators of Angewandte Chemie, the Editor-in-chief of Microchimica Acta, and one of the three editors of Methods and Applications in Fluorescence. Also see: www.wolfbeis.de.

and (3) optical sensors.[7] In view of environmental and health concerns, there is a trend to substitute traditional liquid-filled thermometers by alternative sensors such as thermocouples. These are nontoxic, easy to use, precise, have a wide analytical range (3 to almost 3300 K), and signals can be easily digitized.[3] They have become the most often used industrial sensors but – unless linked to an electronic display – lack the feature of visual read-out of liquid-filled thermometers. Moreover, thermocouples and related systems require an electrical link to the sensor at the sampling site. They also have limitations if applied in harsh or corrosive environments, and are strongly affected by interference from electromagnetic fields. Contact measurements in general require convective heat transfer and thus need to reach equilibrium between the sensor and the object. This can alter the actual T of the sample during the measurement, especially if the size of the sample is small compared to that of the sensor head. Traditional liquid-filled and bimetallic thermometers, thermocouples, pyrometers, and thermistors cannot be easily miniaturized and therefore are not suitable for measurement of T with a spatial resolution of <10 μm which is desirable, however, in microfluidic (integrated) systems or inside cells, for example.

Optical sensors for T, in contrast to other thermometers, possess the unique advantage of contactless measurement and large-scale imaging. Infrared (IR) thermometers based on black body radiation were the first kind of optical sensors for T. They are extremely useful in medicine and wherever direct contact of thermocouples has to be avoided or is even impossible. IR thermometry also lends itself to fast recording of changes in T. However, IR thermometers lack good spatial resolution and their precision depends on the properties of the subject studied. Also, IR thermometry can only be applied to measure the distribution of T on the surface of objects, and does not yield absolute T values so that reliable calibration is mandatory.

Robert J. Meier

Robert J. Meier, born in 1982, studied chemistry and received a doctoral degree in chemistry in 2011 from the University of Regensburg. His research is related to optical (multiple) sensing and imaging schemes for oxygen, pH values and temperature (including lifetime based and RGB techniques), and new (nano)materials including smart polymers and upconversion nanoparticles. In terms of applications of the resulting sensors, the focus is on dermatology (mainly wound research), on microbiology and intracellular sensing, and on pressure-sensitive and temperature-sensitive paints. He has authored or coauthored more than 20 articles over the past five years, and his current h-index is 9 (May 2013). He is now heading his own research group.

IR radiation does not penetrate glass walls and thus cannot be used for thermometry in combination with microscopes or in most microfluidic devices.

Other optical methods such as thermal reflection, absorption, Rayleigh scattering, Raman scattering, magnetic resonance imaging thermometry and luminescent methods are now additionally suggested for use in thermometry. Their principles have been reviewed.[3] Passive optical imaging techniques, such as IR imaging, rely on the natural radiative properties of the material(s) under study, whereas active optical imaging techniques, *e.g.* Raman spectroscopy, utilize an excitation source, such as a laser, to excite molecular vibrations or phonons in the sample. The accuracy of both passive and active imaging techniques is limited by the thermo-optical properties of the sample. For example, IR imaging is limited by low emissivity surfaces and Raman thermography by materials with low phonon energies.[8] Luminescence (fluorescence and phosphorescence) has attracted most attention. Sensing of T *via* luminescence is almost exclusively based on the use of luminescent molecular probes, nanoparticles or nanoaggregates. The probes and nanosensors can be incorporated in the sample to be studied (cells included), or deposited on its surface, often in the form of a thin film of a polymer host containing the probes or particles. Both single-point measurements and imaging have been reported. The probes, nanoparticles and sensor films are typically illuminated with short pulses of light, and the luminescence is detected either as intensity or decay time.

We are aware of different definitions and expressions for the various parameters that describe the performance of a sensor or a molecular probe for T. Therefore, the terms used in this review shall be defined first. *Sensitivity* is defined as the slope of the signal change (ΔS) with T, usually expressed as percent change per Kelvin ([% K^{-1}]). *Resolution* indicates the minimal detectable signal change and usually is given in Kelvin or degree Celsius. The *dynamic range* describes the range between the lowest and the highest T that can be determined with adequate precision and is expressed in K or °C. The *accuracy* of a sensor is the degree of accordance of the measured value with the true value, usually expressed in [%]. *Precision* defines the reproducibility of a measurement by means of the relative standard deviation (given in %, for example).

In this review, we focus on (a) molecular probes, (b) nanosensors, and (c) sensor films for luminescent determination of T. The term *sensor* usually (and like in industry) refers to a complete detection system, not just a (molecular) *probe* that describes a luminescent compound that gives a T-dependent emission. The literature cited here is believed to cover all relevant works after the year 1980 till May, 2013.

1.2. The origins of T-dependent luminescence

Virtually all luminescent molecules and materials display a T-dependent emission.[9] This is due to the Boltzmann distribution, and the dependence on T is a function of the specific electronic band structure of the material.[10] To demonstrate this, let us imagine a simplified material that exclusively allows radiative transitions at low T. At higher Ts, thermal energy

excites the electrons within the excited states (such as S_1, or T_1) transitions to the electronic states with varying vibrational levels that are overlapping at different energy levels, so that non-radiative decays become possible. The rate of non-radiative transitions (k_{nrt}) is related to T *via* the Arrhenius equation:

$$k_{nrt} \sim e^{(-\Delta E/kT)} \quad (1.1)$$

where ΔE is the energy gap between the lowest level of the excited state and the overlap point to a possible non-radiative decay state, and k is the Boltzmann constant. According to this equation, the non-radiative transition rate increases at higher Ts.

The quantum yield (QY) of luminescence represents the ratio of the number of emitted photons to the number of excited photons. It decreases with T according to

$$QY = \Gamma/(\Gamma + k_{nrt}) \quad (1.2)$$

where Γ represents the emissive rate of the luminophore. The luminescence lifetime (decay time) τ is defined as the average time a luminophore remains in its excited state prior to deactivation.[9] The lifetime (or – better – the decay time) of luminescence is defined as the time during which its intensity decays to 1/e of its initial value. In mathematical terms, luminescence intensity at any time can be expressed as

$$I = I_0 e^{-t/\tau} \quad (1.3)$$

where I_0 is the initial intensity (I at $t = 0$). Lifetime is thermally quenched with increasing T via:

$$\tau = 1/(\Gamma + k_{nrt}) \quad (1.4)$$

It shall be kept in mind, though, that the electronic band structures of large parts of the T-sensitive materials often are more complicated and can involve, for example, multiple excited bands that possess varying overlap energies.[11] This leads to a more complex dependency of luminescence on T.

As the T around the fluorophore undergoes changes, its intensity, decay lifetime, spectral positions and shape, and polarization may alter. These effects make all probes (such as for pH or calcium) be T-sensitive probes to some extent. In order to overcome the cross-sensitivity of a (molecular) probe to parameters other than T, and to prevent binding to biomatter such as proteins, they are often incorporated into inert (nano)materials.[12–15]

2. Spectroscopic schemes for read-out

Luminescence often is the observable of choice. It is sensitive, can be applied to even strongly colored or turbid media, and possesses many parameters, all of which may serve to sense T. T-dependent optical properties include the location of excitation and emission wavelength,[16] changes in fluorescence lifetime[17] or emission intensity[18] and changes in anisotropy.[19] Changes in luminescence caused by T are preferably detected, however, by measurement of intensity or of lifetime.[20–22] The following section gives a brief overview of referenced sensing schemes. Reference is made to a review by Schäferling and Duerkop[23] who have critically compared referenced luminescent sensing schemes.

2.1. Measurement of intensity

Luminescence intensity obeys Parker''s law,[9]

$$I = I_0 \phi k \varepsilon d c \quad (2.1)$$

where I is the (measured) luminescence intensity, I_0 the intensity of the exciting (laser) light; ϕ the QY of the luminophore (values range from 0 to 1), k a geometrical factor for the setup used, ε the (molar) absorbance, d the penetrated length, and c the concentration of the luminophore (the probe). Ideally, I is only affected by variations of ϕ with T. Unfortunately, it is also affected by the other parameters of Parker's equation, by photobleaching, and by background luminescence of samples (such as biomatter). Uneven probe distribution and poorly reproducible experimental geometries (such as varying distances or inhomogeneous light fields), in turn, hamper accuracy in the case of imaging. Referenced sensing is highly desirable for these reasons.

2.2. Ratiometric intensity measurement (RIM)

This spectroscopic scheme is simple, straightforward, and widely used for referencing luminescence intensity data.[24–26] In RIM, the intensity of a second (less sensitive or even inert) band is related to the analytical (T-dependent) signal. Ideally, the reference intensity of the second band responds to T in the opposite direction.[27] This ratiometric referencing scheme (usually based on the use of two dyes, one being the probe, the other the reference dye) can cancel out variations in the indicator concentration, geometry, source intensity, and light field. On the other hand, background fluorescence, light scattering and reflections are not compensated for.[28] Two approaches are common in RIMs. The first is based on referencing an indicator signal to a second (reference) dye.[29] The reference dye ideally is photoexcited at the same wavelength, but obviously should have a distinguishable emission wavelength. These methods are popular but can be compromised by FRET, and – more importantly – by different photobleaching rates of probe and reference dye. In a second approach, dual emission wavelength probes are used.[30] However, such probes are rare. Upconversion nanoparticles (see later) fall into this category. Here, the ratio of the intensities of two independent emission bands represents an intrinsically referenced signal. This method can eliminate most limitations and thus is preferred. A recent review[31] has summarized the use of dual-emitting T sensors for nanoscale thermometry, which covers an overview of key photophysical mechanisms of the dual emission of various nanostructures and their relationship with optical ratiometric thermometry. The key features (including tunability, sensitivity, brightness and specificity for T) have been discussed in detail, which offer great potential for their usage *in vivo*.

2.3. Measurement of lifetimes

The measurement of luminescence lifetime is an attractive alternative to intensity-based detection schemes. Besides the definition in the above section, luminescence lifetime (τ) is also defined[32] as the time during which the initial luminescence intensity has dropped to a value of 1/e (assuming single-exponential decay). The time-dependent luminescence intensity I_t is related to the lifetime τ *via* the following equation:

$$I_t = I_0 e^{(-t/\tau)} \quad (2.2)$$

where I_0 equals the luminescence intensity at time $t = 0$. The use of lifetime as the analytical signal overcomes many problems of intensity-based measurements. Lifetime signals are intrinsically referenced and, if proper calibration plots are available, yield corrected values for each T. Lifetime data are independent of dye concentrations, sensor size or thickness, geometry or surface curvature, or photobleaching (to a wide extent). Additionally, there is no need for a second analytical dye or wavelength for referencing, and signals are not affected by inhomogeneous light fields, or changes in the intensity of excitation light. On the other side, they need more sophisticated read-out, and indicators have to possess lifetimes that are adequately long so that low-cost methods for lifetime determination (preferably in the μs range) can be applied.[33] A complication may result from the fact that the decay times of many luminophores in condensed matter are not single-exponential.

Two methods are common in lifetime-based sensing. In the *frequency domain method* (Fig. 1, left), the indicator probe is excited with a sinusoidally modulated light source, typically at modulation frequencies of 0.1 to 10 τ^{-1} (where τ is the decay time). Once the probe is sinusoidally excited, its emission follows the excitation frequency with an additional lifetime-dependent phase shift. The decay time (τ) can be determined from the phase shift Φ according to the following equation:

$$\tau = (\tan \Phi)/(2\pi f_{mod}) \quad (2.3)$$

where f_{mod} is the modulation frequency of the excitation light. Frequency domain measurements are mostly applied to indicators with lifetimes in the μs or ms range. The method is relatively simple and does not require large instrumentation. Dedicated (LED-based) instruments are commercially available having the size of typically two cigarette packs. Measurements become more expensive in the case of fast decaying indicators (those having lifetimes in the ns range), because more expensive (high frequency modulated) light sources are required. The frequency domain method can yield quite accurate results, and is the method of choice for fiber optic sensors and single-spot measurements. It is less applicable to imaging of τ because expensive integrated sinusoidally modulated image intensifiers are required.

In the *time domain method* (Fig. 1, right), square-shape modulated excitation light pulses are applied along with fast gated read-out. The lifetimes typically are gauged from intensity ratios recorded in two successive time gates. There are two common ways to determine lifetimes (''decay times'') as shown in Fig. 2. The first is phase delay rationing (PDR)[34] where a first time gate is recorded in the excitation phase and a second gate in the emission phase shortly after the excitation light pulse. The second scheme is called rapid lifetime determination (RLD).[23,35,36] Here, two time gates (A_{em1} and A_{em2}) are recorded

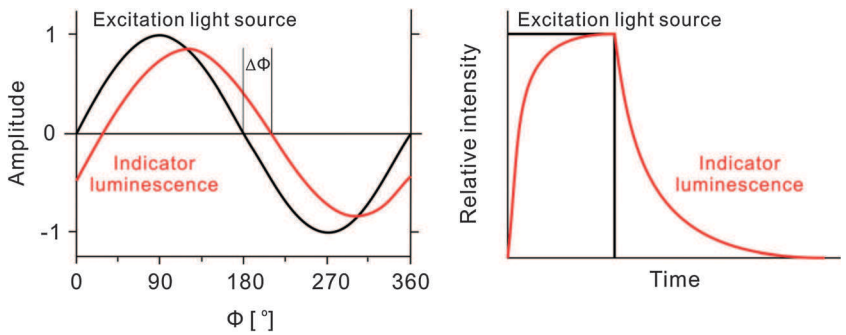

Fig. 1 Schemes of frequency domain (left) and time domain (right) lifetime measurements.

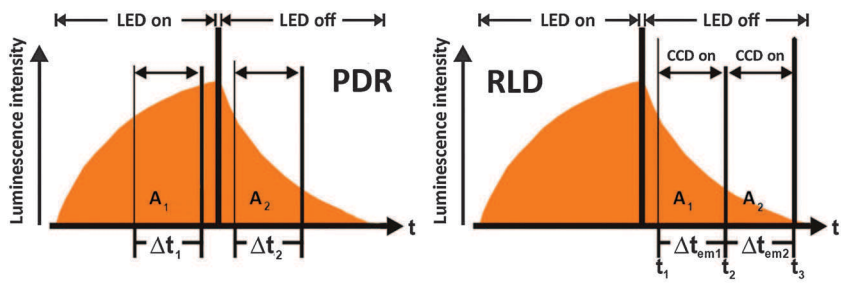

Fig. 2 Spectroscopic schemes for phase delay rationing (left) and rapid lifetime determination (right).

during luminescence decaying after the excitation pulse is switched off.

Assuming monoexponential decay (which however often is not the case, in particular when using solid materials) and identical length of the two time gates (Δt), the lifetime τ can be calculated according to:

$$\tau = (t_2 - t_1)/\ln(A_{em1}/A_{em2}) \quad (2.4)$$

where t_1 and t_2 are the starting times, and A_{em1} and A_{em2} the integrated intensities of the two time gates (A_{em1}, A_{em2}). The RLD scheme additionally offers the important feature of eliminating short-lived background fluorescence, which usually decays within 100 ns. Thus, the background can be excluded by opening the gates after a certain time delay. In contrast to the frequency domain scheme, the time domain method easily allows for both single-spot sensing and 2-dimensional (2-D) imaging. However, instrumental setups are more complex and expensive than in the case of intensity-based detection.

2.4. Measurement of anisotropy

In sensors based on fluorescence polarization (anisotropy),[9,37] the *T*-dependent Brownian (rotational) motion of dissolved molecular *probes* is determined. The scheme is hardly applicable to nanosensors or sensor films. Indicators in fluid solution rotate during the lifetime of their excited state. The movement and rotation of the probes accelerate with increasing *T*. On these grounds, an indicator excited with polarized light will lose more and more emission light intensity of its initial polarization due to rotation. As a result, the degree of anisotropy decreases with increasing *T*.

$$r = (I_{\parallel} - I_{\perp})/(I_{\parallel} + 2I_{\perp}) \quad (2.5)$$

Anisotropy is self-referenced and results in absolute *T* data. Its benefits include intensity-independent data (including insensitivity to photobleaching, fluorophore concentration, or variations in illumination intensity). Tables 1 and 2 summarize the compensations, as well as the advantages and disadvantages of common luminescent and related schemes for sensing *T*.[23,38]

Table 2 Properties of luminescence spectroscopy schemes[a]

Property	LI	DPR	SPDE	FDF	TDF	Anisotropy
Precision	–	0	+	++	++	–
Sensitivity	++	++	+	++	++	0
Photon efficiency	++	+	+	++	–	0
2D-imaging	0	++	++	0	++	–
Availability of portable devices	++	++	++	+	+	+
Robustness	–	+	+	++	++	+
Acquisition speed	++	+	+	0	–	0
Data processing speed	+	0	0	0	0	0
Simplicity	++	+	+	0	0	0
Cost	++	++	++	+	0	+

[a] (++) good; (+) partially good; (0) pendant; (–) bad.

3. Molecular probes for temperature

Luminescent molecular probes enable high spatial resolution and have a fast response, often in a time scale comparable to that of cellular processes. Several features are desirable for a good *T*-sensitive probe: (a) the signal is expected to undergo a large change with *T*; implies good sensitivity. (b) Absorption and emission should occur at long wavelengths so as to reduce interferences by the intrinsic color or fluorescence of samples which is strong in the UV or under UV and shortwave visible photoexcitation. (c) The probes should display good photostability so as to enable long-term monitoring without any photodecomposition during optical interrogation. (d) The probes must not be toxic if an *in vivo* use is intended. (e) High brightness, defined as the product of QY and molar absorbance (QY $\times$ ε), is a highly desirable parameter and supposed to be >20 000, ideally >100 000 cm M^{-1}. The following section discusses molecular probes for *T*, which are subdivided here into organic probes, metal–ligand complexes, and the relatively large group of lanthanide complex-based probes.

3.1. Organic compounds

The luminescence of all fluorescent and phosphorescent organic compounds depends on *T* and thus may be explored for sensing *T*. However, only few display large effects, work in the solid or fluid phase, cover the desired range and have a large QY. Water-soluble indicators are of substantial interest in context with cellular sensing and for bioassays. If not soluble in

Table 1 Commonly encountered interferences in luminescence spectroscopy, and assessment of schemes for compensating such effects.[a] Methods include (a) measurement of luminescence intensity (LI), (b) dual probe ratiometry (DPR), (c) single probe dual emission (SPDE), (d) frequency domain fluorometry (FDF), (e) time-domain fluorometry (TDF), and (f) anisotropy

Interference due to	LI	DPR	SPDE	FDF	TDF	Anisotropy
Instrumental drift (*e.g.* light source, detector)	–	+	+	++	++	+
Optical misalignment	0	++	++	++	++	++
Background luminescence	–	0	0	0	++ for RLD 0 for PDR	0
Optical components (caused, for example, during change of optical filters)	0	–	–	+	++	0
Light scattering by sensor materials	–	+	+	++	++	+
Intrinsic color of sample	–	0	0	++	++	+
Dye leaching or photobleaching	–	0	+	+	+	+
Inhomogeneous dye loading	–	0	++	++	++	+

[a] (++) good compensation; (+) partial compensation; (0) pendant; (–) no compensation.

Table 3 Composition, working ranges (K) and excitation and emission maxima (in nm) of luminescent organic probes for sensing *T*

Probe/matrix	Range (K)	Exc./Em.	Comments	Ref.
Rhodamine B on silica gel or in sol–gel	283–368	545/566	High QY; very good brightness; excitable in the visible range; cheap price; broad working range	42, 44
Rhodamine 6G-labeled DNA	288–308	497/524	High QY; the conformation change of DNA at different *T* influences the lifetime of the labeled Rhodamine G; insensitive to ionic strength	70
Perylene in a copolymer of styrene and *N*-allyl-*N*-methylaniline	298–358	386/475, 551	Resolution about 1 K; monomer emission increases; this is accompanied by an exciplex emission that remains constant; thermo-induced luminescence color change from green to blue at elevated *T*; perylene solely incorporated in polystyrene does not show any *T* dependence	49
BBS-excimer[a] in poly(1,4-butylene succinate)	323–353	366/430, 510	High concentration of dye needed; at first the dyes in poly(1,4-butylene succinate) are quenched; the heat-induced polymer stretching changes the local concentration of BBS and enhances excimer emission	71
7-Nitrobenz-2-oxa-1,3-diazol-4-yl (NBD) derivatives[b]	293–345	475/540	Fluorescent membrane probe; intensity decreases at high *T*s; resolution approximately 2 K; broad sensitive range	39
Laurdan	306–319	365/440, 490	Fluorescent membrane probe; embedded in cell membrane, emission maximum is blue-shifted at high *T*s; resolution approx. 0.1–1 K; narrow working range	39
Dipyren-1-yl(2,4,6-triisopropylphenyl)borane	223–373	410/475	Luminescence undergoes a color change from green to blue at high *T*; wide analytical range; low viscosity and high polarity matrix needed for the formation of TICT state	48
1,3-Bis(1-pyrenyl)propane	298–413	325/376, 476	Fully reversible *T* response and broad *T* range in ionic liquid; self-referenced signal (monomer and excimer interconversion); resolution approx. 0.16–0.30 K	50
Fluorescein labeled starch	273–333	480/523	Linear *T* response; high QY (0.93); response strongly to pH	65
1-(*N*-*p*-Anisyl-*N*-methyl)-amino-3-anthryl-(9)-propane	149–223	360/395, 560	Worked in organic solvent, self-referenced signal (monomer emission decreases, and exciplex emission increases at elevated *T*); high QY (0.44)	51
Acridine yellow in saccharide glass	223–323	410/500, 580	Measured in delayed fluorescence from triplet to singlet excited state; phosphorescent lifetime >100 ms; ratiometric measurement; sensitivity 4.5% K^{-1}; accuracy 1 K	52

[a] BBS = bis(benzoxazolyl)stilbene. [b] 2-(12-*N*-NBD-amino)dodecanoyl-1-hexadecanoyl-*sn*-*glycero*-3-phosphocholine; *N*-(NBD)-1,2-dihexadecanoyl-*sn*-*glycero*-3-phosphoethanolamine, triethylammonium salt; 12-(*N*-NBD-amino)dodecanoic acid.

water, they can be incorporated in particles, however. The use of exogenous fluorescent probes for sensing *T* in single living cells has been reviewed back in 1995.[39]

Rhodamine and its derivatives have long been known for the sensitivity of their fluorescence to *T* (see Table 3). The rhodamine family of fluorophores displays high QYs, brightness, and excitation bands in the visible range. The QY of rhodamine B (RhB) is highly *T*-dependent,[40] in that its QY decreases with an increase in *T* up to 373 K.[41] Their luminescence dependency on *T* is particularly expressed in the range from 273 to 373 K. These features make them most suitable as molecular probes for sensing *T* in microfluidic devices,[42] cells,[43] or in planar sensor films.[44] Other examples of the use of rhodamines will be given in the applications section further below. The group of Bergaud[18] has used dried RhB as a probe for surface *T* mapping, and applied to image the *T* distribution along resistively heated micro- and nanowires (Fig. 3). Similarly, an SU8/RhB thin layer was spin-coated onto a micro-heater to map the in-channel fluid *T*.[45] The surface *T* distribution can be imaged with high spatial resolution in the *T* range of 303–353 K. The *T* resolution can reach 0.1 K, which is very useful in microfluidic devices.

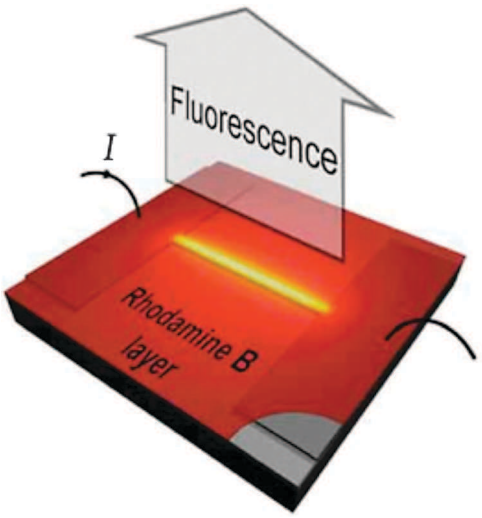

Fig. 3 *T* mapping along resistively heated micro- and nanowires using a dried layer of RhB. (Reprinted with permission from ref. 18. Copyright Wiley-VCH Verlag GmbH & Co. KGaA, Weinheim, 2008.)

Fluorescein is another highly luminescent probe with a QY of almost 1. Fluorescein and its derivatives are mainly used as pH probes. Like all the other fluorophores, fluorescein also undergoes thermal quenching at elevated *T*. It was covalently linked to starch and its response to *T* and pH was studied in detail.[46] The material responds linearly to *T* in the range from 273 to 333 K.

The NBD fluorophore (7-nitrobenz-2-oxa-1,3-diazol-4-yl, see Table 3) has a QY of 0.018 in water and its emission maximum occurs at around 520 nm. Both the fluorescence QY and lifetime of the probes depend on *T* in the range from 293 to 345 K but with moderate resolution. The laurodan (6-dodecanoyl-2-dimethylamino-naphthalene) fluorophore undergoes a gel-to-liquid-crystalline phase transition if incorporated into membranes.[39] This phase transition causes an emission wavelength shift to shorter wavelengths, and enables accurate measurement of *T* in cell membranes within a narrow working range (306–319 K).

The resolution can reach 0.1 K. However, both the NBD and laurodan probes have to be excited in the UV. In general, the thermally induced shift in the emission or excitation spectra is referred to as thermochromism.[47]

In a triarylboron-based fluorescent molecular thermometer (Fig. 4),[48] the probe [dipyren-1-yl(2,4,6-triisopropylphenyl)-borane] is in thermal equilibrium between the local excited state emission (LE) and the twisted intramolecular charge transfer (TICT) excited state emission. If T increases, the TICT emission is transferred into LE emission, and this induces a thermochromatic change of the emission color from green to blue. The probe works in the 223–373 K range, and the color change can be even seen with bare eyes.

Certain fluorophores, if present in typically $>10^{-4}$ M concentration, form exciplexes or excimers that can display T-dependent luminescence. Perylene and *N*-allyl-*N*-methylaniline, for example, form exciplexes in a polystyrene matrix that can be used as a colorimetric sensor for T (Fig. 5).[49] The equilibrium between formation and dissociation of the exciplex shifts to the dissociation side with increasing T. This also induces the increase of the monomer emission at 480 nm, while the exciplex emission remains almost constant. The mixture of the two different emissions undergoes a visible color change from green to blue at elevated Ts. This probe can reach a resolution of approximately 1 K.

A self-referenced luminescent thermometer was reported[50] that is based on a reversible T-dependent monomer–excimer interconversion of 1,3-bis(1-pyrenyl)propane in an ionic liquid. The thermometer can operate in the T range of 298–413 K, and the T response curve is completely identical in the heating and cooling circle. As early as 1977, Pragst *et al.*[51] observed the intramolecular exciplex formation of 1-(*N*-*p*-anisyl-*N*-methyl)-amino-3-anthryl-(9)-propane at elevated T in degassed methylcyclohexane–isopentane solvent. When the T increases from 149 K to 223 K, the monomer emission at 395 nm significantly decreases, and the corresponding exciplex emission at 560 nm increases profoundly. The opposite responses of the dual emission peaks at different Ts enable ratiometric measurement of T. Unfortunately, both the thermometers were used in organic solvents, which are hardly transferred into aqueous media.

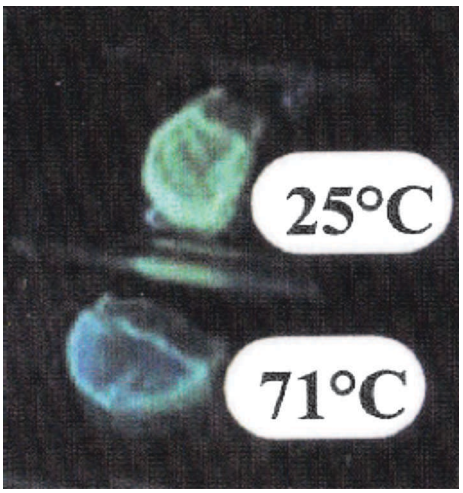

Fig. 5 The fluorescence observed from a copolymer film prepared from styrene and *N*-allyl-*N*-methylaniline at indicated Ts upon UV irradiation. (Reprinted with permission from ref. 49. Copyright American Chemical Society, Washington, DC, 2001.)

The delayed luminescence from a triplet to a singlet-excited state is rather sensitive to T. Fister *et al.*[52] studied the delayed luminescence of acridine yellow in a rigid saccharide glass at different Ts. They observed that the decay time of the delayed luminescence is >100 ms long, and that the fluorescence/phosphorescence intensity ratio is sensitive to T in the range of 223–323 K, with a sensitivity (slope) of 4.5% K^{-1}. The thermometer enables T to be measured with an accuracy of ± 1 K.

The thermally activated delayed fluorescence of fullerene C_{70} strongly depends on T. This was exploited to sense T by incorporating C_{70} into polymer films.[53] In the absence of oxygen and at Ts above 293 K, the red fluorescence of C_{70} in the films is so intense that the bare eyes can perceive it. Fluorescence increases with T by a factor of up to 90, depending on the polymer used. This results in a working range from 193 K to at least 413 K. Perylene was incorporated as an internal reference in order to enable ratiometric measurements. The sensitivity of the lifetime of the delayed fluorescence to T is also high, and results in an even wider working range. The method

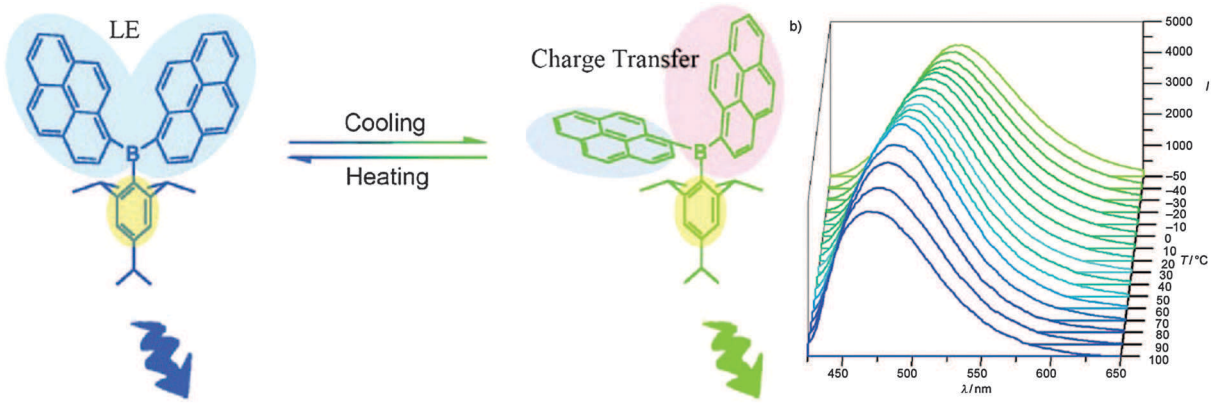

Fig. 4 Function of the triarylboron-based fluorescent probe. An increase of T causes the green TICT emission to disappear in favor of the blue local excited state emission. (Reprinted with permission from ref. 48. Copyright Wiley-VCH, Weinheim, 2011.)

was also applied to image *T*. The properties of commonly used organic luminescent *T* probes are summarized in Table 3. Fig. 6 depicts the corresponding chemical structures of the organic luminescent *T* probes.

The limitations of using free molecular probes include the contamination of the surrounding material[54] due to absorption onto surfaces, and (non-*T* related) time dependent changes in fluorescence intensity.[55] Such shortcomings can be overcome by encapsulating the probes into microparticles or nanoparticles made from organic polymers.[15,56–66] However, organic polymer–fluorophore hybrids have limited *T* stability.[67] Mapping *T* of above 398 K is a highly desirable property for thermal optical sensors, especially when recording the *T* profile of high-power electronic devices.[68,69]

3.2. Metal–ligand complexes

Luminescent metal–ligand complexes form a large group of molecular probes for sensing *T*. They often possess lifetimes in the μs range, absorption in the visible range, moderate brightness, and large Stokes shifts. Their luminescence (mostly phosphorescence) is often sensitive towards oxygen due to their long lifetimes. The use of gas-blocking materials can shield them from being quenched by oxygen (see Section 6). The *T* sensitive luminescence of these probes can be easily separated from scattered excitation light due to the long lifetimes and the usually large Stokes shifts.

Characteristics of typical probes are listed in Table 4 and their respective chemical structures are shown in Fig. 7. The $Ru(bpy)_3$ complex absorbs in the blue part of the spectrum (400–480 nm) and an intense emission peaking at ~620 nm. It is water-soluble and has a μs lifetime. Thus, it can also be used for lifetime-based sensing and imaging *T* in aqueous solutions or in aqueous biosystems. It was also immobilized in sol–gel films[72] or nanoparticles.[80] Among the ruthenium polypyridyl complexes, $Ru(phen)_3$ has the highest sensitivity towards *T*, but it also suffers from quenching by oxygen. If, however, incorporated in gas-blocking polymers, such as polyacrylonitrile or poly(vinylidene chloride-*co*-acrylonitrile), this cross-sensitivity can be eliminated.[74] The probe $Ru(phen)_3$ is very photostable, has a working range of 273–393 K, a large Stokes shift (160 nm), and a lifetime as long as 3 μs, which is easily determined using time-gated devices (see Section 2).

Similar to the ruthenium complexes, iridium polypyridyl complexes have lifetimes in the μs range, and their luminescence is sensitive to *T*. The probe $Ir(ppy)_2(carbac)$ has a particularly high sensitivity to *T* and a low cross-sensitivity to oxygen if dissolved in the gas-blocking polymer polyacrylonitrile.[61,75] Both, intensity and lifetime linearly depend on *T* over a wide

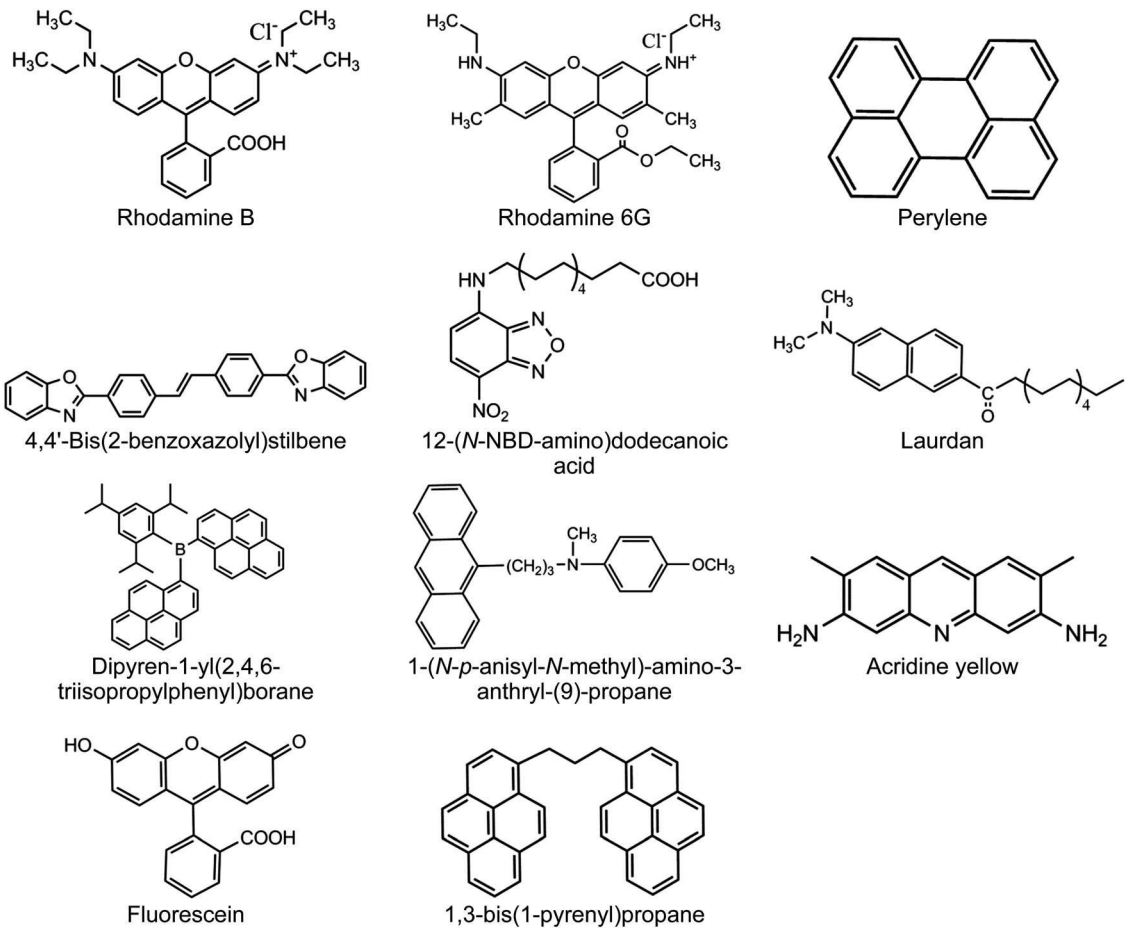

Fig. 6 Chemical structures of selected luminescent organic probes for *T*.

Table 4 Working ranges (in K), spectral maxima of excitation and emission (in nm) of luminescent metal–ligand probes for sensing *T*

Probe	Range (K)	Exc./Em.	Comments	Ref.
$Ru(bpy)_3$	50–290	458/575	Water-soluble; can be excited with blue LEDs; resolution up to 0.1 K; fair photostability; luminescence quenched by oxygen	72
$Ru(phen)_3$	273–393	470/580	High sensitivity to *T*; can be excited with blue LEDs; wide working range; photostable; luminescence quenched by oxygen	15, 64, 73, 74
$Ir(ppy)_2(carbac)$	274–323	405/519	High sensitivity and brightness; linear relationship between lifetime and *T*; low cross-sensitivity to oxygen in polyacrylonitrile; but poor photostability	61, 75
Brph-thq Pt	273–333	405/501	Blue LED excitable; good QY; slight oxygen response; low cross-sensitivity to oxygen in poly(vinylidene chloride-*co*-acrylonitrile)	59, 76
Ni tetraazamacrocyclic complex	300–338	—/340	The probe undergoes *T*-dependent spin interconversion equilibrium; fluorescence enhanced at elevated *T*; emission at UV	77
$[Cu_4I_4(PPh_2(CH_2)_2Si(OCH_2CH_3)_3)_4]$	8–120	300/420, 600	Emission undergoes a thermochromatic shift; ratiometric read-out possible, polymerizable using the sol–gel method	78
PtOEP in polystyrene	300–450	387/650	Lifetime based thermal imaging; accuracy about 0.25 K; cross-sensitivity to oxygen; enables imaging of thermal pulse induced *T* change	79

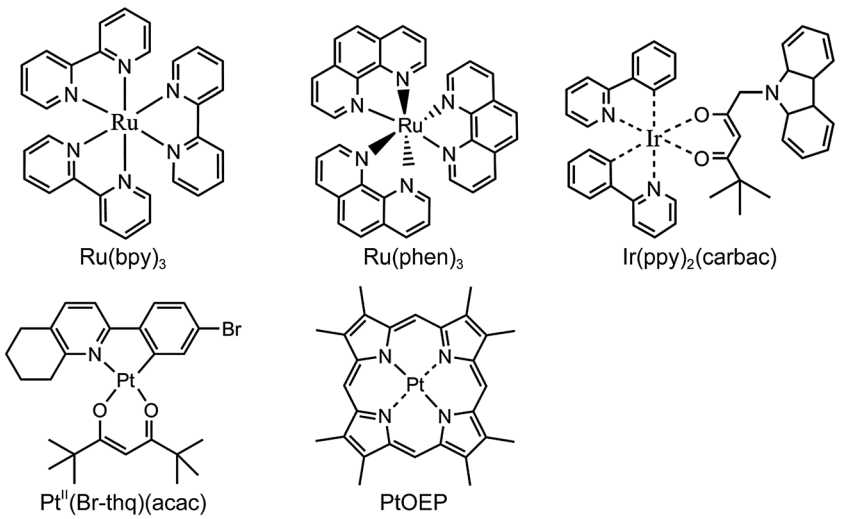

Fig. 7 Chemical structures of selected luminescent metal–ligand probes for *T*.

range (274–323 K). However, the absorption coefficient of the iridium complexes in the visible range is rather weak.

Luminescent platinum complexes for sensing *T* have been described recently.[76] A series of yellow-green to blue-green light-emitting heteroleptic, cyclometalated [(C^N)Pt(II)(acac)] complexes were reported that can be excited using 405 nm LEDs. They possess lifetimes of several μs and QYs of up to 0.15. The luminescence of the dyes incorporated in polystyrene films only shows a weak response to oxygen, and luminescence is virtually independent of oxygen tension if they are embedded in a gas-blocking polymer. The best candidate of this class of *T* probes is the Pt(II) complex of (4-bromophenyl)-5,6,7,8-tetrahydroquinoline (Brph-thq Pt) which offers a fairly good response in the range from 273 to 333 K.

A nickel complex with a macrocycle was covalently attached to a naphthalene fluorophore, and then undergoes a highly *T*-dependent interconversion from a high-spin state to a low-spin state.[77] It can be used as a molecular thermometer in solution because the equilibrium between the two states is shifted towards the low spin form as *T* is increased. The naphthalene fluorophore reports the increase in *T* as an enhancement in its QY. In other words, the probe lights up as the sample is heated.

Polynucleic metal complexes are known to undergo thermochromic shifts in their luminescence. This phenomenon originates from two different emission bands.[81,82] The emission band that is distinct at room *T* (the low energy band) is attributed to metal centered d → s,p transitions resulting in a so-called ''cluster centered'' triplet emission. At cooled *T*, this low energy emission band is extremely weak and a higher energy band dominates the visible luminescence. This high energy band can be attributed to a triplet center-to-ligand charge transfer. Copper(I) cluster complexes are the most powerful probes and give visually observable thermochromic shifts in luminescence. An example for this can be seen in Fig. 8. The thermochromic behavior was first described by Hardt and Pierre[83,84] who reported on $Cu_4L_4J_4$ type complexes, with L representing a varying cyclic nitrogen base as a ligand.[83] Piperidine, morpholine and pyridine were studied as ligands, displaying a distinct red shift of the emission spectra upon heating from 84 and 201 K. The group of Boilot[78,85,86] further

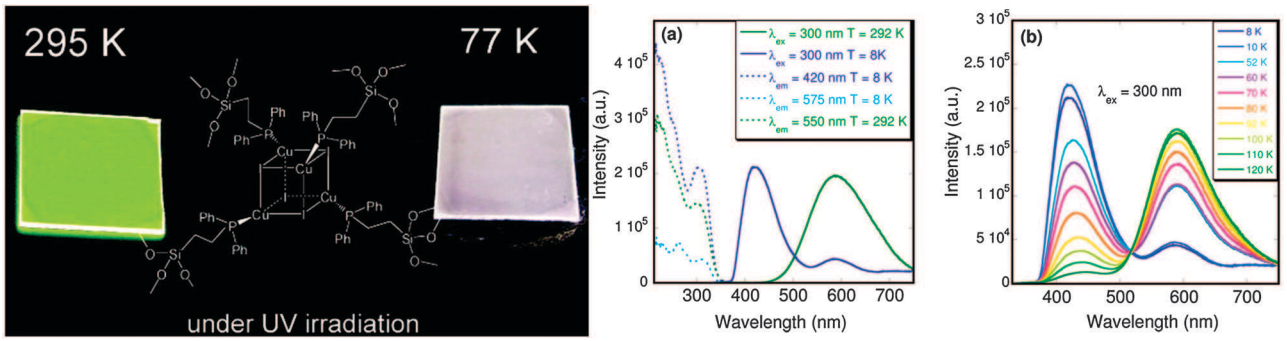

Fig. 8 Thermochromic behavior and structure of a polymerizable copper clusters using alkoxysilane modified phosphine ligands along with the sol–gel polymerization. The complex displays a change in emission color from green at room *T* towards violet 77 K. The right panel depicts the change in excitation and emission spectra of the complex at varying *T*s. (Reprinted with permission from ref. 78. Copyright American Chemical Society, Washington, DC, 2008.)

investigated copper iodide clusters with phosphine-based ligands. These display two intense emission bands, *viz.* a bright green-yellow band at room *T* and a blue one at lower *T*. These probes cover a whole range from 8 to 290 K. Furthermore, phosphine ligands render the complexes more stable than the pyridine-based clusters. The group also realized polymerizable copper clusters using alkoxysilane modified phosphine ligands along with the sol–gel polymerization technique.[78] Films prepared from this material allow for ratiometric (2-wavelength) measurement of *T* in the range from 8 to 120 K. Further, a trizwitterionic dicationic Cu_5 cluster was reported[87] that exhibits an excellent thermochromic *T*-dependent luminescence in the range between 228 and 353 K with a high sensitivity and temporal (sub-millisecond) as well as spatial (sub-micrometer) resolution. Besides copper cluster complexes, thermochromism was reported for many other coinage metal clusters including for example gold, silver, or platinum.[88,89] This field has been reviewed by Ford *et al.*[90] and Yam and Lo.[91] After the publication of these reviews there were numerous articles reporting examples for thermochromatic clusters, but unfortunately, we cannot list all of these complexes due to the limited space. Nearly all of these complexes were not investigated for sensing purposes, which provide a great potential for future investigation.

Metalloporphyrins have lifetimes that can range from tens to hundreds of μs. Normally, their absorption peaks of the Soret bands are located at around 400 nm so that they can be photoexcited with 405 nm laser diodes or purple LEDs. These probes have long been known as oxygen-sensitive probes. However, they also exhibit strong thermal quenching with increasing *T*. Lupton *et al.*[79] have incorporated platinum(II) octaethylporphyrin (PtOEP) in a polystyrene matrix and spin-coated this material on an electrically heated device for thermal imaging. PtOEP has a lifetime of 50 μs that strongly depends on *T*, and lifetime-based thermal imaging was accomplished with an accuracy of about ±0.25 K. The system also enables imaging of temporal *T* change that was induced by short thermal pulses (in the order of μs). However, the sensing film suffers from the cross-sensitivity to the quencher oxygen because polystyrene is oxygen permeable.

3.3. Lanthanide complexes

Luminescent lanthanide chelates, especially those of europium(III) and terbium(III), have decay times between several hundred μs up to 2 ms, sharp emission bands, large Stokes shifts, but moderate brightness. They are very sensitive to *T*. Lanthanide ions (without any organic ligand) have particularly weak absorption so that direct use of them for optical sensing is difficult. If chelated (in most cases, with β-diketonate ligands, see Fig. 9), much larger absorption coefficients are warranted. The organic ligands – which can be easily introduced – are referred to as sensitizers. The resulting complexes display good sensing capabilities but absorb light in the 350–450 nm region only.

The europium thenoyltrifluoroacetonate chelate complex, referred to as $Eu(TTA)_3$, was used in a matrix of poly(methyl methacrylate) to image *T* on an integrated circuit.[92] The spatial resolution of the sensor can reach 0.7 μm. The probe was also injected into cells for thermal imaging of receptor-activated heat production in living cells.[93] A detailed study[94] on the effect of sensitizers, polymer matrix and concentration on europium β-diketonate based probes for *T* revealed that all these parameters play a role in terms of the *T* sensing performance of the probes and their applicability in *T*-sensitive paints for use in aerodynamic studies.

The luminescence of the $Eu(TTA)_3$ complex is not quenched by oxygen. It was immobilized in polymers including polystyrene, poly(methyl methacrylate), polyurethane and model airplane dope.[95] The decay time of $Eu(TTA)_3$ depends on the polymer matrix. All the sensor materials respond to increasing *T* with a decrease in intensity, but there is a large variation in terms of signal change. Plots of normalized intensity *versus T* are linear or almost linear for $Eu(TTA)_3$ in polystyrene and in polyacrylates, whilst they are nonlinear in polyurethane. The maximum sensitivity of the luminescence lifetime of $Eu(TTA)_3$ in polystyrene is between 283 and 333 K. The co-immobilization of a relatively inert reference dye (such as perylene) and the *T*-probe $Eu(TTA)_3$ in a polystyrene matrix also enables ratiometric read-out.[96] $Eu(TTA)_3$ is a good *T* probe in oxygen impermeable polymers, but its luminescence degrades quickly in (highly gas-permeable) silicone.[97] The chemically related complex $Eu(TTA)_3$phen was incorporated[98] into nm-thin Langmuir–Blodgett films of poly-(*N*-dodecylacrylamide). Such films respond to *T* in the range of 320–370 K with a sensitivity of 1.2% K^{-1}.

As shown in Table 5, currently used lanthanide probes can be photoexcited in the 350–450 nm region only. By increasing

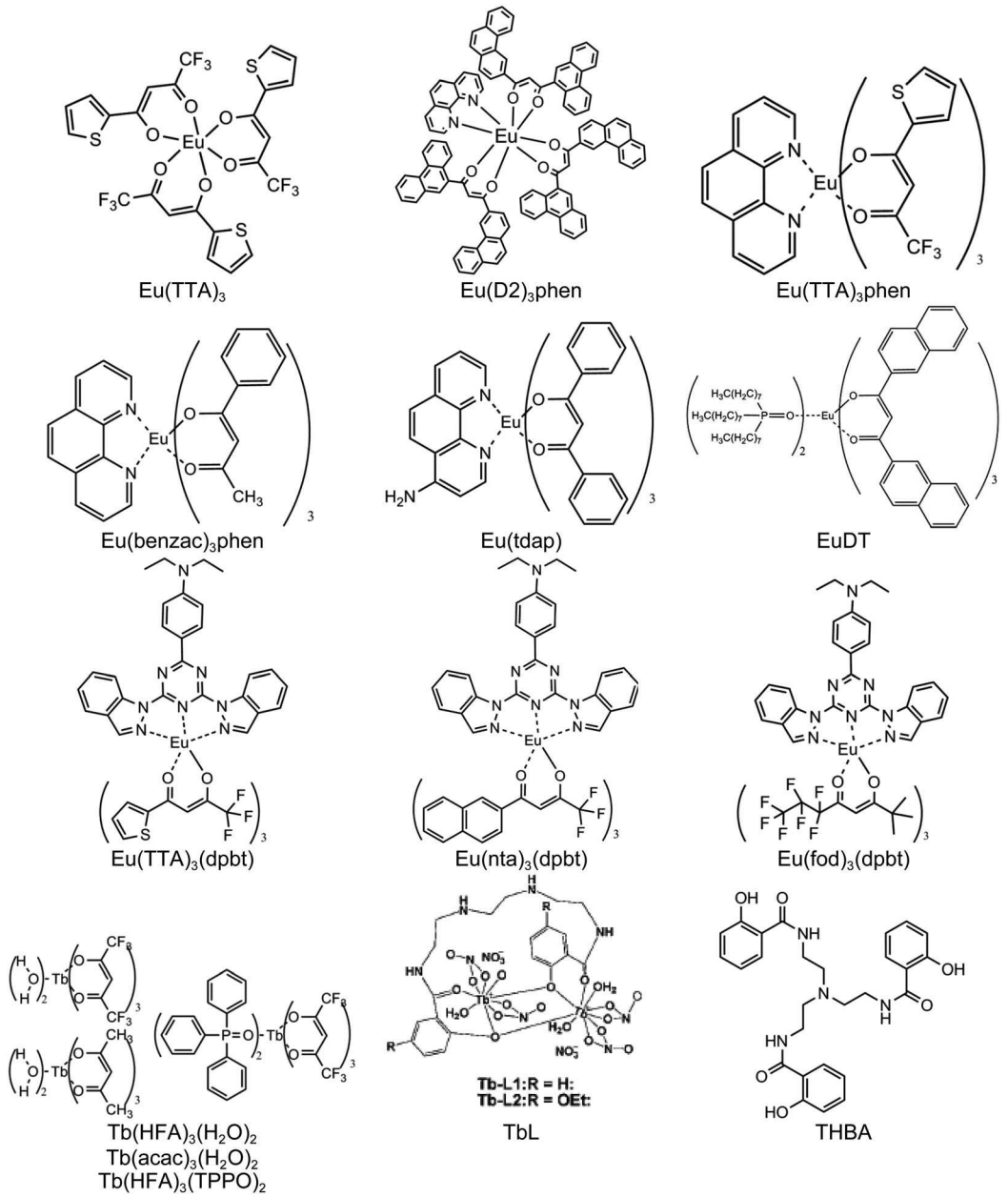

Fig. 9 Chemical structures of lanthanide complexes based probes for *T*.

the size of the conjugated π-electron system of the sensitizer (*i.e.*, by increasing the number of conjugated double bonds), the excitation maximum of the probe can be longwave shifted. Derivatives of dipyrazolyltriazine (dpta) were coordinated to various tris(β-diketonato) Eu(III) complexes to result in probes that were referred to as $Eu(tta)_3(dpbt)$, $Eu(nta)_3(dpbt)$, and $Eu(fod)_3(dpbt)$.[63,99,100] They display enhanced luminescence QYs, absorption coefficients, and excitation peaks near or in the visible range. The resulting complexes often are compatible with 405 nm LEDs and lasers. On the other side, they are not very stable in polar solvents (water included), because the sensitizer is easily replaced by the solvent. This process usually is irreversible. Thus, the selection of proper solvents and polymer matrices is critical when dissolving or immobilizing such probes.

Rather surprisingly, terbium(III) chelate complexes have rarely been used as optical probes for *T*.[101] Such complexes have longer decay times than those of Eu(III), and therefore are likely to be superior in terms of lifetime-based sensing. Their long lifetimes can be measured more easily and with better precision and accuracy. The terbium(III) tris[(2-hydroxybenzoyl)-2-aminoethyl]amine chelate[102] was found to be a viable probe for sensing *T*. It has high color purity, a long lifetime and a good QY, but requires shortwave excitation. Both its luminescence intensity and lifetime strongly depend on *T* in the range from 288 to 338 K. The probe displays the typical green emission of terbium(III) complexes if photoexcited at 341 nm, with the strongest peak at 546 nm and a typical decay time of 1.15 ms at 288 K. Notwithstanding their performance, it

Table 5 Working ranges (in K), spectral maxima of excitation and emission (in nm) of luminescent europium(III) and terbium(III) chelates for sensing *T*

Probe/matrix	Range	Exc./Em.	Comments	Ref.
$Eu(TTA)_3$ [a] in poly(methyl methacrylate)	—	365/612	*T* resolution 0.01 K; spatial resolution 0.7 μm	92
$Eu(TTA)_3$ in cells	288–313	357/612	Hydrophobic, attachable to biological membranes; luminescence quenched rapidly in aqueous solution	93
$Eu(TTA)_3$ in polystyrene $Eu(TTA)_3$ in polyurethane $Eu(TTA)_3$ in poly(methyl methacrylate) $Eu(TTA)_3$ in a model airplane dope	278–333	377/615	Good sensitivity; insensitive to oxygen; degrades rapidly in a silicone matrix; lifetime based measurement; response to *T* is nonlinear in polyurethane, but linear in other polymers; highest sensitivity in a polystyrene matrix	95
$Eu(D2)_3$phen in FIB[b]	278–318	370/615	Not sensitive to oxygen; highly sensitive to *T*; high resolution up to 0.001 K; several other complexes were also studied in detail, but all can only be excited in the UV	94, 105
$Eu(TTA)_3$phen and poly(*N*-dodecylacrylamide) as a Langmuir–Blodgett film	320–370	350/613	Lifetime 714 μs; 2-D imaging demonstrated; linear calibration plot	98
Eu(benzac)$_3$(phen)[c]	278–328	381/611	High sensitivity to *T*; insensitive to oxygen; poor stability in polar solvent; used poly(vinylidene dichloride-*co*-acrylonitrile) based nanoparticles	29
Eu(tdap[d]) in poly(methyl methacrylate)	283–343	400/613	Lifetime based measurement; high sensitivity; can be excited with a 405 nm LED	106
EuDT[e] in poly(methyl methacrylate) and 2-bis(trimethoxysilyl)decane nanoparticles	298–318	375/616	Excitable using a 405 nm LED; high QY; resolution of 0.3 K; suitable for biological systems; luminescence lifetime can be adjusted by varying the concentration of dye in the nanoparticles (size 20–30 nm); insensitive to oxygen if placed in nanoparticles	107, 108
$Eu(TTA)_3$(dpbt)[f] in poly(vinylidene dichloride-*co*-acrylonitrile)	274–323	425/619	Excitable using a blue LED; large absorption coefficient (63 900 M^{-1} cm^{-1}); high QY (0.4 in toluene at 298 K); in-sensitive to oxygen; good photostability; rather poor stability in polar solvents; cannot be immobilized in PAN polymer; but in poly(vinylidene chloride-*co*-acrylonitrile); various other polymers also studied	63, 99
Eu(nta[g])$_3$(dpbt)	273–343	403/615	Excited with a 405 nm LED; large molar absorption coefficient (61 300 M^{-1} cm^{-1}); high QY (0.52 in toluene at 298 K); high brightness; not stable in polar solvents such as DMF or ethanol; not sensitive to oxygen in poly(vinyl methyl ketone)	100
Eu(fod[h])$_3$(dpbt)	273–343	397/615	Excited with a 405 nm LED; large absorption coefficient (62 300 M^{-1} cm^{-1}); high QY (0.42 in toluene at 298 K); high brightness; not stable in polar solvents such as DMF or ethanol; not sensitive to oxygen in poly(vinyl methyl ketone)	100
[i]$Tb(HFA)_3(H_2O)_2$ $Tb(HFA)_3(TPPO)_2$ $Tb(acac)_3(H_2O)_2$	283–323	363/543 345/543 370/543	$Tb(HFA)_3(H_2O)_2$ and $Tb(HFA)_3(TPPO)_2$ are very sensitive to *T*. $Tb(acac)_3(H_2O)_2$ is less sensitive. The luminescence of terbium(III) nitrate is not at all sensitive to *T*. QYs: $Tb(acac)_3(H_2O)_2$: 0.59; $Tb(HFA)_3(TPPO)_2$: 0.30. Poor stability in hydroxylic solvents (water included)	109
TbL	273–343	334/546	Luminescence lifetime ~1 ms; strong *T* dependence; good QY (~0.14); broad excitation band, compatible with 405 nm LED; decomposes at 580 K; resolution of 0.1 K	110
Tb-THBA[j]	288–338	341/546	Multiple emission at 488, 546, 584, and 619 nm; good QY (0.22 in dimethylsulfoxide); high sensitivity to *T*; decay time 1.15 ms in acetonitrile at 288 K	102
$[Tb(hfa)_3(dpbp)]_n$ coordination polymer	200–500	380/543	High-*T* sensing probe; decomposition *T* at 590 K; QY = 0.4; lifetime: 0.35 ms at room *T*; sensitivity 0.64% K^{-1}; the corresponding Eu complex is not sensitive to *T*	104
$[Tb_{0.99}Eu_{0.01}(hfa)_3(dpbp)]_n$ coordination polymer	200–500	380/543, 613	Ratiometric probe (emission at 543 nm is sensitive to *T*, but the emission at 613 is not); high thermostability; sensitivity 0.83% K^{-1}	104

[a] TTA = thenoyltrifluoroacetonate. [b] D2 = tris(4,4,4-trifluoro-1-(2-thienyl)-1,3-butanediono); phen = 1,10-phenanthroline; FIB = poly(hexafluoro-isopropylmethacrylate-*co*-heptafluoro-*n*-butyl methacrylate). [c] benzac = benzoylacetonato. [d] tdap = tris(dibenzoylmethane) mono(5-amino-1,10-phenanthroline). [e] DT = tris(dinaphthoylmethane)-bis(trioctylphosphine oxide). [f] dpbt = 2-(4-diethylaminophenyl)-4,6-bis[(3,5-dimethylpyrazol-1-yl)-1,3,5-triazine]. [g] nta = 4,4,4-trifluoro-1-(2-naphthyl)butane-1,3-dione. [h] fod = 6,6,7,7,8,8,8-heptafluoro-2,2-dimethyloctane-3,5-dione. [i] HFA = hexafluoroacetylacetone; TPPO = triphenylphosphineoxide; acac = acetylacetone. [j] THBA = tris[(2-hydroxy-benzoyl)-2-aminoethyl]amine.

is desirable to use probes that can be photoexcited with more longwave (laser) light.

The development of probes that can efficiently absorb visible light is highly desired. Tb(III) chelates have also been used as membrane dyes for the preparation of self-assembled *T* sensitive unilamellar vesicles.[103] These compounds are very sensitive towards *T* between 273 and 305 K, and the sensitive range can be tuned *via* the phase transition *T* and the constituents used in the vesicles.

Thermostable lanthanide coordination polymers were designed and synthesized in order to improve the thermosensing performance and allow for high-temperature measurements.[104] The polymers were prepared *via* introducing the Tb^{III} ion and hexafluoroacetylacetonato (hfa) ligands into coordination polymer frameworks. The typical structure of the polymer is given in Fig. 10. The triplet state of hfa (22 000 cm^{-1}) is very close to the emitting level of the Tb^{III} ion (20 500 cm^{-1}). This induces effective

energy transfer (EnT1) and energy back transfer (BEnT), and thus results in high-performance thermosensing dyes. In the molecular structure, the phosphane oxide ligands acted as a bi-dentate bridge between lanthanide ions in one-dimensional polymeric chains.

The coordination polymer prepared from solely Tb^{III} ion offers a high emission QY (40% for $[Tb(hfa)_3(dpbp)]_n$ at room T) and a T sensitivity over a wide T range of 200–500 K. Thermogravimetric analysis revealed that the coordination polymers $[Eu(hfa)_3(dpbp)]_n$ and $[Tb(hfa)_3(dpbp)]_n$ have decomposition points of 581 and 590 K, respectively, which is significantly higher than the $Tb(hfa)_3(H_2O)_2$ (450 K). The superior thermal stability of the coordination polymers enables high-T sensing with the probe.

Quite interestingly, the $[Eu(hfa)_3(dpbp)]_n$ is not sensitive to T in the range of 200–300 K. Therefore, co-doping with both Eu^{III} and Tb^{III} to the coordination polymer may result in probes that possess the ability of ratiometric sensing. Thus, the polymer $[Tb_{0.99}Eu_{0.01}(hfa)_3(dpbp)]_n$ was synthesized for investigation of its T response in the range of 200–450 K. As shown in Fig. 11, the characteristic emission bands at 543 and 613 nm are attributed to the f–f transitions of Tb^{III} ($^5D_4$–$^7F_5$) and Eu^{III} ($^5D_0$–$^7F_2$), respectively. The emission intensities at 543 nm decrease dramatically with increasing T. In contrast, the emission intensities at 613 nm increase slightly. The polymer exhibits brilliant green, yellow, orange, and red photoluminescence under UV irradiation (365 nm) at 250, 300, 350, and 400 K, respectively.

3.4. Thermo-responsive luminescent bioprobes

The green fluorescent protein (GFP) can act as a T-sensitive intracellular nanoprobe,[37] because its fluorescence polarization anisotropy (FPA) depends on T (see Fig. 12). The method was applied to GFP-transfected HeLa and other cancer cell lines to monitor the heat generated after photothermal heating using gold nanorods surrounding the cells. A spatial resolution of 300 nm and a T resolution of about 0.4 K were achieved. The method excels by the biocompatibility of the GFP, its high spatial and good T resolution as well as a fast response. Therefore, it possesses the potential ability to unravel intimate cellular processes that involve heating at the single cell level. It also provides a noninvasive tool for fundamental and applied research in areas ranging from molecular biology to therapeutic and diagnostic studies.

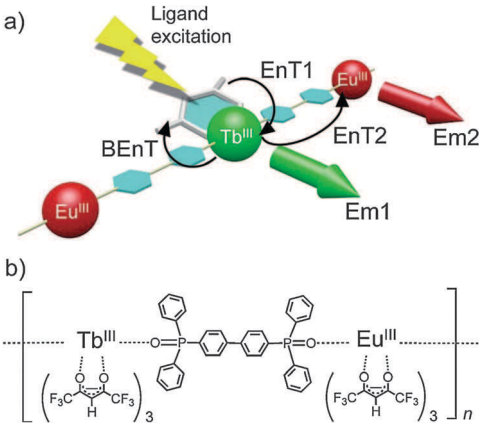

Fig. 10 (a) Energy transfer processes of the Eu^{III} and Tb^{III} coordination polymer (EnT: energy transfer, BEnT: energy back transfer, Em: emission). (b) Chemical structure of $[Ln(hfa)_3(dpbp)]_n$ (Ln = Eu, Tb). (Reprinted with permission from ref. 104. Copyright Wiley-VCH, 2013.)

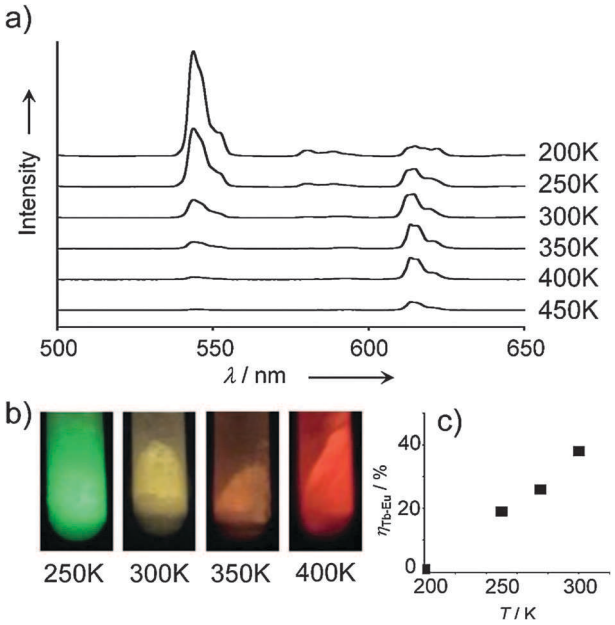

Fig. 11 (a) T-dependent emission spectra of $[Tb_{0.99}Eu_{0.01}(hfa)_3(dpbp)]_n$ in the solid state in the T range of 200–450 K (λ_{ex} = 380 nm). (b) Color pictures of $[Tb_{0.99}Eu_{0.01}(hfa)_3(dpbp)]_n$ under UV (365 nm) irradiation show brilliant green, yellow, orange, and red emission. (c) T-dependence of the energy transfer efficiency. (Reprinted with permission from ref. 104. Copyright Wiley-VCH, 2013.)

Furthermore, T dependent blinking of fluorescent proteins was investigated using fluorescence correlation spectroscopy (FCS).[111] The enhanced green fluorescent protein (EGFP) offers an attractive feature. Protonation of the Tyrosine-66 hydroxyl group on the chromophore brings the molecule from a deprotonated state (fluorescent upon 488 nm excitation), to a protonated state (non-fluorescent upon 488 nm excitation). The fluctuations in the fluorescence signal caused by this reversible reaction are referred to as blinking and strongly vary along with changing T. The associated relaxation time (<1 ms) can be measured with FCS and provides a self-referenced signal. Thereby, fluorescent proteins can be used as molecular thermometers in the range of 283 to 338 K. However, the T response is still sensitive towards changes in pH or buffer composition.

4. Nanomaterials for sensing temperature

It is fair to say that probably all kinds of luminescent nanomaterials (examples being quantum dots, carbon dots, polymer dots, photon up-conversion nanoparticles, nanodiamonds and the like) display T-dependent luminescence. However, only few have been studied in detail. Certain aspects of the use of nanomaterials for sensing T have been reviewed recently.[11,112,113]

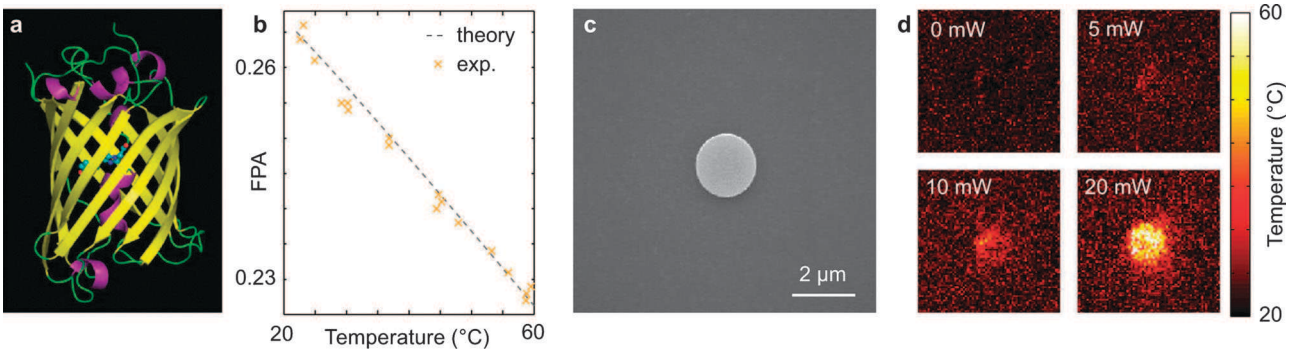

Fig. 12 GFP as a probe for sensing and imaging of *T*. The figures show (a) a 3D model of the structure of GFP; (b) a calibration plot that relates the fluorescence polarization anisotropy (FPA) of GFP to *T*; (c) a scanning electron microscopic image of a lithographically imprinted gold microdisc; and (d) the *T* map obtained by imaging the FPA of GFP around the microdisc while heating with an IR laser. (Reprinted with permission from ref. 37. Copyright American Chemical Society, Washington, DC, 2012.)

4.1. Quantum dots

Quantum dots (QDs) of the CdX type (with X = S, Se or Te) possess high QYs, bright luminescence, wide excitation spectra and – of capital importance – size-tunable absorption and emission colors. They have been widely used for purposes of fluorescent labeling and imaging.[114] In general, the luminescence intensity of QDs decreases with an increase in *T*, and this is accompanied by a widening and a red shift of the emission spectra. Water-soluble CdTe QDs respond to *T* over a wide range (77–300 K) and with an unusual anti-quenching effect.[115] Their luminescence is completely quenched if cooled to below 230 K, and it recovers upon increasing *T* to 280 K. However, if *T* exceeds 280 K, the luminescence of these QDs exhibits normal thermal quenching. The anti-quenching effects of the QDs at lower *T* can be attributed to the inter-QD dipole–dipole interactions.[115,116] Ultrathin films of CdTe QDs assembled on a positively charged layered double hydroxide nanosheet respond[117] linearly and reversibly to *T* in the range of 396–353 K (see Fig. 13). These QDs can also be co-immobilized with other probes to achieve multiple sensing[118] and have also been used for *T* compensation in sensors.[119]

QDs normally exhibit lifetimes in the ns time regime, and the lifetime of core–shell QDs, for example CdSe–CdS–ZnS,[120] is strongly reduced at 300–500 K. If *T* increases from 300 to 433 K, the lifetime of the QDs decreases from 35 to 5 ns, respectively. QDs of the CdTe and of the CdSe type were used[121] for lifetime based thermal sensing in microfluidic devices. They exhibit high sensitivity and linear response in the range of 300–323 K. In addition, the *T* response sensitivity is strongly dependent on and is inversely proportional to the size of the QDs. The highest sensitivity was obtained using smallest size QDs. However, it should be mentioned that the small size QDs always have low QYs and short emission wavelength, which is not beneficial for their use *in vivo*.

A study[11] on the *T* dependence of the luminescence of QDs of the type CdTe, Mn^{2+}-doped ZnS (ZnS:Mn), and Mn^{2+}/Eu^{3+}-double-doped ZnS (ZnS:Mn,Eu) showed that their fluorescence intensity of CdTe QDs strongly and reversibly decreases with *T* in the range of 303–333 K, with a sensitivity of 1.1% K^{-1}.

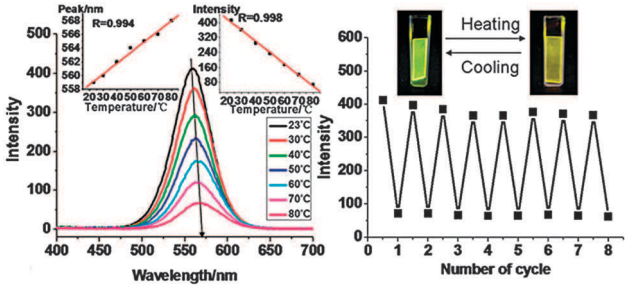

Fig. 13 The left panel depicts the luminescence spectra of the *T* sensitive $(CdTe\ QDs–LDH)_{30}$ QDs ultrathin film in the *T* range 296–353 K (inset: the emission position or intensity as a function of *T*, respectively). The right panel shows the reversible fluorescence response of eight consecutive cycles (the inset shows photographs of the ultrathin film at 296 and 353 K, respectively). (Reprinted with permission from ref. 117. Copyright Royal Society of Chemistry, 2013.)

However, *T*s of <400 K induce irreversible quenching, possibly due to decomposition. Uncapped ZnS:Mn nanoparticles also show linear and reversible response (between 303 and 423 K), which is accompanied by a shift of the emission spectra (0.05 nm K^{-1}). The double-doped nanoparticles (ZnS:Mn,Eu) respond differently in that both emission intensities (from Mn^{2+} and Eu^{3+}) decrease with increasing *T*. The ratio of the two intensities enables ratiometric measurement of *T*. Heat-induced luminescence *enhancement* was found for other doped nanoparticles including $ZnS:Eu^{3+}$ and $Y_2O_3:Eu^{3+}$. This was attributed to a heating process that possibly cures the defects on the nanoparticle surface and increases QYs.

Mn^{2+}-doped ZnSe QDs with different dopant concentrations undergo pronounced high-*T* dependent dual emission (Fig. 14, left panel).[30] Their luminescence results from two distinct but interconnected excited states. The respective intensity ratio shows a *T*-dependence with a resolution of 0.2 K. The *T* window can be tuned by changing the energy gap during nanocrystal growth. This unique combination of properties makes these nanocrystals a new class of intrinsic dual emitters that are highly attractive for ratiometric thermometry.

Other types of Mn^{2+}-doped QDs capable of ratiometric sensing of *T* (Fig. 14, right panel) have a core–shell structure

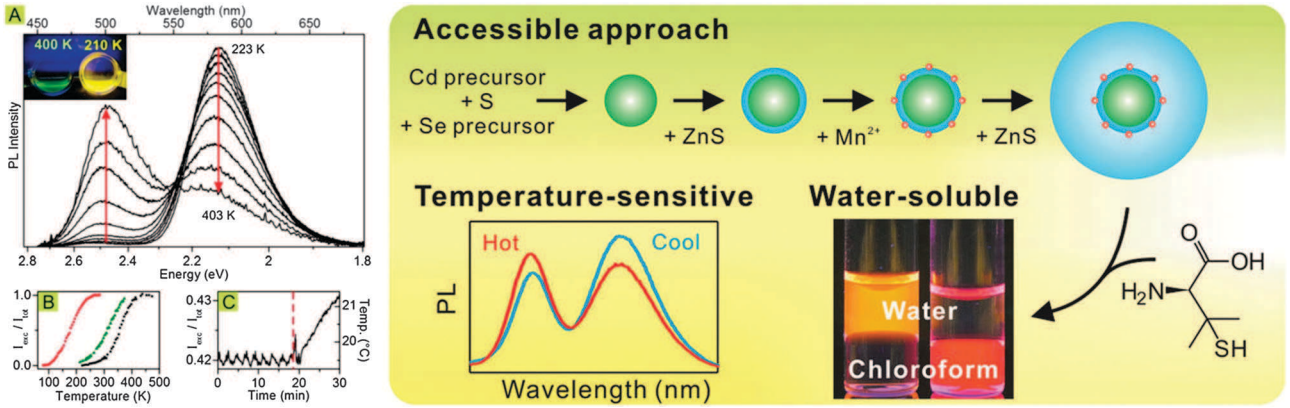

Fig. 14 *T*-dependence of the luminescence of Mn^{2+}-doped QDs for ratiometric *T* sensing. The exciton emission band at ~520 nm increases while the Mn^{2+} emission band at ~600 nm decreases with increasing *T*. (Reprinted with permission from ref. 30 and 122. Copyright American Chemical Society, Washington, DC, 2011.)

of the type CdSSe–ZnS, with the Mn^{2+} dopant residing in the shell.[122] The Mn^{2+} ions were sandwiched between an initial thin ZnS shell and a thicker protective ZnS shell. As the thickness of the ZnS shell increases, the exciton emission band (peaking at ~520 nm) is shortwave shifted, while the Mn^{2+} emission band (peaking at ~600 nm) is red-shifted. The relative intensity of the exciton emission decreases with increasing thickness of the ZnS shell. It is noteworthy that the chemical structure of these Mn^{2+}-doped QDs is different from those prepared by Vlaskin *et al.*,[30] but the *T* sensing mechanism is the same. The method of preparation enables the Mn^{2+}-doped QD structure to be varied at different stages. Therefore, not only its *T*-sensing properties for optical readouts can be tuned, but also the (ratiometric) response to *T* by varying the thickness of the ZnS shell and the concentration of the Mn^{2+} dopant. The precision is further improved by increasing the ZnS shell and dopant concentration. A resolution of 0.59 K is obtained in the range from 293 to 323 K. Citrate-capped $Zn_{1-x}Mn_xSe$–ZnS–CdS–ZnS nanocrystals with a diameter of 5 nm display intrinsic dual emissions at 520 and 600 nm.[123] They possess robust photo and thermal stability and attractive thermal sensitivity (0.83% K^{-1}) over a broad range from 133 to 373 K. The dual emission of QDs enables ratiometric measurement of *T*, and a precision of 0.15 K was obtained.

Mn^{2+} doped CdS–ZnS core–shell QDs are also found to possess a *T*-sensitive luminescence.[124] The doping location of Mn^{2+} can be controlled either at the interface between the CdS core and ZnS shell or in the ZnS shell. Results revealed that the dopant at the interface shows higher sensitivity (0.5% K^{-1} at 293 K). The *T* response is not influenced by surrounding chemical environment change (such as polarity, phase and pH). The sensor can be used to measure *T* in the range of 77–380 K.

QDs can be pumped to higher energy levels using two-photon excitation (2-PE), which cause less fluorescence background if NIR excitation sources are used. Maestro *et al.*[125] compared the effect of *T* on the emission of CdSe QDs under one-photon excitation (1-PE) and 2-PE. An increase in *T* causes a red shift of maximum intensity and, simultaneously, a reduction in the optical conversion efficiency that is independent of the excitation mechanism. However, with *T* increasing, the luminescence intensity decreases much more apparently under 2-PE than that under the 1-PE. This is attributed to the thermally induced effects on both the fluorescence QY and the 2-PE absorption cross-section. The different *T* dependencies caused by the two excitation mechanisms make CdSe QDs "dual thermal sensors" capable of sensing *T* by two complementary methods. The higher sensitivity under 2-PE leads to higher quality thermal images. These properties enable the acquisition of high quality thermal gradient images in fluids, and even to measure *T* in single cells.

Normally, QDs are synthesized using highly toxic elements such as Cd, Se, and Te. Low-toxic QDs of the type ZnS–$AgInS_2$ were synthesized[126] and studied with respect to their *T*-response between 293 and 353 K. The new QDs exhibited higher photostability than the commonly used CdSe–ZnS, and the *T*-sensitivity can reach 1% K^{-1}. In addition, oxygen does not quench their luminescence.

Clusters of CdSe QDs with an average diameter of 27 nm and made from 2–5 nm QDs were investigated with respect to the effect of *T* on their luminescence.[127] They exhibit a reversible response to *T* between 298 and 353 K in that intensity decreases with increasing *T*. The spectral maximum also undergoes a reversible red-shift upon heating the solution of the clusters.

QDs are widely used in solution, but also in immobilized form (in an inert host polymer), for example in the form of solid-state sensors films or particles. Rhee and Duong[128] in 2008 studied the response of CdSe–ZnS QDs to *T* in a modified silica host prepared from 3-glycidoxypropyl trimethoxysilane (GPTMS) and 3-aminopropyl trimethoxysilane (APTMS). This matrix prevents the QDs from forming large aggregates. The resulting sensing film displays a fluorescence whose intensity is responsive to *T* in the range from 273 to 373 K. The same QDs were immobilized in a highly *T*-resistant plain silica (SiO_2) matrix.[129] Their emission peak undergoes a red-shift upon increasing *T* from 295 to 525 K. The determination of the peak maximum under thermal cycling enables self-referenced continuous measurement of *T* with a sensitivity of 0.11 nm K^{-1}.

QDs with a CdSe–ZnS core–shell structure were immobilized[130] in a poly(lauryl methacrylate) matrix where they display a strong *T*-dependence of their luminescence intensity in the range of 100–315 K. In addition, the peak of the emission band undergoes a red shift of 20 nm over the same *T* range. The decrease in photoluminescence is linear (1.3% K^{-1}) and reversible at ambient *T*. However, the glass-transition *T* of the polymer limits its analytical range. This polymer may also show defects such as cracks at cryogenic *T*s. Anodized-aluminum,[131] in contrast, is a very stable support for QDs to construct a global sensor for imaging *T*. It covers the 100 to 500 K range.

An overview on quantum dots as sensors for *T* is given in Table 6. Notwithstanding these results, the use of QDs for sensing *T* is associated with problems such as limited long-term stability, undesired and unpredictably effects of surface chemistry, irreversible surface oxidation, loss of ligands, and small signal changes with *T*. There is still a large potential to improve these new fluorescent nanomaterials for purposes of sensing *T*.

4.2. Luminescent metal clusters

Nano-sized metal clusters can become luminescent with proper surface capping agents, because of the quantum confinement effect. These nanomaterials include luminescent gold nanoparticles,[132,133] luminescent silver nanoparticles,[134,135] luminescent gold(I)–silver(I) cluster complexes[136] and recently reported luminescent copper clusters.[87] Unfortunately, the *T* dependence of their luminescence properties was rarely studied. Copper clusters composed of five copper atoms (Cu_5) and strongly bound to three highly conjugated dianionic cationic ligands ($(EtNC(S)PPh_2NPPh_2C(S)NEt)^-$) possess a broad absorption band at below 450 nm, and their emission is centered at 660 nm in the solid state.[87] Unlike QDs, the copper cluster has a rather long lifetime (38.9 μs at 77 K and 490 ns at room *T*), and this enables lifetime imaging of *T* using time-gated devices. The QY and lifetime of the Cu_5 clusters are strongly influenced by *T* in the range of 228–353 K, so that *T* can be measured with a resolution of 0.1 K over a wide range. These clusters are also suitable for sensing *T* in the physiological range. However, they do not show good dispersibility in aqueous solutions, which limits their applications *in vivo*.

4.3. Photon upconverting (lanthanide) nanoparticles

Photon upconverting nanoparticles[137] (UCNPs) form another kind of luminophores for sensing *T*. Their emission peaks are at shorter wavelength than that of excitation (typically 850 to 980 nm) so that the autofluorescence from samples (if occurring at all) does not interfere. The UCNPs exhibit multiple and sharp emission peaks that depend on the lanthanide dopants. They possess obvious advantages in the field of *in vivo* imaging,[138] including excellent signal-to-noise ratio, good tissue penetration, lack of photobleaching, and no phototoxicity. Similar to the respective and much larger bulk luminophores described in the next section, UCNPs most often are prepared from a lanthanide-doped host material as the starting material. UCNPs can be photoexcited using near infrared (NIR) continuous-wave diode lasers (mostly operated at 980 nm). This is advantageous when compared with probes based on 2-PE, which requires pulsed (expensive) lasers.

Most of the UCNPs are of the type $NaYF_4:Yb^{3+}$, X (where X is a another trivalent lanthanide ion).[139] *T* exerts an individual effect on the intensity (but not spectral maximum) of each emission peak of UCNPs, but – unlike in the case of QDs – the particle size has no effect on the spectral maxima. The use of UCNPs for nanoscale thermometry has been highlighted.[26] Examples of new materials are given in Table 7. In this section, we focus on UCNPs with a size of <1 μm. Materials of larger size are treated in the section on bulk materials further below.

Discovered more than four decades ago,[139] systems doped with Er^{3+}, Yb^{3+} and Tm^{3+}, Yb^{3+} remain the key constituents for the majority of UCNPs with blue, green, red or NIR luminescence. In these systems, Yb^{3+} with its large absorption cross-section in the NIR usually acts as a photosensitizer to overcome the small absorption cross sections of Er^{3+} or Tm^{3+} ions. The UC efficiency of rare earth oxides is still low because of the high phonon energies of the host matrix employed.

Table 6 Composition, emission maxima (in nm), optical parameters, particle sizes (in nm), sensitivities (in K^{-1}) and working ranges (in K) of quantum dot (QD)-based nanothermometers

QDs	Matrix	λ_{em} [a]	Spectral parameter	Size	Sensitivity	Range	Ref.
CdSe	SiO_2 NPs	535	Peak shift	4.2	0.095 nm	303–373	118
CdTe	Layered double hydroxides	558	Intensity	2.7	−1.47%	296–353	117
CdSe	Aqueous solution	650	Lifetime	4.0	−0.08%	300–323	121
CdTe	Aqueous solution	510	Lifetime	1.0	−0.17%	300–323	121
CdTe	Solution	518	Intensity		−1.1%	303–333	11
$ZnS:Mn^{2+}$	Solution	589	Intensity	10	−0.5%	303–423	11
$ZnS:Mn^{2+}$, Eu^{2+}	Solution	595, 611	Intensity	5	—	303–423	11
CdSe–ZnS	Poly(lauryl methacrylate)	590	Intensity	4.8–5.5	−1.3%	100–315	130
$CdSSe–ZnS:Mn^{2+}$	Aqueous solution	520, 600	Intensity ratiometric	~11	−0.4%	293–323	122
$Zn_{1-x}Mn_xSe–ZnS–CdS–ZnS$	Toluene or water	520, 600	Intensity ratiometric	~5	−0.83%	133–373	123
$CdS–Zn:Mn^{2+}$	Solution or in poly(methyl methacrylate)	600, 650	Intensity ratiometric	~7.8	−0.5%	77–380	124
CdSe cluster	Aggregations of 2–5 nm QDs	560	Intensity	~27	—	298–353	127
CdSe–ZnS	Ormosils[b]	600	Intensity	—	−0.7%	273–373	128
CdSe–ZnS	SiO_2	606	Peak shift	3–4	0.11 nm	295–525	129
$ZnS–AgInS_2$	Dried state	533	Intensity	—	−1%	293–353	126

[a] Maximum peak position at room *T*. [b] Ormosil = organically modified silicate.

Table 7 Composition of typical UCNP-based nanothermometers, particles sizes, spectral data, and useful *T* ranges. The arrows indicate the direction of the change in intensity with increasing *T*

Host	Dopant ions	λ_{em}/nm	Excitation density[a]	Particle size/nm	Temperature range/K	Ref.
Al_2O_3	Yb^{3+}, Er^{3+}, Mo^{3+}	522↑, 546↓	20 W cm^{-2}	57	295–973	140
$LiNbO_3$	Yb^{3+}, Er^{3+}	530↓, 550↑	0.6 W	160	285–453	141
$NaYF_4$	Yb^{3+}, Tm^{3+}	475↓, 695↓	3–4 W	26–30	293–333	142
$NaYF_4$	Yb^{3+}, Er^{3+}	541↓, 656↓	3–4 W	26–34	293–333	142, 143
$NaYF_4$	Yb^{3+}, Ho^{3+}	541↓, 656↓	3–4 W	26–30	293–333	142
$NaYF_4$	Nb^{3+}	863↑, 870↑	0.5 W	25	273–423	144
CaF_2	Yb^{3+}, Tm^{3+}	790↑, 800↑	100 fs laser	11	298–323	145
$KZnF_3$	Yb^{3+}, Mn^{2+}	585↓	0.5 W cm^{-2}	~200	300–573	146

[a] Typically, NIR lasers with wavelengths of 760–980 nm are employed.

$NaYF_4$ is a preferred host matrix because of its low phonon energy, and it is the most widely used for synthesizing UCNPs with rare-earth dopants. Vetrone *et al.*[147] synthesized UCNPs of the type $NaYF_4$:Er^{3+}, Yb^{3+} and used them for measuring *T* inside a cell. This is the first paper on intracellular sensing of *T* using UCNPs, and the measurement resolution can reach 0.5 K. A more recent article[142] reports on a study on the *T*-dependence of the luminescence of various UCNPs of the type $NaYF_4$:Yb^{3+},X (X = Er^{3+}, Ho^{3+} and Tm^{3+}). It was found that the *T*-response of these UCNPs is strongly dependent on the dopants and also on the crystal type. The UCNPs of the type $NaYF_4$:Yb^{3+}, Er^{3+} in the hexagonal phase are a good choice for *T* measurements in the physiologically important range (293–318 K), because of their brightness and their excellent *T* resolution of 0.45 K. By contrast, the *T* resolution of Ho^{3+} and Tm^{3+} doped $NaYF_4$ UCNPs is less good. Similarly, the ratio of the luminescence intensities at 863 and 870 nm of Nd^{3+} doped $NaYF_4$ UCNPs[144] strongly depends on *T* and is governed by the Boltzmann law. The sensor works in the *T* range of 273–423 K, and is beneficial for deeper tissue penetration because of the two emissions in the NIR. However, their sensitivity is much lower than the UCNPs of the type $NaYF_4$:Yb^{3+}, Er^{3+}.

The sensitivity of these UCNPs can be further improved by exploring the FRET between UC emission and Rhodamine 6G.[148] Rhodamine 6G can efficiently absorb the green UC emission of $NaYF_4$:Er^{3+}, Yb^{3+} in the region of 525–560 nm, and give a separate emission peak centered at 575 nm. Since Rhodamine 6G is more sensitive to *T* than the UC emission, the ratio between Rhodamine emission and the UC emission offers higher sensitivity than that of the solely UC emissions. The average temperature sensitivity is estimated to be 1% K^{-1} over the whole physiological temperature range (298–318 K) and 2.7% K^{-1} in the higher-temperature region (320–330 K).

Nanocrystalline Er^{3+}–Mo^{3+}:$Yb_2Ti_2O_7$ phosphors were prepared[149] by a sol–gel method and used as optical thermometers. The Mo^{3+} co-doping enhances intensities such as the $^2H_{11/2} \rightarrow {}^4I_{15/2}$ transition (at 522 nm) that increases with *T*, while that of the $^4S_{3/2} \rightarrow {}^4I_{15/2}$ transition (at 554 nm) decreases. The fluorescence intensity ratio of the two green emission bands increases from 0.90 to 3.05 upon increasing *T* from 290 to 610 K. The maximum sensitivity (slope) is 0.74% K^{-1}, and the resolution is 0.1 K. The same group[150] prepared UCNPs of the type Er^{3+}–Yb^{3+}–Mo^{3+}:Al_2O_3 and observed an extraordinary enhancement (compared to the UCNPs synthesized without Mo^{3+}) of green UC emissions under 976 nm laser diode excitation. The measurement of the intensity ratio of the two green emissions of this material enables *T* to be determined with a resolution of 0.3 K in the range of 294–973 K. Similarly, Tm^{3+}–Yb^{3+}–Mo^{3+} dopants in oxidic matrix materials of the type Al_2O_3, TiO_2, Gd_2O_3 or $Yb_3Al_5O_{12}$ cause an enhancement of UC efficiency.[140] A further enhancement by four orders of magnitude relative to Er^{3+}–Yb^{3+} and Tm^{3+}–Yb^{3+} oxides without Mo^{3+} doping was reported.[140] Among these UCNPs, the $Yb_3Al_5O_{12}$ matrix doped with Er^{3+} and Mo^{3+} has the best response to *T* and works well between 295 and 973 K. The resolution can reach 0.3 K at an excitation power of 2 mW. All these results suggest that the Mo^{3+} co-doped UCNPs with high green UC emissions efficiency are very promising materials for optical sensing of *T*. The Tm^{3+}–Yb^{3+} doped CaF_2 UCNPs with an average size of 11 nm exhibit remarkable strong Tm^{3+} ion emission at around 800 nm.[145] The UCNPs can be excited using 920 nm pulsed laser and enable deep tissue imaging of *T* with a penetration depth as large as 2 mm. The material is biocompatible and can be used for *in vivo* imaging of *T* with high penetration depth.

A host made from $LiNbO_3$ and doped with Er^{3+} and Yb^{3+} ions[141] resulted in UCNPs with an average size of 160 nm, and a response to *T* in the range from 285 to 453 K. The sensitivity is 0.7% K^{-1} at physiological *T*s, but the maximum sensitivity (1.4% K^{-1}) was obtained at 623 K.

Rare earth doped UCNPs show fixed and very sharp emission peaks. It is very difficult to get a broad UC emission band. Compared with the f–f transitions of rare earth ions, the d–d transitions of transition metal (TM) ions are much more sensitive to the local environment, the emission can be easily tuned by changing the chemical composition. Mn^{2+} doped perovskite nanocrystals $KZnF_3$:Yb^{3+}, Mn^{2+} show intense yellow upconversion emission upon excitation with a 976 nm laser diode.[146] This broad yellow luminescence band is centered at 585 nm and identified as the $^4T_{1g}(G) \rightarrow {}^6A_{1g}(S)$ transition of Mn^{2+}. The emission is sensitive to *T*, which enables *T* measurement in the range of 300–573 K. The response is fully reversible, but the response curve is not linear. In addition, unlike the rare earth doped UCNPs, the TM doped UCNPs only showed a single broad emission peak, which is not possible to achieve an

intrinsically referenced ratiometric measurement. However, the thermo-quenching effect is more profound than that of the rare earth doped UCNPs. Co-doping of rare earth and TE ions in such crystals may pave a new way for ratiometric sensing of T with much larger sensitivity.

4.4. Other lanthanide-doped inorganic nanoparticles

Obviously, lanthanide doped nanoparticles can be excited by conventional 1-PE at short wavelengths, typically at below 400 nm. If 30 nm YAG:Ce^{3+} nanophosphors are photoexcited at 346 nm, their decay time varies over the T range from 280 to 350 K.[151] The T dependent change in the lifetime of the 550 nm emission is approximately 150 ps K^{-1}. There is a linear relationship between the luminescence lifetime and T in the range of 298–313 K. The nanomaterial undergoes a 33% variation (from 18 to 27 ns) in lifetime upon increasing T from 280 to 350 K, with nominal lifetimes in the range of ~20 ns. However, the need for UV excitation compromises the utility of these materials.

4.5. Dye-doped nanoparticles

The encapsulation of luminescent dyes into nanoparticles is a straightforward way to prepare T-sensitive nanomaterials. Among the various techniques, the precipitation method is the simplest and easiest way to prepare nano-sized T sensors.[74] Typically, the probe and the host material (such as a polymer) are dissolved in an organic solvent to form a homogeneous solution. Then, another solvent, in which both the probe and the host material do not have good solubility (typically water), is added. The host material is precipitated and the probes are encapsulated inside the precipitant simultaneously. This method is applicable, in principle, to all kinds of luminescent probes for T, for example,[152] to the probes $Eu(TTA)_3$(dpbt) and $Ir(Cs)_2$(acac) in a gas-blocking copolymer. Similarly, reversible T nanosensors for visual (bare-eye) read-out were reported.[29] Two dyes of different color were incorporated in poly(vinylidene chloride-*co*-acrylonitrile) nanoparticles (85 nm). The first (a blue reference dye) is not sensitive to T in the 278–323 K range, whilst the second (a red-emitting Eu^{3+}-probe) is very sensitive. The mixture of the two colors in different intensity ratios results in distinct colors at various Ts. The nanosensors undergo a reversible response and enable both rapid colorimetric T estimation with the bare eye and quantitative two-dimensional thermo-imaging using the RIM method for imaging (see Section 2). Heat-exchange induced fluid motion was, for the first time, rapidly imaged by just taking color pictures, and good temporal and spatial resolution was accomplished when studying heat-driven hydrodynamics (Fig. 15). Such nanosensors are useful in micro/nanoscale research and also for the fabrication of sensor films for macroscopic study.

T-sensitive nanoparticles with a size of 20–30 nm were obtained[107] by incorporation of the probe Eu-DT in a silica coated hybrid matrix consisting of 2-bis(trimethoxysilyl)decane and poly(methyl methacrylate). Unlike many other lanthanide-based sensors (that require UV-excitation), these nanosensors can be excited using blue LEDs (405 nm). The incorporation of

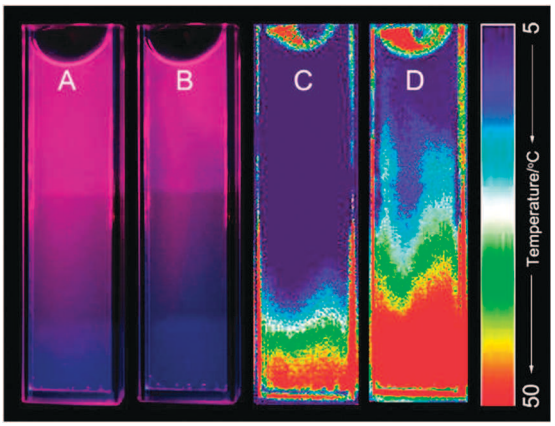

Fig. 15 Colorimetric sensing and imaging of T using nanoparticles made from (vinylidene dichloride)-*co*-(acrylonitrile) and doped with the probe $Eu(benzac)_3$(phen) and a blue reference dye. The heat-induced fluid convection can be imaged using a photographic technique.[153] (Reprinted with permission from ref. 29. Copyright American Chemical Society, Washington, DC, 2010.)

Eu-DT into nanoparticles also enhances their photostability. They display a strong T dependency on both fluorescence intensity and lifetime over the physiological range (298–318 K) and a resolution of typically 0.3 K. The hybrid nanomaterials were also doped[102] with the probe Tb-THBA to perform lifetime-based sensing of T, and with Eu-DT along with a green-emitting reference dye for ratiometric signal generation.[108] Brites *et al.*[154] incorporated both a Eu^{3+} and a Tb^{3+} probe into organic–inorganic hybrid magnetic nanoclusters of 100–400 nm in size. These were formed from a maghemite (γ-Fe_2O_3) magnetic core and coated with an orthosilicate/aminopropyltriethoxysilane organosilica shell. The resulting luminescent nanothermometers allow absolute T to be determined in the range from 10 to 350 K, with a sensitivity of maximally up to 4.9% K^{-1}. Their working range can be flexibly tuned by varying the ratio of the Eu^{3+} and Tb^{3+} complexes. Photo-excitation occurs at 357 nm.

The tris(bipyridine)ruthenium(II) complex was doped[80] into silica NPs with a size of 130 nm. In this approach, the dye is placed in the outer shell of the particles where it maintains the photophysical properties of its dissolved form. The silica shell additionally hinders the probe from undergoing oxygen quenching or being influenced by anionic quenchers. The NPs work in the 293–333 K range with a linear decrease in signal with rising T. However, these nanosensors suffer from a slight decrease in signal upon repeated cycling.

The triarylboron compounds mentioned in Section 3.1 were used to prepare T-sensitive microcapsules.[155] The probe 1,1′-(6,6′-((2,4,6-triisopropylphenyl)boranediyl) bis(pyrene-6,1-diyl)-dipyrrolidine) was first dissolved in tetrahydronaphthalene containing 5% of polystyrene. Droplets of this solution were coated with cross-linked poly(urea-formaldehyde) as a shell material to form the microcapsules. The microsensors undergo a visible color change from orange towards green on rising T from 243 to 413 K. These microcapsules can also be used for referenced dual wavelength read-out. Thereby the fluorescence emission ratio of 530/650 nm can be used to determine T.

The calibration plot is linear in the range from 303 to 413 K, and the sensitivity is 0.059% K^{-1}.

4.6. Thermo-responsive organic (nano)gels

Poly(*N*-isopropylacrylamide) (PNIPAM) is a thermo-responsive polymer that undergoes a phase transition in aqueous solution at ~305 K. Below this *T*, the polymer is in a fully swollen state and has a flexible and loose structure. At *T*s above the phase transition, the polymer becomes coiled and forms colloidal nanoparticles smaller than 100 nm. The core of the resulting nanoparticles is relatively hydrophobic. Thus, the fluorescence of a labeled polymer backbone will be altered due to the phase transition. The phase transition is in the physiological *T* range. Probes with suitable spectral features, such as NIR probes, can be easily attached to this kind of polymer, which then can extend the flexibility of this approach for sensing *T in vivo*. The properties of selected fluorophore-labeled PNIPAM nanogels are summarized in Table 8.

The copolymerization of 4-(4-dimethylaminostyryl)pyridine (a hemicyanine dye; HC) with NIPAM yields a copolymer [poly(NIPAM-*co*-HC)] which, dissolved in water, displays weak fluorescence if *T* is <298 K, but a strong fluorescence if *T* rises to 298 K or higher.[156] Saturation occurs at >313 K. Thus, the material enables the determination of *T* between 298 and 313 K. The fluorescence enhancement is driven by a heat-induced phase transition of the polymer from a coiled to a globular state. The HC unit exists in the non-fluorescent benzenoid form within the coil state of the polymer. The less polar domain formed inside the globular state of the polymer leads to a transformation of the HC into the fluorescent quinoid form. This results in a heat-induced fluorescence enhancement. The fluorescence intensity measured at 313 K is more than 20-fold higher than the intensity at <298 K. All changes are fully reversible. A related material, with HC being replaced by BODIPY, yields a *T*-sensitive co-polymer for the 296 to 308 K range.[157]

The co-polymerizations of various benzofurazans with NIPAM led to five new *T*-responsive co-polymers.[158] They undergo a *T*-induced phase transition at ~305 K in water. The fluorescence intensities of the copolymers concurrently increase with *T*. In the case of the co-polymer of 4-*N*-(2-acryloyloxyethyl)-*N*-methylamino-7-*N*,*N*-dimethylaminosulfonyl-2,1,3-benzoxadiazole (DBD-AE) and NIPAM, the fluorescence intensity at 310 K is 13.3-fold higher than that at 302 K. The *T*-sensitive range of these fluorescent thermometers can be changed by replacing the NIPAM units by *N*-isopropylmethacrylamide or *N*-propylacrylamide units. The response of these fluorescent thermometers assumed to result from a decrease in the micropolarity near the main chains of the copolymers. The responses are reversible and exactly repeatable over at least 10 cycles of heating and cooling. These co-polymers can sense changes in *T* in aqueous solution within the ranges of 318–327, 302–310, and 291–297 K, respectively.

The same group[159] studied the *T*-dependent fluorescence lifetime of a copolymer of NIPAM and the an environmentally sensitive fluorescent benzoxadiazole monomer (DBD-AA). The average fluorescence lifetime of poly(NIPAM-*co*-DBD-AA) in aqueous solution increased sharply (from 4.2 to 14.1 ns) as the *T* changed from 303 to 308 K. This was attributed to a decrease in the local polarity around the fluorescent DBD-AA units and to the loss of hydrogen bonding between the DBD-AA units and water. Since fluorescence lifetime imaging is independent of the luminophore concentration, the method enabled thermal mapping of small spaces such as microchannels and living cells with very high sensitivity (a 27% change in fluorescence lifetime per 1 K).

A copolymer prepared from DBD-AE and NIPAM exhibits an even higher sensitivity[17] but has a multiexponential fluorescence decay in aqueous solution. The average lifetime of this highly sensitive probe increases from 3.0 ns to 13.5 ns between 296 and 311.3 K. The phase transition causes the fluorophore to be displaced from an aqueous environment (where it has a fluorescence lifetime of ~2 ns) to a hydrophobic environment (with lifetimes of ~15 ns). The copolymer was used for studying spatial variations of microfluidic *T* using fluorescence lifetime imaging microscopy (FLIM). Resolution was better than 0.1 K (Fig. 16). The good water solubility of the copolymer and its response at physiological *T*s make it particularly useful as a FLIM probe in lab-on-a-chip devices and for biomedical applications, where precise control of *T* is crucial.

A sulfonated poly-NIPAM containing DBD-AA units was prepared[160,161] (Fig. 17) for use in intracellular imaging of *T*. The sulfate groups create a highly hydrophilic surface, which prevents the precipitation of this nanogel even at high ionic

Table 8 Fluorophore-labeled polymeric nanogels for sensing *T*

Name	Working range (K)	Exc./Em. (nm)	Comments	Ref.
Poly(NIPAM-*co*-HC)	298–313	510/580	20-fold fluorescence enhancement at higher *T*; reversible; pH insensitive (2–12)	156
Poly(NIPAM-*co*-BODIPY)	296–308	490/600	Fluorescence enhanced about 8-fold at high *T*; reversible	157
Poly(NIPMAM-*co*-DBD-AE)	318–327	444/556	Reversible; tunable *T* sensing range; high sensitivity; many other polymers synthesized and studied	158
Poly(NIPAM-*co*-DBD-AE)	302–310	444/563		
Poly(NNPAM-*co*-DBD-AE)	291–297	444/566		
Poly(NIPAM-*co*-DBD-AA)	303–308	444/560	Used for fluorescence lifetime imaging; lifetime changes from 4.2 to 14.1 ns; fully reversible	159
Poly(NIPAM-*co*-DBD-AE)	296–312	444/563	Used for fluorescence lifetime imaging; lifetime changes from 3.0 to 13 ns; fully reversible; non-linear calibration curve; resolution <0.1 K	17
Poly(NIPAM-*co*-DBD-AA-*co*-FPA)	300–306	444/560	The introduction of the sulfo group improves the stability of the nanogel in biological media; sharp *T* response; suitable for *in vivo* studies; good *T* resolution (0.18–0.58 K); suitable for fluorescence lifetime based imaging	160, 161

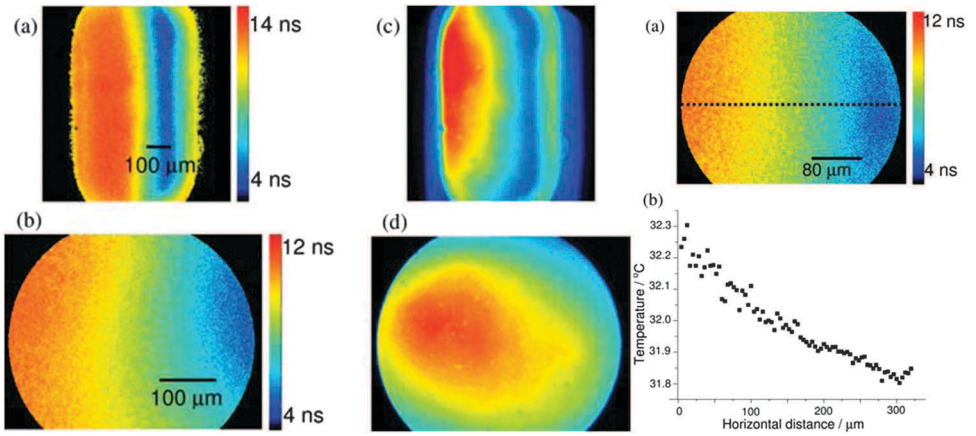

Fig. 16 FLIM based thermo-imaging using the fluorescently labeled hydrogel poly(NIPAM-*co*-DBD-AE). (Reprinted with permission from ref. 17. Copyright Royal Society of Chemistry, 2010.)

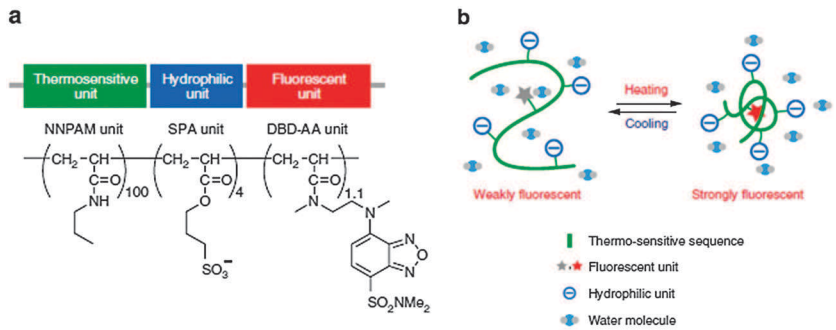

Fig. 17 Chemical structure of the sulfonated *T*-responsive poly(NIPAM-*co*-DBD-AA-*co*-SPA) nanogel. (Reprinted with permission from ref. 160. Copyright Nature Publication Group, 2009.)

strengths and its deposition on the cytoplasmic membrane. The fluorescence response of the material to *T* is independent of environmental pH, ionic strength, and even surrounding proteins. The nanogels were delivered inside COS7 cells by microinjection and were shown to be capable of monitoring the heat generated by external chemical stimuli. The fluorescence of the nanogels sharply changed between 300 and 306 K in COS7 cells. The use of FLIM pushes the spatial and *T* resolution of nanothermometry to the diffraction limited level (200 nm) and 0.18–0.58 K, respectively.[160] In addition, the photostability of this nanogel can be enhanced by a factor of 10 *via* replacing an oxygen atom in the fluorescence unit with a sulphur or selenium atom.[162]

Poly-NIPAM was also labeled[163] with 3-hydroxyflavone (3-HF) to obtain another optical sensor material for *T*. The probe 3-HF displays dual-band emissions that are associated with (a) a normal excited state intramolecular charge transfer (denoted as ESICT), and (b) a tautomer excited state intramolecular proton transfer (denoted as ESIPT). In polar and aprotic solvents, 3-HF displays a greenish fluorescence emission originating from the coupled ESICT/ESIPT processes (Fig. 18). The ESIPT is suppressed in highly polar, protic solvents, and this results in strong blue fluorescence. With increasing *T*, the fluorescence of the material changes from a bluish to a greenish color, thus providing sensitive and reversible response to *T* in the range of 306–314 K, and making it suitable for intracellular thermo-imaging. The dual emission from these nanothermometers enables self-referenced ratiometric *T* measurement.

A thermo-responsive material with a sharp transition was obtained from NIPAM and an ionic liquid. It forms nanoparticles after the addition of a fluorescent benzothiazole due to hydrophilic/hydrophobic and electrostatic interactions.[164] The fluorescence of these nanoparticles is strongly dependent on pH and *T*. Its intensity is 50-fold enhanced if the pH is increased from 7 to 10, and it is effectively doubled within 1 K around its lower critical solution *T* (309 K) in solution of pH 9. The response to *T* is reversible over more than five cycles. These nanoparticles are intended for medical uses, because of the sharp signal enhancement at around 309 K. However, fluorescence is cross-sensitive to pH and requires UV excitation.

Ultra-bright single-nanoparticle *T*-sensitive polymer dots (PDs) were obtained *via* the precipitation. RhB was chemically linked to polystyrene and blended with the semiconducting polymer (either poly[(9,9-dioctylfluorenyl-2,7-diyl)-*co*-(1,4-benzo-2,1′,3-thiadiazole)] (PFBT) or poly-[(9,9-dioctyl-2,7-divinylene-fluorenylene)-*alt*-*co*-(2-methoxy-5-(2-ethylhexyloxy)-1,4-phenylene)] (PFPV)). The fluorescence intensity of the PDs decreases with increasing *T*. Under excitation at 450 nm, the labeled PDs exhibit dual

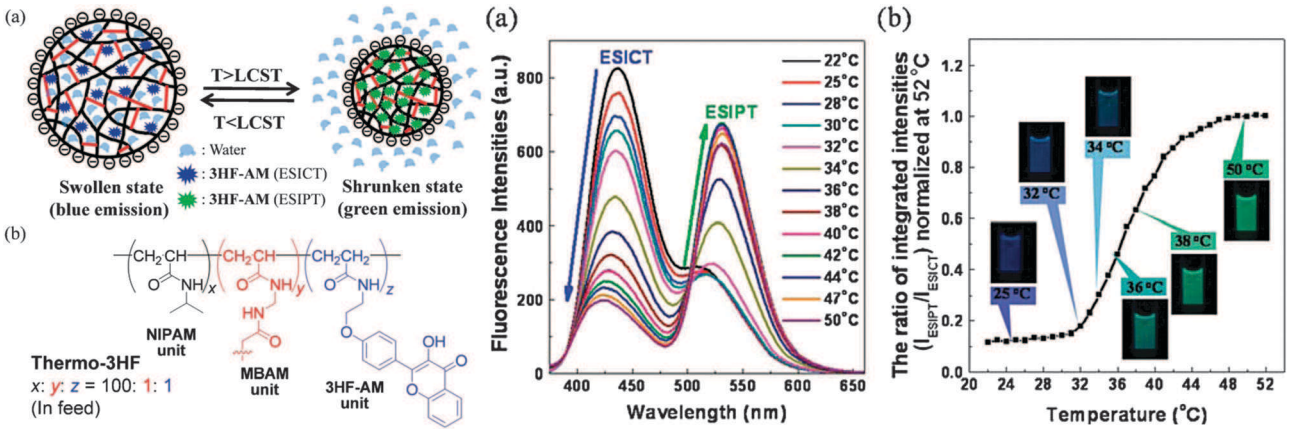

Fig. 18 Ratiometric sensing of *T* using poly-NIPAM labeled with 3-hydroxyflavone. (Reprinted with permission from ref. 163. Copyright Royal Society of Chemistry, 2011.)

emissions with peaks at 510 and 570 nm, and this enables ratiometric read-out. The two peaks are assigned to the emissions of the conjugated polymer and the RhB. There is a linear response in the range between 283 and 333 K. The PDs were further employed for measurement of *T* in living cells.[43] The size of PDs was tuned from 22 to 160 nm by varying the nanoscale precipitation conditions, the molecular weight or type of semiconducting polymer, or the amount of polystyrene–RhB blended into the PDs.

Other organic gel-based nanosensors were obtained[165] by coating luminescent silver nanoparticles with a hybrid nanogel composed of poly(ethylene glycol) and hyaluronic acid (PEG-HA). *T* induces shrinking of the hydrogel shell that leads to enhancement of luminescence intensity of the emissions in the Ag–Au@PEG-HA hybrid nanogels. The enhancement of the intensity was attributed to an increase in the local refractive index, and the reduction of the number of surface defects of the noble metal nanoparticles. These nanosensors work fully reversibly in the *T* range of 278–323 K. However, the luminescence has to be excited in the UV range (~334 nm), which limits their applicability to biological systems. Another smart hydrogel[166] exhibits linear and reversible thermo-response in the 283–323 K range. It consists of Eu(III)-doped poly(styrene-*co*-NIPAM)–poly-NIPAM in the form of core–shell nanoparticles. Upon increasing *T*, the nanoparticles shrink (from ~500 to ~300 nm) and induce the Eu(III) phthalate loaded into the PNIPAM chains to get closer. This leads to a decrease in the intensity of the emission of the Eu(III) phthalate complex. However, the luminescence of the material appears to be weak.

5. Bulk materials

Bulk materials, unlike nanomaterials, possess comparatively large structures and morphology, and lack any effects that are inherent to nanomaterials only. They can be shaped as films, rods, planar glasses, fibers, and the like. This chapter is subdivided into sections on *T*-sensitive inorganic bulk materials, lanthanide-doped bulk materials, upconversion bulk materials, and (organic) bulky polymer materials.

5.1. Inorganic luminescent phosphors for sensing temperature

Fiber optic *T* sensors were developed quite some time ago using phosphors[167] such as (ZnS):Cu; (ZnS):Al, Ag, Cu; (ZnCd)S:Ag; (ZnCd)S:Cu, Al, Ag; $(ZnS_{0.8}CdS_{0.2})$:Ag, Cu; $(ZnS_{0.7}CdS_{0.3})$:Al, Cu; $(ZnS_{0.5}CdS_{0.5})$:Cu; $(ZnS_{0.2}CdS_{0.8})$:Ag, Al. These are commonly used as color correctors in TV picture tubes. The decay time of the luminescence is a function of *T*, and this enables measurement of *T* in high-voltage machines. Among these phosphors, (ZnCd)S:Ag offers strong luminescence and long lifetime (12 ms at 263 K), and its *T* response possesses the highest sensitivity. The fiber optic *T* sensor using (ZnCd)S:Ag works well in the range of 263–423 K with an accuracy of ±1 K.

5.2. Lanthanide-doped bulk materials

The luminescence of inorganic bulk materials doped with Eu^{3+} and Tb^{3+} is very sensitive to *T*. Such materials can be excited using UV light and this results in a sharp emission band at 611 nm, which corresponds to the $^5D_0 \rightarrow {}^7F_2$ transition. The decay time of the luminescence of $La_{1.92}Eu_{0.08}Zr_2O_7$ and $La_{1.92}Eu_{0.08}Hf_2O_7$, if photoexcited at 337 nm, varies[168] with *T* in the range of 700–1100 K. The host Sr_2CeO_4 doped with various Eu^{3+} concentrations also undergoes thermal quenching and this was used[169] for sensing low *T*s (273–523 K). The decay time of Y_2O_3:Eu (4.52% w/w) and YAG:Tb (5% w/w) drops from 1000 to 0.4 μs on going from 823 to 1273 K.[20] The accuracy is ±5%. Y_2O_3:Eu is said to be better suited for turbine engine applications because its emission at elevated *T*s is stronger than that of YAG:Tb. Phosphorescent inorganic materials of the type Gd_2O_2S:Tb and Mg_4FGeO_6:Mn exhibit good (and reversible) response to *T* and are resistant to oxidizing and reducing environments.[170] The phosphors provide complementary *T* sensitivity in that Gd_2O_2S:Tb is more suitable for *T*s from 303 to 453 K, while $Mg_4(F)GeO_6$:Mn works best from 473 to 923 K.

Y_2O_3 is quite stable even at high *T*s and thus a viable hosting material for lanthanide doping. In a systematical study on the *T* dependency of the luminescence of Y_2O_3:Eu (6% Eu), Y_2O_3:Tb (4% Tb) and Y_2O_3:Tm (1% Tm),[28] microparticles with an

average size of 1.5 μm were prepared and shown to be present in a monoclinic phase and a cubic phase. Their fluorescence spectra vary with the phase. Under UV excitation, Y_2O_3:Eu phosphors with both phases give sharp and strong emission. The emission intensities vary uniquely with elevating *T* due to the change in absorption and the thermal quenching effect. The decay time of the Y_2O_3:Eu phosphors was also found to be sensitive to *T*.[171] The emission intensities of the Y_2O_3:Tb phosphors, in contrast, became weaker at elevated *T*, especially those of the cubic phase at above 650 K. In addition, the intensity ratios of the peak emissions undergo rather small variations with *T* so that their resolutions are quite poor. The Y_2O_3:Tm phosphors display another behavior in that only a few sharp emission peaks are obtained whose intensities are hardly affected at ~1200 K. Even worse, the intensity ratios are almost constant between 300 and 1300 K. Consequently, Y_2O_3:Tb and Y_2O_3:Tm cannot be read out by the intensity ratio method.

A luminescent mixed lanthanide metal–organic framework (MOF) $Eu_{0.0069}Tb_{0.9931}$-DMBDC (DMBDC = 2,5-dimethoxy-1,4-benzenedicarboxylate) has dual emission from Tb^{3+} at 545 nm and Eu^{3+} at 613 nm while excited using 488 nm laser.[172] The whole MOF structure acted as a sensitizer for the doped lanthanide ions. The two emissions have abnormal response to *T*, the Tb^{3+} emission decreases when *T* increases, but the Eu^{3+} emission increases. The opposite response of the dual emission of $Eu_{0.0069}Tb_{0.9931}$-DMBDC enables self-referenced sensing of *T* in the range of 50–200 K. In addition, the material displayed different colors at different *T*s (green color at low *T*; red color at high *T*), and can be read out with bare eyes. The authors also compared the MOF with a single lanthanide dopant, and observed that the luminescence intensity decreases with increasing *T* for either the Tb^{3+} or Eu^{3+} doped MOF.

A fiber optic sensor based on Yb^{3+}-doped silica was reported to be capable of sensing *T* in the range of 303–883 K with a resolution of ±1 K.[173] Another optical fiber sensor uses an Nd^{3+}-doped silica fiber and works over the 223–1773 K range.[174] Its resolution (~2.5 K) was improved to ~1.3 K (ref. 175) *via* annealing the Nd^{3+}-doped silica fiber at 1023 K for 100 h. An oxyfluoroborate glass is doped with Sm^{3+}, the material can be used for ratiometric luminescent monitoring of *T* up to 500 K with a (moderate) sensitivity of 0.00126% K^{-1} at room *T*.[176] The YAG:Dy^{3+} phosphor can be excited with a 355 nm Nd:YAG laser to give emissions peaking at 458 and 493 nm.[21] The intensity ratios correlate well with *T* in the relatively wide range of 300–1500 K. YAG:Dy was doped in a $(ZrO_2)_{1-x}$–$(Y_2O_3)_x$ (named YSZ) matrix, and was capable of sensing *T* between 773 and 1673 K.[177] The lifetime of Ga-substituted YAG:Ce materials ($(Y_{1-x}Ce_x)_3Al_{2.5}Ga_{2.5}O_{12}$; where x = 0.1 and 0.2) was also found to change over the 293–393 K range.[178] The substitution of Ga^{3+} by Al^{3+} causes the luminescence lifetime of Ce^{3+} to be quenched at much lower *T*s compared to YAG. This is attributed to the non-radiative transitions of the material and makes the material suitable for sensing room *T*s.

The luminescence decay time of the chromium(III)-doped yttrium aluminum borate (YAB) phosphor was found[179] to be highly sensitive to *T*. The material can be excited in blue (422 nm) and red (600 nm) parts of the spectrum, and emits very bright luminescence in NIR. Its brightness is comparable to that of a well-known lamp phosphor, a Mn^{4+}-doped magnesium fluorogermanate. Luminescent decay time decreases with rising *T* with a slope of about 1% K^{-1} in the range of 253–343 K. The phosphor has good chemical and photochemical stabilities and no cross-sensitivity to oxygen. Its long lifetime (237 μs at 274 K) enables imaging of *T* using time-gated devices. The same group encapsulated $Eu(TTA)_3$ and $Gd(TTA)_3$ into an acridone–polystyrene matrix to form ultra-thin (250 nm) sensing layers for *T*.[180] The acridone in the polymer acts as an antenna to capture excitation energy and transfers the energy to the luminescent lanthanide complex. The luminescence of the $Eu(TTA)_3$ doped sensing layer is only slightly affected by oxygen but highly sensitive to *T* in the physiological range (293–313 K). The $Gd(TTA)_3$ has long phosphorescence lifetime (up to 1 ms) and is very sensitive to oxygen. The co-immobilization of both luminophores in the acridone–polystyrene polymer enables dual sensing of *T* and oxygen simultaneously.

5.3. Lanthanide-doped upconversion bulk materials

These represent a rather important class of materials as can be seen in Table 9. They are prepared by doping lanthanide ions (typically Er^{3+}, Yb^{3+}, Tm^{3+}) in host crystals or glasses. The hosting material (such as $NaYF_4$) is always co-doped with Yb^{3+}, which has a larger absorption cross-section at NIR wavelengths. Yb^{3+} acts as a good photosensitizer. This co-doping overcomes difficulties associated with the rather smaller absorption cross-section of Er^{3+} or Tm^{3+} due to the dipole-forbidden nature of intra-4f transitions. After annealing at around 673 K, they display strong UC luminescence under NIR cw laser excitation. They are suitable for high *T* sensing over a wide range. In general, the Er^{3+}-doped materials have two green UC emission peaks (at ~520 and ~550 nm, respectively). These result from the two thermally coupled $^2H_{11/2}$ and $^4S_{3/2}$ levels. The luminescence intensity at ~520 nm increases with *T*, while the one at ~550 nm decreases. Tm^{3+}-doped materials possess two blue UC emission peaks (at ~475 and ~488 nm, respectively). The luminescence intensity at ~475 nm increases with *T*, and the one at 488 nm decreases. This also enables ratiometric measurement of *T*.

The selection of proper hosting materials is critical.[181] Fluoride glasses proved to be efficient matrices. They are superior to other oxidic glasses because of their low phonon energy, low melting point, high refractive index and high chemical, mechanical and thermal stability. Fluoride glasses have been used[182] as hosting materials as early as 1990. They have a broad transmissive range, high melting points and crystallization *T*s, low sensitivity to humidity, and can even be manufactured in the form of optical fibers. Er^{3+} and Yb^{3+} were doped into BIZYT fluoride glass (BIZYT stands for barium, indium, zinc, yttrium, and thorium)[182] and were shown to enable sensing of *T* in the range of 303–433 K. The Er^{3+}–Yb^{3+} co-doped fluoride glass can also be fabricated in particles with a diameter of ~1 μm. They were placed at the scanning tip of an atomic force microscope

Table 9 Lanthanide ion doped upconversion bulky materials for *T* sensing based on the measurement of luminescence intensity

Host	Dopant	λ_{em} [a]/nm	λ_{exc}/nm	Excitation density	Resolution/K	Temperature range/K	Ref.
Fluoride glass BIZYT[b]	Er^{3+}	520↑, 550↓	972	40 mW		303–433	182
Fluoride glass particle (1 μm)	Er^{3+}, Yb^{3+}	520↑, 550↓	980	—	—	312–417	183
Fluorotellurite glass	Er^{3+}	530↑, 550↓	800	5 W mm^{-2}	—	300–550	185
Fluoride glass ZBLALiP[c]	Er^{3+}	522↑, 546↓	805	10, 450 mW	1	150–850	195
Bi_2O_3–Li_2O–BaO–PbO glass	Er^{3+}	521↑, 547↓	800	—	—	295–600	186
Silicate glass	Er^{3+}, Yb^{3+}	526↑, 549↓	978	—	0.2	296–723	187
Silica fiber	Er^{3+}	525↑, 555↓	800	200 mW	1.3	295–873	196
Ga_2S_3:La_2O_3 chalcogenide glass	Er^{3+}, Yb^{3+}	530↑, 555↓	1060	10–200 mW	0.5	293–498	188
Al_2O_3	Er^{3+}	523↑, 545↑	978	4 W mm^{-2}	0.3	295–973	189, 190
Al_2O_3	Er^{3+}, Yb^{3+}	523↑, 545↓	978	4 W mm^{-2}	—	300–825	191
Al_2O_3	Er^{3+}, Y^{3+}	523↑, 546↓	978	1.2 W mm^{-2}	0.3	295–973	192
Al_2O_3	Er^{3+}, Yb^{3+}, Mo^{3+}	522↑, 546↓	976	0.2 W cm^{-2}	0.3	294–973	150
ZrO_2	Er^{3+}, Yb^{3+}, Li^{+}	517↑, 562↓ 646↑, 678↓	976	50 mW		323–673	193
Y_2O_3	Tm^{3+}, Yb^{3+}	476↑, 488↓	976	86.7–500 W cm^{-2}	—	303–753	194
$Yb_2Ti_2O_7$	Er^{3+}, Mo^{3+}	522↑, 554↓	976	0.5 W cm^{-2}	0.1	290–610	149
Gd_2O_3	Er^{3+}, Yb^{3+}	523↑, 548↓	976	280 mW		300–900	197

[a] ↑: increase with *T*; ↓: decrease with *T*. [b] BIZYT = barium–indium–zinc–yttrium–thorium. [c] ZBLALiP = ZrF_4–BaF_2–LaF_3–AlF_3–LiF–PbF_2.

to obtain a scanning thermal microscope.[183,184] *T* is determined by rationing the integrated relative intensities of the two green emissions (peaking at 527 and 550 nm). It has a well-defined *T* dependency, allows for the determination of *T* near the tip, and enables thermal imaging (Fig. 19). A fluorotellurite glass doped with an Er^{3+} ion was also used as a *T* sensor.[185] The material exhibits bright green UC emissions upon excitation with a continuous-wave diode laser at 800 nm. The emission and its changes can be observed with the bare eyes. The sensor works over a wide *T* range and up to 540 K.

Other glasses doped with lanthanide ions include a Bi_2O_3–Li_2O–BaO–PbO glass[186] doped with Er^{3+}, which can sense *T*s up to 600 K; a silicate glass[187] doped with Er^{3+}–Yb^{3+} that works in the range from 296–723 K; and a Ga_2S_3:La_2O_3 chalcogenide glass[188] co-doped with Er^{3+}–Yb^{3+} for the *T* range 293–498 K upon excitation at 1060 nm.

Metal oxides may also be used as hosting materials. Al_2O_3 doped with Er^{3+} works over a wide *T* range (295–773 K) and with high resolution (up to 0.3 K).[189,190] Addition of the co-dopants Yb^{3+} or Y^{3+} to this material further extends the dynamic range (up to 825 K[191] and 973 K,[192] respectively). ZrO_2 was also used as a host material,[193] and Er^{3+}–Yb^{3+}–Li^{+} were employed as dopants. The introduction of Li^{+} strongly enhances the emission of Er^{3+}. This is attributed to an increased asymmetry in the local environment surrounding the rare earth ions, and to the neutralization of hydroxy groups on the surface of the particles. The peak positions of the UC emission do not alter with increasing *T*, but the intensity of the emission from the upper levels ($^2H_{11/2}$ and upper sublevel of $^4F_{9/2}$) increases, while a decrease appears for the lower level transitions ($^4S_{3/2}$ and lower sublevel of $^4F_{9/2}$). As a result, the intensity ratio of the green emission (generated from Er^{3+} $^2H_{11/2}$ and $^4S_{3/2}$ levels) and red

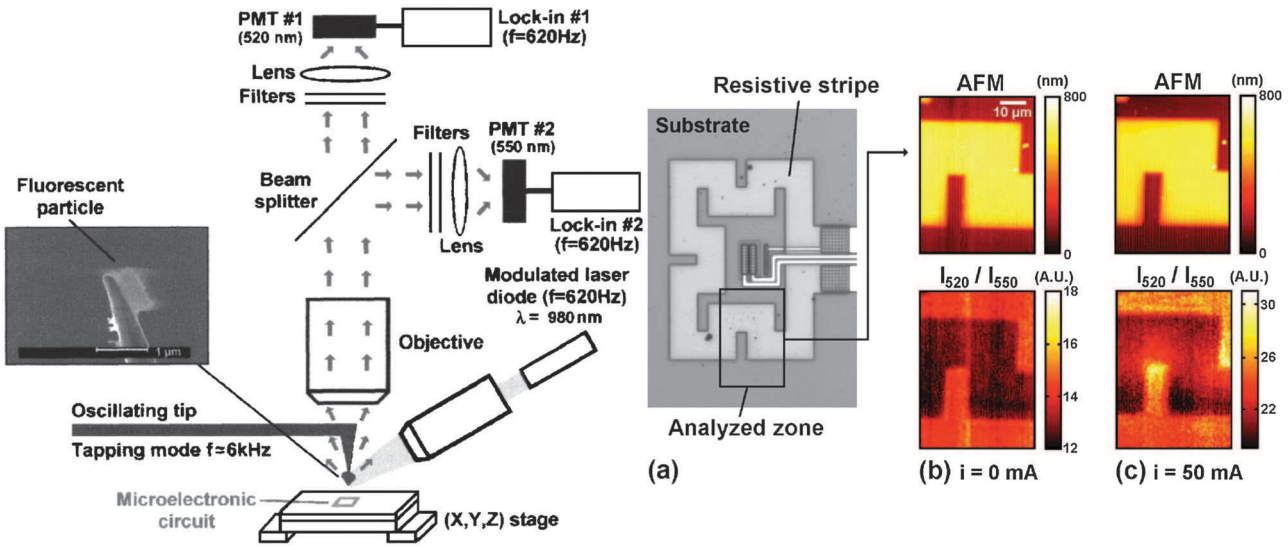

Fig. 19 Fluorescent imaging of *T*. An Er^{3+}–Yb^{3+} co-doped fluoride glass was prepared in the form of microparticles and placed at the scanning tip of an atomic force microscope to obtain a scanning thermal microscope. (Reprinted with permission from ref. 183. Copyright American Institute of Physics, 2005.)

emission (generated from the sublevels of Er^{3+} $^4F_{9/2}$ level) varies with *T*. The maximum sensitivities are 1.34% K^{-1} and 1.04% K^{-1} and observed in the range of 323–673 K. Others[194] have used Y_2O_3 as a hosting material, which was doped with Tm^{3+}, Yb^{3+}. The material exhibits typical blue UC emission of thulium and is sensitive to *T* in the range of 303–753 K.

5.4. Luminescent bulky (organic) polymer materials

Certain organic polymers display intrinsic luminescence that changes with *T*, polydiacetylene (PDA) being one typical representative (Table 10). Its emission color changes from blue to red in response to *T*. In parallel, it is converted from a non-fluorescent to a fluorescent form. PDA was embedded in a host PVA polymer matrix to work as a nano/microscale layer for sensing *T*.[198] The material was used[198] to monitor *T* gradients on an integrated circuit chip and to uncover sub-μm size defects in a resistance random access memory device structure (Fig. 20, left panel). The thermally induced fluorescence is irreversible and remains unchanged upon cooling to room *T*. This is beneficial to investigate the maximal *T* reached and allows for post-analysis. This new method can be widely applied in *T* distribution analysis on semiconductor and micro-electro-mechanical system devices where the detection of local heat deviations of small-scale components is critical. PDA was also used[199] in the form of droplets to measure the *T* of single droplets in microfluidic devices. Fig. 20 (right panel) shows that the PDA droplets emit red fluorescence when traveling over the micro-heated areas in the channel. The fluorescent signal of PDA is linearly proportional to the *T* in the 313 to 333 K range. However, the response is irreversible, so that it can be used only once and does not enable reversible (*i.e.* true) sensing.

The luminescence of the dye bis(benzoxazolyl)stilbene is quenched at very high concentrations (excimer effect, see Section 3.1) if incorporated in a poly(1,4-butylene succinate) matrix.[71] The polymer matrix undergoes a thermo-induced stretching that implicates a change in the local indicator concentration. This causes an enhancement of the excimer emission at high *T*s. This sensor layer works in the range from 323–353 K, but the resolution is rather poor.

The luminescence of rhodamine-labeled poly(isobutyl-methacrylate-*co*-trifluoroethylate), referred to as poly(IBM-*co*-TFEM), decreases almost linearly upon increasing *T* from 273 to 333 K. The solubility of RhB in the polymer was dramatically improved by conjugation to the polymer chain.[200] The labeled polymer is soluble in toluene to yield a sprayable paint. The *T*-sensitivity of the polymer is 0.37% K^{-1} and independent of air pressure or, more precisely, not quenched by oxygen. In addition, poly(IBM-*co*-TFEM) is highly permeable to oxygen. It was used to immobilize oxygen-sensitive probes to obtain a paint for dual sensing of oxygen and *T* in aerodynamic research.[201]

The monomers 2-(2-methoxyethoxy)ethyl methacrylate and oligo(ethylene glycol) monomethyl ether methacrylate were copolymerized[202] in the presence of a quinoline-based Zn^{2+}-recognizing moiety (ZQMA) *via* reversible addition–fragmentation chain transfer polymerization. The fluorescence of ZQMA undergoes a ~6.0-fold increase over the rather narrow *T* range of 299–305 K. This is due to the fact that the microenvironment of ZQMA becomes more hydrophobic. This co-polymer requires to be photo-excited in the UV and emits in the blue region.

6. High-sensitivity luminescent temperature probes

The preceding paragraphs have categorized luminescent indicators and probes according to their molecular or structural features. This section focuses on probes for high-sensitivity sensing of *T* which is often needed in practice and frequently is needed over a fairly narrow range of *T*s. Table 11 gives an overview of probes with remarkably large resolution. High-sensitivity probes are needed to measure small changes in *T* as they are observed in physiological and (intra)cellular studies. Transition metal based probes are quite sensitive, but they are outmatched by lanthanide based probes such as

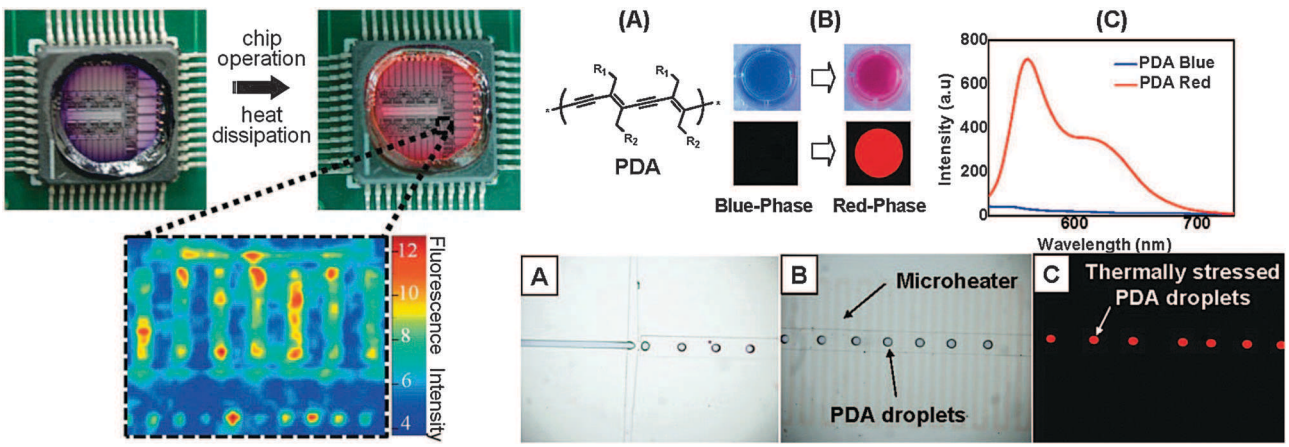

Fig. 20 Polydiacetylene-based irreversible imaging of *T* integrated circuit (left, reprinted with permission from ref. 198. Copyright Wiley-VCH, 2011) and in microfluidic devices generated droplets (right, reprinted with permission from ref. 199. Copyright American Chemical Society, Washington, DC, 2009).

Table 10 Intrinsically fluorescent and fluorophore-labeled bulky polymers for sensing and imaging of *T*, their working ranges (in K) and wavelengths (in nm) for fluorescence excitation and emission

Material	Range	Exc./Em.	Comments	Ref.
Polydiacetylene (PDA)	313–333	540/650	Irreversible color change from blue to red; accompanied by a transition from a non-fluorescent state to a luminescent state	198, 199
Poly(IBM-*co*-TFEM-*co*-RhB)	273–333	541/570	Gas permeable polymer; suitable for multiple sensing; suitable for *T* sensitive paints	200
PEG-*b*-P(MEO_2MA-*co*-OEGMA-*co*-ZQMA)	299–305	364/482	Sensitive to *T* and Zn^{2+}; 6-fold sharp fluorescence enhancement; tunable dynamic range	202

Table 11 Probes that display a particularly high sensitivity

Probe (or sensor)	Useful *T* range (K)	Exc./Em.	Max. sensitivity[a] (% K^{-1})	Ref.
$Ru(phen)_3$	273–393	470/580	-2.0^c	15, 60, 64, 74
$Ir(ppy)_2(carbac)$	274–323	405/519	-0.4^b	61, 75
$Eu(TTA)_3$	274–323	377/615	-4.28^b -1.8^c	94, 95
$Eu(D2)_3$phen in FIB	278–318	370/615	-4.42^b -4.0^d	94, 105
$Eu(benzac)_3(phen)$	278–328	381/611	-4.0^b	29
EuDT	298–318	375/616	-3.07^b -2.2^c -4.0^d	107, 108
$Tb(HFA)_3(H_2O)_2$	283–323	363/543	-1.80^b	109
$Tb(HFA)_3(TPPO)_2$	283–323	345/543	-1.90^b	109
$[Tb_{0.99}Eu_{0.01}(hfa)_3(dpbp)]_n$	200–500	380/543, 613	-0.64^d	104
CdTe (layered double hydroxides)	296–353	405/535	-1.47^b	117
$Zn_{1-x}Mn_xSe$–ZnS–CdS–ZnS	133–373	405/520, 600	-0.83^d	123
Poly(NIPAM-*co*-HC)	298–313	510/580	$+500^a$	156
Poly(NIPAM-*co*-BODIPY)	296–308	490/600	$+83^a$	157
Poly(NIPMAM-*co*-DBD-AE)	318–327	444/556	$+79^a$	158
Poly(NNPAM-*co*-DBD-AE)	302–310	444/563	$+266^a$	158
Poly(NIPAM-*co*-DBD-AE)	291–297	444/566	$+166^a$	158
Poly(NIPAM-*co*-DBD-AA-*co*-FPA)	300–306	444/560	$+27^b$	160, 161
$Yb_2Ti_2O_7$ with Er^{3+}, Mo^{3+} dopant	290–610	976/522, 554	-0.74^c	149

[a] The maximum sensitivity is not always ensured over the whole working range. [b] Intensity signal change. [c] Lifetime signal change. [d] Ratiometric signal change.

Eu- or Tb-complexes. Lanthanide complexes are suitable for application in the physiological range, but unfortunately they often possess limited stability in aqueous solution or suspension. Some also require UV excitation which can cause a large fluorescence background in the case of studies on biological matter. This can be partially overcome in the case of long-lived probes (such as those based on lanthanide ions) if gated measurements are performed. *T*-sensitive polymers such as the poly(NIPAM-*co*-DVB) derivatives are also highly promising. These offer a very sharp *T*-dependent fluorescence transition. Compared to other indicators, they offer reversed *T*-dependent fluorescence leading to an increase in intensity upon increasing *T*. This results in very distinct signal changes.

7. Polymeric matrices for immobilizing temperature sensitive probes and particles

Polymer matrices or supports are used in various situations in order to immobilize molecular probes and sensor nanoparticles for *T*. The host material then can be shaped in forms such as sensor particles, planar sensor films, sensor coatings on optical fiber tips, or as host-coated nanoparticles. Both organic and inorganic polymers have been used. The host materials are expected to remain completely inert (unless a second sensor function is to be introduced[203,204]), to firmly retain the probes, not to quench luminescence, to be stable even at elevated *T*s, and to rapidly conduct heat. Obviously, micro-and nanosized films and sensors respond more rapidly due to more rapid *T* equilibration than sensors based on the use of thick or bulky host materials.

Solubility in polymers is an issue in the case of ionic molecular probes. Ionic probes possessing a counter anion (such as many complexes of ruthenium or europium) usually are not well soluble in organic polymers, and are virtually insoluble in silicone rubber where they tend to aggregate and to lose their functionality. The exchange of the (hard) counter ion by a soft (organic) counter[205] offers a generally applicable method to make ionic probes (not only for *T*) soluble in apolar organic polymers. Organic polymers often are not stable at *T*s of >573 K. Inorganic materials, sol–gels in particular, are much better in that respect.

Oxygen is a notorious quencher of luminescence. If probes are used whose luminescence is quenched by oxygen, host materials may be chosen that have a poor solubility for oxygen and that may even prevent oxygen from entering the sensor

materials. Oxygen is also a major cause for photobleaching in that singlet oxygen is being formed, which is highly reactive. The oxygen-sensitive probe $Ru(bpy)_3$ has been immobilized in a sol–gel film and was able to sense *T* in the range of 15–340 K with a resolution of 0.1 K.[72] RhB immobilized in a silica gel (28–200 mesh) or in a sol–gel film also served[44] as a solid state optical sensor for *T*. Their dynamic ranges are between 283 and 368 K and 273–333 K, respectively. The sensors are not interfered by pH or oxygen, and their shelf lifetime exceeds 3 months. Sol–gels usually are processed such that porous materials are obtained that are permeable to gases. This is not desirable in the case of sensing *T*. However, by drying the sol–gel solution rapidly at 313 K under vacuum,[15] the resulting sol–gel condensed film is impermeable to gases and henceforth suitable for specific sensing of *T*.

There is a variety of other polymers that are hardly permeable to oxygen.[206] These include poly(vinyl chloride) (PVC), poly(vinyl alcohol) (PVA), and polyacrylonitrile (PAN), see Table 12. The luminescence of $Eu(TTA)_3(dpbt)$ is highly sensitive to *T*, but is also slightly affected by oxygen. Stich *et al.*[63] minimized this interference to almost zero by shielding the fluorophores with PVC. The hydrophilic polymer PVA is also hardly permeable to gases and was used as a matrix for immobilizing the green-emitting probe Tb-THBA to obtain a sensor for *T*.[102] Among the various ruthenium polypyridyl complexes, $Ru(phen)_3$ possesses a good sensitivity for *T*, but its luminescence is also quenched by oxygen. It has effectively been shielded towards oxygen with the use of polyacrylamide (PAN).[15,64,73,74] PAN has a gas permeability that is typically five orders of magnitude lower than that of silicone rubber, thus drastically reducing oxygen crosstalk of the sensor response. Moreover, it has a low uptake of water, which generates a shielding ability towards pH-dependencies. $Ru(phen)_3$ is well soluble in PAN, and this allows the formation of nm-thin but highly luminescent sensing films. $Ru(phen)_3$ in PAN also displays an extraordinarily long decay time (3.6 μs at 283 K).

QDs are fairly good probes for *T* and can be incorporated into almost any polymer, but in the case of soft and hydrophobic polymers they tend to aggregate and to lose their luminescence. However, in the case of amino-modified sol–gel films,[128] aggregation is strongly reduced due to the electrostatic interaction between the amino groups on the film and the negatively charged groups on the surface of the QDs. This method enabled QDs to be distributed evenly in a sensor film.

Table 12 Oxygen permeability (*P*) data of commonly used polymers for sensing *T*

Polymer [acronym]	Chemical structure	P [10^{-13} cm^2 s^{-1} Pa^{-1}]
Poly(acrylonitrile) [PAN]	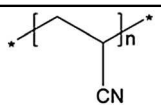	0.00015
Poly(vinyl chloride) [PVC]	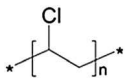	0.034
Poly(vinylidene chloride-*co*-acrylonitrile) [PVDC-AN]	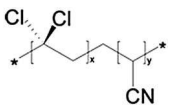	n.s.
Poly(styrene-*co*-acrylonitrile) [PSAN]	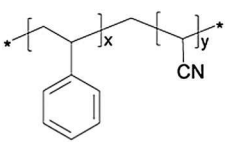	0.0032
Poly(vinyl alcohol) [PVA]	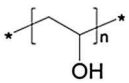	0.0065

8. Application formats

Sensors for *T* are mainly used in four kinds of application formats, *viz.* as molecular probes in solution, as micro- and nanosized sensor particles (for example inside cells), in optical fiber sensors, and as 2-dimensional sensor films for use in imaging of *T*. These fields will be discussed in the following sections.

8.1. Molecular probes in solution

T-sensitive molecular fluorophores and nanoparticles can offer nm-scale resolution and the possibility of sensitivity down to a single-molecule level.[207] Molecular probes for *T* have been used in solutions, for example, in microfluidics, to perform kinetic measurements and thermodynamics of reactions.[27,42,208,209] Fig. 21, left panel shows thermal pseudocolor-images of Joule-heating of electrokinetically pumped buffered solutions in a *T*-shaped microfluidic system.[42] The indicator RhB in aqueous buffers was used to visualize thermal changes within the microfluidic channels with a precision of 0.03–3.5 K and a spatial resolution of down to 1 μm limited by the optical setup. The saturated solutions of RhB along with a second less *T*-sensitive rhodamine derivative were used for referenced two-color laser-induced *T*-mapping in microfluidic devices.[209] The group of deMello[208] substantially improved referenced thermal imaging in microfluidic devices by acquiring lifetime-based 2D images of the *T* of a fluid in a microchannel network. They also reported on 3D mapping of *T via* 2-PE using this system, allowing for enhanced quantitation of *T* (±1 K) with a μm-spatial resolution. Graham *et al.*[17] extended referenced fluorescent lifetime imaging by using the water soluble polymer poly(DBD-AE-*co*-NIPAM). They were able to map microfluidic heat deviations on a μm-scale with a *T* resolution of less than ±1 K.

Dissolved molecular probes were additionally used in cellular and microscopic studies.[39,93] Molecular probes can be injected into cells, directly taken up by cells (membrane-permeable), or used as membrane probes if sufficiently lipophilic. However, they (i) have to be non-toxic and biocompatible, (ii) must not be quenched by oxygen, (iii) must not suffer from photodecomposition or effects caused by other sample ingredients (such as proteins). The use of a reference dye may help in some cases. Exemplarily for cellular and microscopic *T*-measurements using dissolved probes, Fig. 21 (right panel) displays temporal resolved *T*-imaging of a

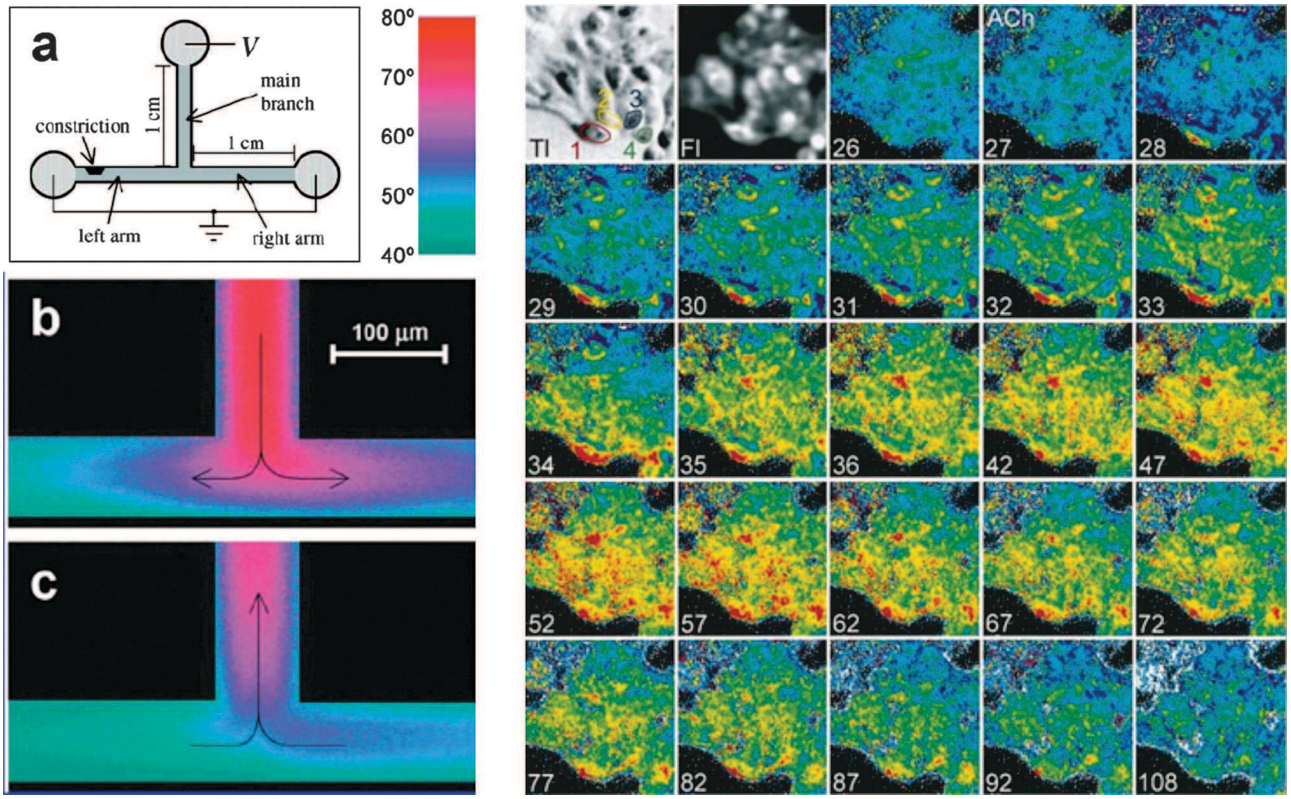

Fig. 21 Thermal imaging of Joule-heating caused by electrokinetically pumping buffers in microfluidic channels (reprinted with permission from ref. 42. Copyright American Chemical Society, Washington, DC, 2001) or of cellular heat waves evoked after activation with acetylcholine using dissolved molecular *T*-probes. (Reprinted with permission from ref. 93. Copyright Elsevier, 1998.)

biphasic heat wave caused by applying acetylcholine to a Chinese hamster ovary (CHO) cell. The hydrophobic $Eu(TTA)_3$ was stained in the CHO cell membrane and served to visualize the heat waves with an excellent temporal and spatial resolution.

8.2. Micro- and nanosensors

Many of the limitations of probes in solution can be overcome by incorporating the molecular probe into a protective polymer in the form of micro- and nanoparticles. Dissolved indicators have limited use in the case of application in vessels or cells. In most cases, they simply reflect average values over certain areas of the samples, because they are not spatially fixed. The use of particles has indeed the advantage of hampered indicator mobility inside samples such as cells. The polymer matrix also prevents direct contact of biomatter (*e.g.* proteins) in the sample with the probes. Therefore, interferences by interactions with oxygen or due to local pH values can be prevented. Furthermore, the use of particles allows for co-embedding of reference dyes for ratiometric $(2-\lambda)$ measurements. Encapsulation usually makes the dyes more photostable and thus prolongs the shelf and usage times of the sensors. However, on the other side, the addition of sensor particles to a sample implicates a possible risk of contamination and intoxication.

There are numerous examples of the use of nano- and micromaterials for cellular research[2,37,160,161,210,211] and imaging,[26,29] microscopy,[112,160,198,212] or fluidic research.[17,112,213] For example, *T* sensor particles were placed at the tip of an atomic force microscope to build a device for thermal imaging with a good spatial resolution (Fig. 19).[183] Wang *et al.*[29] used polymer-nanoparticles-based sensors for mapping heat-driven thermodynamics of solutions (Fig. 15). QDs can be used to visualize nano-heating of carbon nanotubes in an optofluidic chip device.[213]

Thermal imaging in cells is another emerging and exciting field of research. Thermoresponsive luminescent core–shell nanoparticles, for example, enable[165] simultaneous targeting of cancer cells and optical imaging of *T*. Similarly, intracellular heat mapping was accomplished[160] with a spatial resolution at the diffraction limit (200 nm) and a resolution of 0.18–0.58 K *via* the use of a polymeric nanogels (see Fig. 22). These authors reported that this intracellular heat mapping was probably the first to show that intracellular *T* distribution is not uniform. Both the nucleus and centrosome of a COS7 cell possess a higher *T* than its cytoplasm. The *T* gap between the nucleus and the cytoplasm differed depending on the respective cell cycle. The heat production from mitochondria was also observed as a proximal local *T* increase. These results showed that intracellular thermometry demonstrated an intrinsic relationship between local *T* and organelle function. A local heterogeneous *T* progression in cells subsequent to a chemical calcium stress and a physical cold shock was observed[211] *via* the use of QDs based nano thermometers. Superparamagnetic nanoparticles

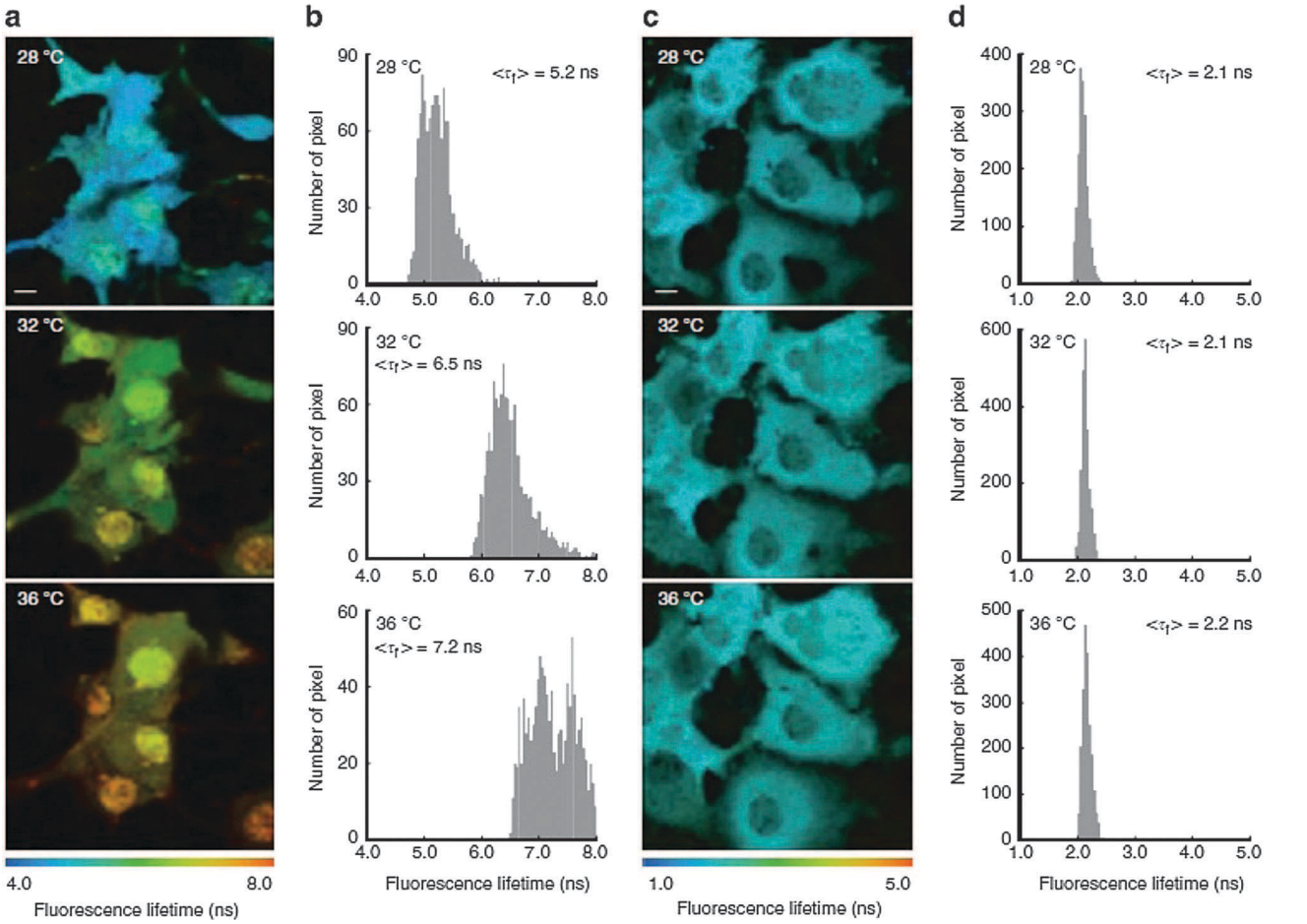

Fig. 22 Thermal imaging in living cells using a *T*-sensitive polymer nanogel. The thermal distribution in the cells is not uniform and the *T* near the nucleus is clearly higher than that in other regions. (Reprinted with permission from ref. 160. Copyright Nature Publication Group, 2012.)

were described[214] that can induce and simultaneously measure local *T* and its changes over time. In our opinion, the use of optical intracellular nanothermometry is still in its fledgling stages but will gain exciting new insights into cellular mechanisms and will substantially push the understanding biological processes.

8.3. Fiber-optic sensors

The state of the art in fiber optic sensing of *T* by the year 1991 has been reviewed.[215] Such sensors[216] often rely on probes that are immobilized at the tip (distal end) or on the core of an optical fibers waveguide (see Fig. 23 left panel), mostly in an organic polymer, a sol–gel, or related kinds of matrices.[217,218] The group of Grattan[10,219,220] has pioneered fiber optic thermometry. Such sensors have gained much popularity.[4] Optical fiber sensors are lightweight, small, and thus enable microsensing.[217] The typical size of fiber-based microsensors is around 20 to 200 μm in diameter.

Fiber optic microsensors can be minimally invasive due to their small size (10–20 μm tip diameter) and often are inserted *via* syringes.[64] They are applicable at sites that are inaccessible to other spectroscopic methods, *e.g.* the inside of the body, in chemical reactors or bioreactors, in turbine engines, soil or sediments, *etc.*[216,218,221] Such sensors also work in strong magnetic fields.[222] Fiber optic sensors are used routinely for years in medicine especially to determine clinical hyperthermia.[223–225] Reviews by Samulski[226] and Michalski *et al.*[4] discuss the role of luminescent thermometry in medicine. Fiber optic thermometers also enable long distance measurements and distributed sensing along the fibers.[227] For example, neodymium(II)-doped fibers were reported[228] that enable *T* to be measured between 223 and about 373 K with a spatial resolution of 15 m along the fiber.

Fiber optic sensors for *T* are used in commercial devices. The Luxtron type system is one such device.[229] It employs a UV light source with dichroic mirrors for wavelength separation and relies on the fact that the luminescence of a rare earth phosphor strongly depends on *T*. The change in the ratio of the emissions at two different wavelengths is rationed to give a referenced signal for calculating *T*. The ASEA company (www.abb.com) in Sweden had commercialized a device that exploited *T*-dependent changes in the luminescence of an aluminum gallium arsenide semiconductor material[230] which is excited using LEDs. Emission intensity varies with *T* and the two distinct emissions in separated spectral regions can be used for ratiometric read-out. *T*s in the region of 273 to 473 K

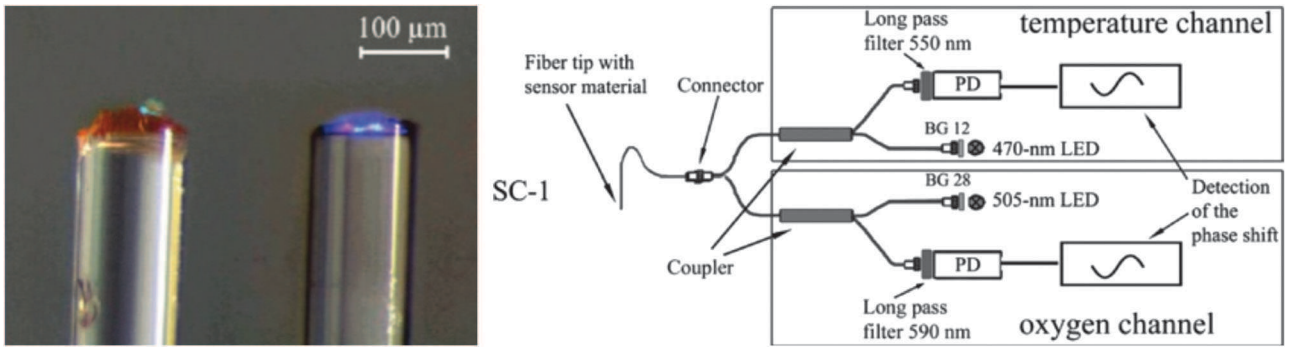

Fig. 23 Microscopic images of a fiber optic sensor for dual sensing of oxygen and *T*. (Reprinted with permission from ref. 64. Copyright American Chemical Society, Washington DC, 2007.) A *T*-indicator probe embedded in a polymer matrix is immobilized at the tip (distal end) of an optical fiber waveguide (left panel). The distinct colors of the sensing layer on top of the tip result each from a combination of the excitation light (LED) and the emitted light (probe). The right panel displays a schematic of the fiber-optic *T*-sensor within this dual sensor approach.

can be determined with an accuracy claimed to be about 1 K. LEDs are attractive light sources in terms of size, energy consumption, brightness and long term stability. On the other side, LEDs undergo a small change in their operating characteristics with *T* as the peak wavelength of emission increases as the device heats up. This is highly disadvantageous in the case of single wavelength intensity measurements, but usually is compensated for by ratiometric (2-wavelength) measurements and in decay time-based sensing.

Fiber-optic sensors are not limited for the use of luminescence intensity based measurements. One may also determine the characteristic decay time of a sensor material (see Section 2.3). This method has quite a long history in terms of sensing *T* and is based on photoexcitation of phosphors such as ZnCdS and ZnSe. The state of the art in thermographic sensing using inorganic phosphors has been reviewed.[231] Others[232] have discussed the application of the decay time sensing scheme to monitoring *T*s in the 303 to 323 K range using the emission of a ruby crystal. Ruby crystals, when pumped with LEDs, emit deep red light with a peak at 694 nm that undergoes a large change in decay time with *T*. This material is extremely stable, inexpensive in its impure form, and completely inert. A detailed study of a ruby based fluorescence decay time sensor has been published.[233] Resolutions of 0.04 K have been demonstrated under laboratory conditions. A fiber optic sensor was produced using the commonly used visible wavelength phosphor $BaClF:Sm^{2+}$.[234] This sensor operates up to 423 K by monitoring the *T*-dependent decay time of the material excited by a mechanically modulated conventional lamp source. Lifetime based sensing is exploited[235] in a sensor that uses a chromium-doped crystal. The device can sense *T*s up to 473 K.

Materials such as neodymium dopants and alexandrite were used[236] in decay time-based fiber-optic thermometry. The Nd(III) doped glasses or crystals (such as YAG) possess strong absorption bands in the near IR (750 to 810 nm), and this makes them amenable to photoexcitation by low-cost LEDs or high-power diode lasers. The strongest emission occurs at extremely long wavelength (at 1.06 μm). However, the decay time of Nd(III) does not display a large change with *T*,[237] and response is ambiguous because decay times initially increase with *T* but then decrease. On the other hand, if Nd(III) is doped into glass at high concentrations (7 to 9%), the obtained material undergoes a fairly large change (a drop in decay time of about 10%) with *T* and over a range of 273 to 423 K. It is advantageous that the decay times are in the order of 0.1 to 1 ms (compared to the μs decay times of many phosphors) so that fairly simple electronic circuits can make these measurements accurately.

Alexandrite can be pumped with a He–Ne laser.[238] If the intensity of the laser is modulated in a sinusoidal form, the phase shift of the emission (compared to the phase of the laser) is a direct measure for *T* over a large range from 293 to 413 K. The mathematics relating the decay time to this phase lag has also been discussed.[239]

Additionally the fiber optic sensor format can be implemented in multiplexed sensing, or used for imaging purposes using fiber bundles.

8.4. Planar sensing and 2-D imaging using sensor films

The distribution of *T* on surfaces can be imaged using sensing films or so-called *T*-sensitive paints (TSPs).[240,241] Fig. 24 shows a sensor film exposed to 273 (iced water) and 333 K (heated air), respectively.[74] The observable red luminescence intensity is distinctly quenched at elevated *T*. Such thin sensor films have extremely low heat capacity.[183] Further, the *T* dependent effects occur at the molecular level. These two reasons allow sensing and imaging of very fast changes in *T*. The 2-D sensor formats are also quite flexible in terms of application compared to dissolved indicators, particles, or fiber based sensors. One major virtue compared to, for example, fiber-optic sensors, is the fact that no direct contact of the fiber or measurement device and the sensor is needed. Therefore, this method is referred to as a so-called contactless or non-invasive method.

Heat transfer in sensor films deserves a special discussion. On one side, one would like such sensors to rapidly equilibrate with its environment in order to enable real-time monitoring of local *T*. On the other side, rapid heat transfer will limit spatial resolution in that heat not only is transferred from the object of interest to the sensor film, but also vertically inside the film, thereby blurring borderlines. There are only a handful of

Fig. 24 Response of a planar *T* sensitive paint (film size 4 × 7 cm). (Reprinted with permission from ref. 74. Copyright Wiley-VCH, 2006.) A heated planar sensor foil is dipped into ice water. The bright orange-red luminescence at 273 K (bottom) is less quenched compared to the less distinct luminescence at 333 K (top).

ratiometric probes and sensors that display a very high spatial resolution in the 293–333 K *T* range as reported by reviews of Brites *et al.*,[112,242] and Jaque and Vetrone,[113] as well as in more recent articles.[60,126,144] Therefore, sensing *T* with spatial resolution below 10 μm still remains a major challenge, demanding in most cases the development of new materials and sensing instruments.

Optical sensing can be contactless, for example through transparent flasks or walls, with the inherent advantage of sterile sensing. This is of special interest if sensors are operated in bioprocess control, or *in vivo*. A contactless optical *T*-sensor system was realized for example for use in neonatal care (Fig. 25).[243] In this monitoring system, two sensor spots enable ratiometric determination of *T*. Each of the panels is composed of a (varying) fluorescent dye embedded in a skin-friendly chitosan gel matrix. The panels are applied to the subject, excited using an LED as well as monitored *via* a camera from the outside of the incubator. The gel can easily be wiped off the subject after use and does not cause skin irritation.

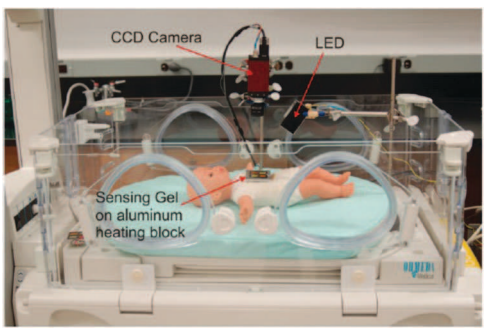

Fig. 25 Experimental setup of a neonatal care *T* sensor. The sensor consisting of a *T* sensitive probe and a reference dye in a chitosan gel is displaced on the skin and can be monitored in a contactless manner *via* a CCD camera. (Reprinted with permission from ref. 243. Copyright IOP Publishing, 2012.)

Planar *T* sensors are mostly used for visualization of two dimensional *T* patterns on surfaces, with a main application in aerodynamics and wind tunnel tests.[241,244–247] *T* is a critical parameter in high speed wind tunnel tests.[247] For example, TSPs were used to study the whole-field *T* distribution in heat transfer enhancement applications,[248] and in short-duration Mach 6 wind tunnels.[249] TSPs in wind tunnel experiments are more often than not used to compensate effects of *T* in pressure sensitive paints (PSPs), because all luminescent indicators are sensitive to *T*. Dual sensor paints consisting of a TSP and a PSP have become known in the last few decades in order to eliminate those errors caused by *T* differences and produce reliable PSP measurements.[14,105,250,251] For instance, Gouterman *et al.*[245,252] co-incorporated a *T* sensitive magnesium complex and a platinum porpholactone oxygen indicator in a highly fluorinated FIB polymer to form a dual sensor paint. They sprayed the so-called sensor cocktail onto an automotive model and determined local air pressures on the model in the wind tunnel and after correction for effects of *T* (Fig. 26).

The specific features of sensor paints also allow for imaging of moving objects. The application benefits from the fast response times and the contactless sensing mode. For example, thermometry in turbine engines is difficult, because fast moving parts prevent conventional contact thermometry, but TSP works well.[21,226,227] However, the luminescence lifetimes of the indicators have to be short in the ns range to obtain non-blurred 2-D *T* images of fast moving rotor blades.

Luminescent *T* sensors – unlike electrical sensors – can be operated in the presence of electrical fields. Thus, TSPs are, for instance, also used in the maintenance of electrical machinery to locate hot spots inside the rotor.[253] TSPs are also used in high voltage distribution power lines, such as for electric trains, or on various components, like surge suppressers, power bars, bus-bars or on integrated circuits.[92] The measurement of *T* on micro- and nanowires in circuits has, in fact, attracted substantial interest because it cannot be performed easily with methods other than luminescence based assays. Examples for respective studies include thermal imaging of a microwire with fluorescent nanocrystals[254] and high-spatial-resolution surface-*T* mapping of nanowires using fluorescent thermometry.[18]

9. Prospects

The wealth of luminescent probes and (sold) materials paves the way to an almost endless number of opportunities to design sensors for *T*. There is hardly any luminophore known that would not possess a *T*-dependent luminescence. In addition, there are an increasingly large number of smart methods for luminescent read-out that can be adapted to someone's specific problem. However, all probes and sensors have their merits and shortcomings. Development of future sensors for *T* should be focused on probes that meet several of the following requirements: (i) they should be brighter with higher QYs and (ii) offer higher signal changes along with *T* over a specific range. This implies higher sensitivity. Most notably for nanosensors, the sensitivity should be in the order of ±0.01 K to detect very small

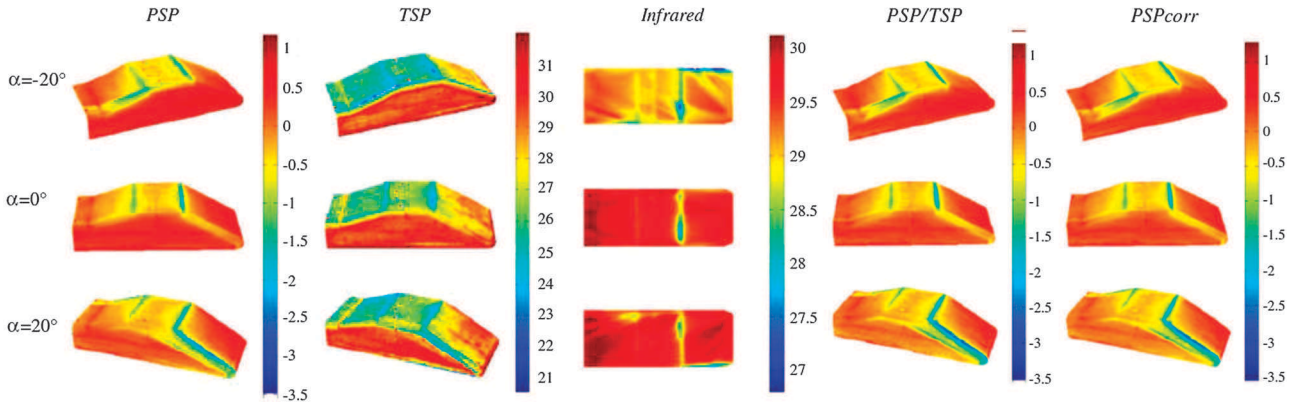

Fig. 26 Application of a TSP and a PSP for aerodynamic wind tunnel experiments with a model of a car. (Reprinted with permission from ref. 245. Copyright IOP Science, 2004.)

changes, and to sense and visualize for example *T*-changes caused by cellular processes. (iii) Probes are supposed to be more photostable (unless solid-phase particles are used). Although, some probes can be combined with read-out techniques that are not prone to photobleaching (such as LLI, or intrinsic 2-wavelength referencing), the overall signal intensity should be sufficiently stable to extend their operational lifetime and allow for long-term monitoring. Especially, photostability is very critical in microscopy studies, since high excitation light intensity is focused on a relatively small assembly of *T*-probes. Photobleaching caused by high power laser excitation is even worse in this case. (iv) New probes are needed, which have spectral properties shifted towards long-wavelength (laser) excitation and emission. This will minimize interferences caused by the intrinsic color of the sample or background fluorescence of samples. Background luminescence is particularly strong under UV and shortwave visible photoexcitation. Furthermore, lower energy long-wavelength excitation reduces photobleaching of the probes. (v) Sensors are to cover wider dynamic ranges (>300 K) with adequate resolution and (vi) the probes need to be thermally stable. Thus, (vii) more probes and sensors for high *T* measurements are needed. (viii) Additionally, the *T*-indicators must not be toxic or harmful to the organisms if an *in vivo* use is intended.

There is no need for a universal optical thermometer, however. In fact, we envision the design of numerous sensing approaches that match the specific needs in a given situation. Material science – more than anything else – will push respective developments, and the option of using nanosensors to be able to look into a nanostructured (bio)system will further accelerate research. It was challenging in the past, and will be challenging in the future, to theoretically substantiate the effects found. Most research is still a kind of empirical research, and results often come incidentally. Notwithstanding this, the luminescent probes and sensors will enable *T* to be sensed in situations and with a precision not anticipated some 20 years ago.

The authors declare no competing financial interest.

Acknowledgements

This work was financially supported by the Alexander von Humboldt foundation (Bonn) by a fellowship for XW, and by the Deutsche Forschungsgemeinschaft (DFG; Bonn) within project SCHA 1009/7-1 (covering the employment of RJM). Both are gratefully acknowledged.

References

1 E. F. J. Ring, *Infrared Phys. Technol.*, 2007, **49**, 297–301.
2 J. B. Weaver, *Nat. Nanotechnol.*, 2010, **5**, 630–631.
3 P. R. N. Childs, J. R. Greenwood and C. A. Long, *Rev. Sci. Instrum.*, 2000, **71**, 2959–2978.
4 L. Michalski, K. Eckersdorf, J. Kucharski and J. McGhee, *Temperature measurement*, Wiley, Chichester, UK, 2001.
5 N. Ashcroft and N. Mermin, *Solid state physics*, Saunders College, Philadelphia, 1976.
6 S. Maekawa, *Physics of transition metal oxides*, Springer Verlag, 2004.
7 G. Beheim, *Integrated Optics, Microstructures, and Sensors*, 1995, pp. 285–313.
8 A. Sarua, J. Hangfeng, M. Kuball, M. J. Uren, T. Martin, K. P. Hilton and R. S. Balmer, *IEEE Trans. Electron Devices*, 2006, **53**, 2438–2447.
9 J. R. Lakowicz, *Principles of fluorescence spectroscopy*, Kluwer Academic/Plenum Publishers, New York, London, Moscow, 2006.
10 K. Grattan and Z. Y. Zhang, *Fiber optic fluorescence thermometry*, Springer, 1995.
11 S. P. Wang, S. Westcott and W. Chen, *J. Phys. Chem. B*, 2002, **106**, 11203–11209.
12 M. A. Woodmansee and J. C. Dutton, *Exp. Fluids*, 1998, **24**, 163–174.
13 L. M. Coyle, D. Chapman, G. Khalil, E. Schibli and M. Gouterman, *J. Lumin.*, 1999, **82**, 33–39.
14 L. M. Coyle and M. Gouterman, *Sens. Actuators, B*, 1999, **61**, 92–99.

15 G. Liebsch, I. Klimant and O. S. Wolfbeis, *Adv. Mater.*, 1999, **11**, 1296–1299.
16 S. Li, K. Zhang, J.-M. Yang, L. Lin and H. Yang, *Nano Lett.*, 2007, **7**, 3102–3105.
17 E. M. Graham, K. Iwai, S. Uchiyama, A. P. de Silva, S. W. Magennis and A. C. Jones, *Lab Chip*, 2010, **10**, 1267–1273.
18 P. Löw, B. Kim, N. Takama and C. Bergaud, *Small*, 2008, **4**, 908–914.
19 G. Baffou, C. Girard and R. Quidant, *Phys. Rev. Lett.*, 2010, **104**, 136805.
20 S. D. Alaruri, A. J. Brewington, M. A. Thomas and J. A. Miller, *IEEE Trans. Instrum. Meas.*, 1993, **42**, 735–739.
21 R. Hasegawa, I. Sakata, H. Yanagihara, B. Johansson, A. Omrane and M. Alden, *Appl. Phys. B: Lasers Opt.*, 2007, **88**, 291–296.
22 M. D. Chambers and D. R. Clarke, *Annual Review of Materials Research*, Annual Reviews, Palo Alto, 2009, vol. 39, pp. 325–359.
23 M. Schäferling and A. Duerkop, in *Standardization and Quality Assurance in Fluorescence Measurements I*, ed. U. Resch-Genger, Springer, Berlin, Heidelberg, 2008, vol. 5, pp. 373–414.
24 A. Heyes, S. Seefeldt and J. Feist, *Opt. Laser Technol.*, 2006, **38**, 257–265.
25 J. Linden, G. Särner, M. Richter and M. Alden, Proceedings of the European Combustion Meeting, 2009.
26 L. H. Fischer, G. S. Harms and O. S. Wolfbeis, *Angew. Chem., Int. Ed.*, 2011, **50**, 4546–4551.
27 C. Gosse, C. Bergaud and P. Löw, in *Thermal Nanosystems and Nanomaterials*, ed. S. Volz, Springer, Berlin, Heidelberg, 2009, vol. 118, pp. 301–341.
28 N. Ishiwada, T. Ueda and T. Yokomori, *Luminescence*, 2011, **26**, 381–389.
29 X. D. Wang, X. H. Song, C. Y. He, C. J. Yang, G. N. Chen and X. Chen, *Anal. Chem.*, 2011, **83**, 2434–2437.
30 V. A. Vlaskin, N. Janssen, J. van Rijssel, R. m. Beaulac and D. R. Gamelin, *Nano Lett.*, 2010, **10**, 3670–3674.
31 E. J. McLaurin, L. R. Bradshaw and D. R. Gamelin, *Chem. Mater.*, 2013, **25**, 1283–1292.
32 J. R. Lakowicz, H. Szmacinski, K. Nowaczyk, K. W. Berndt and M. Johnson, *Anal. Biochem.*, 1992, **202**, 316–330.
33 M. I. J. Stich, PhD thesis, University of Regensburg, 2010.
34 P. Hartmann, W. Ziegler, G. Holst and D. W. Lübbers, *Sens. Actuators, B*, 1997, **38**, 110–115.
35 R. Woods, S. Scypinski and L. J. C. Love, *Anal. Chem.*, 1984, **56**, 1395–1400.
36 R. M. Ballew and J. Demas, *Anal. Chem.*, 1989, **61**, 30–33.
37 J. S. Donner, S. A. Thompson, M. P. Kreuzer, G. Baffou and R. Quidant, *Nano Lett.*, 2012, **12**, 2107–2111.
38 R. J. Meier, L. H. Fischer, O. S. Wolfbeis and M. Schäferling, *Sens. Actuators, B*, 2013, **177**, 500–506.
39 C. F. Chapman, Y. Liu, G. J. Sonek and B. J. Tromberg, *Photochem. Photobiol.*, 1995, **62**, 416–425.
40 J. Ferguson and A. Mau, *Aust. J. Chem.*, 1973, **26**, 1617–1624.
41 Y. Y. Chen and A. W. Wood, *Bioelectromagnetics*, 2009, **30**, 583–590.
42 D. Ross, M. Gaitan and L. E. Locascio, *Anal. Chem.*, 2001, **73**, 4117–4123.
43 F. Ye, C. Wu, Y. Jin, Y.-H. Chan, X. Zhang and D. T. Chiu, *J. Am. Chem. Soc.*, 2011, **133**, 8146–8149.
44 H. D. Duong and J. I. Rhee, *Sens. Actuators, B*, 2007, **124**, 18–23.
45 W. Jung, Y. W. Kim, D. Yim and J. Y. Yoo, *Sens. Actuators, A*, 2011, **171**, 228–232.
46 X. Guan, X. Liu, Z. Su and P. Liu, *React. Funct. Polym.*, 2006, **66**, 1227–1239.
47 J. Verhoeven, *Pure Appl. Chem.*, 1996, **68**, 2223–2286.
48 J. Feng, K. Tian, D. Hu, S. Wang, S. Li, Y. Zeng, Y. Li and G. Yang, *Angew. Chem., Int. Ed.*, 2011, **50**, 8072–8076.
49 N. Chandrasekharan and L. A. Kelly, *J. Am. Chem. Soc.*, 2001, **123**, 9898–9899.
50 G. A. Baker, S. N. Baker and T. M. McCleskey, *Chem. Commun.*, 2003, 2932–2933.
51 F. Pragst, H. J. Hamann, K. Teuchner, M. Naether, W. Becker and S. Daehne, *Chem. Phys. Lett.*, 1977, **48**, 36–39.
52 J. C. Fister, D. Rank and J. M. Harris, *Anal. Chem.*, 1995, **67**, 4269–4275.
53 C. Baleizão, S. Nagl, S. M. Borisov, M. Schäferling, O. S. Wolfbeis and M. N. Berberan-Santos, *Chem.–Eur. J.*, 2007, **13**, 3643–3651.
54 T. Glawdel, Z. Almutairi, S. Wang and C. Ren, *Lab Chip*, 2008, **9**, 171–174.
55 J. L. Pittman, C. S. Henry and S. D. Gilman, *Anal. Chem.*, 2002, **75**, 361–370.
56 H. A. Clark, S. L. R. Barker, M. Brasuel, M. T. Miller, E. Monson, S. Parus, Z. Y. Shi, A. Song, B. Thorsrud and R. Kopelman, *Sens. Actuators, B*, 1998, **51**, 12–16.
57 Y. E. Lee, R. Smith and R. Kopelman, *Annu. Rev. Anal. Chem.*, 2009, **2**, 57–76.
58 V. M. Chauhan, G. R. Burnett and J. W. Aylott, *Analyst*, 2011, **136**, 1799–1801.
59 L. H. Fischer, C. Karakus, R. J. Meier, N. Risch, O. S. Wolfbeis, E. Holder and M. Schäferling, *Chem.–Eur. J.*, 2012, **18**, 15706–15713.
60 X. D. Wang, R. J. Meier and O. S. Wolfbeis, *Adv. Funct. Mater.*, 2012, **22**, 4202–4207.
61 L. H. Fischer, S. M. Borisov, M. Schäferling, I. Klimant and O. S. Wolfbeis, *Analyst*, 2010, **135**, 1224–1229.
62 M. I. J. Stich, M. Schäferling and O. S. Wolfbeis, *Adv. Mater.*, 2009, **21**, 2216–2220.
63 M. I. J. Stich, S. Nagl, O. S. Wolfbeis, U. Henne and M. Schäferling, *Adv. Funct. Mater.*, 2008, **18**, 1399–1406.
64 A. S. Kocincova, S. M. Borisov, C. Krause and O. S. Wolfbeis, *Anal. Chem.*, 2007, **79**, 8486–8493.
65 X. Guan and Z. Su, *Polym. Adv. Technol.*, 2008, **19**, 385–392.
66 K. Oyama, M. Takabayashi, Y. Takei, S. Arai, S. Takeoka, S. Ishiwata and M. Suzuki, *Lab Chip*, 2012, **12**, 1591–1593.
67 H. F. Arata, P. Löw, K. Ishizuka, C. Bergaud, B. Kim, H. Noji and H. Fujita, *Sens. Actuators, B*, 2006, **117**, 339–345.

68 P. Dreike, D. Fleetwood, D. King, D. Sprauer and T. Zipperian, *IEEE Trans. Compon., Packag., Manuf. Technol., Part A*, 1994, **17**, 594–609.
69 M. Willander, M. Friesel, Q. Wahab and B. Straumal, *J. Mater. Sci.*, 2006, **17**, 1–25.
70 S. Jeon, J. Turner and S. Granick, *J. Am. Chem. Soc.*, 2003, **125**, 9908–9909.
71 A. Pucci, F. Di Cuia, F. Signori and G. Ruggeri, *J. Mater. Chem.*, 2007, **17**, 783–790.
72 K. Maruszewski, D. Andrzejewski and W. Strek, *J. Lumin.*, 1997, **72–74**, 226–228.
73 C. Baleizao, S. Nagl, M. Schäferling, M. N. Berberan-Santos and O. S. Wolfbeis, *Anal. Chem.*, 2008, **80**, 6449–6457.
74 S. M. Borisov, A. S. Vasylevska, C. Krause and O. S. Wolfbeis, *Adv. Funct. Mater.*, 2006, **16**, 1536–1542.
75 L. H. Fischer, M. I. J. Stich, O. S. Wolfbeis, N. Tian, E. Holder and M. Schäferling, *Chem.–Eur. J.*, 2009, **15**, 10857–10863.
76 C. Karakus, L. H. Fischer, S. Schmeding, J. Hummel, N. Risch, M. Schäferling and E. Holder, *Dalton Trans.*, 2012, **41**, 9623–9632.
77 M. Engeser, L. Fabbrizzi, M. Licchelli and D. Sacchi, *Chem. Commun.*, 1999, 1191–1192.
78 C. d. Tard, S. Perruchas, S. b. Maron, X. F. Le Goff, F. o. Guillen, A. Garcia, J. Vigneron, A. Etcheberry, T. Gacoin and J.-P. Boilot, *Chem. Mater.*, 2008, **20**, 7010–7016.
79 J. Stehr, J. M. Lupton, M. Reufer, G. Raschke, T. A. Klar and J. Feldmann, *Adv. Mater.*, 2004, **16**, 2170–2174.
80 M. Mirenda, V. Levi, M. L. Bossi, L. Bruno, A. V. Bordoni, A. E. Regazzoni and A. Wolosiuk, *J. Colloid Interface Sci.*, 2013, **392**, 96–101.
81 K. R. Kyle, C. K. Ryu, J. A. Dibenedetto and P. C. Ford, *J. Am. Chem. Soc.*, 1991, **113**, 2954–2965.
82 P. C. Ford and A. Vogler, *Acc. Chem. Res.*, 1993, **26**, 220–226.
83 H. D. Hardt and A. Pierre, *Inorg. Chim. Acta*, 1977, **25**, L59–L60.
84 H. D. Hardt, *Naturwissenschaften*, 1974, **61**, 107–110.
85 S. Perruchas, X. F. Le Goff, S. Maron, I. Maurin, F. Guillen, A. Garcia, T. Gacoin and J. P. Boilot, *J. Am. Chem. Soc.*, 2010, **132**, 10967–10969.
86 S. Perruchas, C. Tard, X. F. Le Goff, A. Fargues, A. Garcia, S. Kahlal, J.-Y. Saillard, T. Gacoin and J.-P. Boilot, *Inorg. Chem.*, 2011, **50**, 10682–10692.
87 D. Cauzzi, R. Pattacini, M. Delferro, F. Dini, C. Di Natale, R. Paolesse, S. Bonacchi, M. Montalti, N. Zaccheroni, M. Calvaresi, F. Zerbetto and L. Prodi, *Angew. Chem., Int. Ed.*, 2012, **51**, 9662–9665.
88 M. A. Omary, M. A. Rawashdeh-Omary, M. A. Gonser, O. Elbjeirami, T. Grimes, T. R. Cundari, H. V. Diyabalanage, C. S. P. Gamage and H. R. Dias, *Inorg. Chem.*, 2005, **44**, 8200–8210.
89 A. A. Rachford and F. N. Castellano, *Inorg. Chem.*, 2009, **48**, 10865–10867.
90 P. C. Ford, E. Cariati and J. Bourassa, *Chem. Rev.*, 1999, **99**, 3625–3648.
91 V. W.-W. Yam and K. K.-W. Lo, *Chem. Soc. Rev.*, 1999, **28**, 323–334.
92 P. Kolodner and J. A. Tyson, *Appl. Phys. Lett.*, 1983, **42**, 117–119.
93 O. Zohar, M. Ikeda, H. Shinagawa, H. Inoue, H. Nakamura, D. Elbaum, D. L. Alkon and T. Yoshioka, *Biophys. J.*, 1998, **74**, 82–89.
94 G. E. Khalil, K. Lau, G. D. Phelan, B. Carlson, M. Gouterman, J. B. Callis and L. R. Dalton, *Rev. Sci. Instrum.*, 2004, **75**, 192–206.
95 B. B. J. Basu and N. Vasantharajan, *J. Lumin.*, 2008, **128**, 1701–1708.
96 B. J. Basu and S. Venkatraman, *J. Fluoresc.*, 2009, **19**, 479–485.
97 J. Gallery, M. Gouterman, J. Callis, G. Khalil, B. McLachlan and J. Bell, *Rev. Sci. Instrum.*, 1994, **65**, 712–720.
98 M. Mitsuishi, S. Kikuchi, T. Miyashita and Y. Amao, *J. Mater. Chem.*, 2003, **13**, 2875–2879.
99 S. M. Borisov and I. Klimant, *J. Fluoresc.*, 2008, **18**, 581–589.
100 S. M. Borisov and O. S. Wolfbeis, *Anal. Chem.*, 2006, **78**, 5094–5101.
101 S. Katagiri, Y. Tsukahara, Y. Hasegawa and Y. Wada, *Bull. Chem. Soc. Jpn.*, 2007, **80**, 1492–1503.
102 L. N. Sun, J. B. Yu, H. S. Peng, J. Z. Zhang, L. Y. Shi and O. S. Wolfbeis, *J. Phys. Chem. C*, 2010, **114**, 12642–12648.
103 M. Bhuyan and B. Koenig, *Chem. Commun.*, 2012, **48**, 7489–7491.
104 K. Miyata, Y. Konno, T. Nakanishi, A. Kobayashi, M. Kato, K. Fushimi and Y. Hasegawa, *Angew. Chem., Int. Ed.*, 2013, **52**, 6413–6416.
105 B. Zelelow, G. E. Khalil, G. Phelan, B. Carlson, M. Gouterman, J. B. Callis and L. R. Dalton, *Sens. Actuators, B*, 2003, **96**, 304–314.
106 H. Lam, G. Rao, J. Loureiro and L. Tolosa, *Talanta*, 2011, **84**, 65–70.
107 H. S. Peng, M. I. J. Stich, J. B. Yu, L. N. Sun, L. H. Fischer and O. S. Wolfbeis, *Adv. Mater.*, 2010, **22**, 716–719.
108 H. S. Peng, S. H. Huang and O. S. Wolfbeis, *J. Nanopart. Res.*, 2010, **12**, 2729–2733.
109 S. Katagiri, Y. Hasegawa, Y. Wada and S. Yanagida, *Chem. Lett.*, 2004, 1438–1439.
110 J. B. Yu, L. N. Sun, H. S. Peng and M. I. J. Stich, *J. Mater. Chem.*, 2010, **20**, 6975–6981.
111 F. H. Wong, D. S. Banks, A. Abu-Arish and C. Fradin, *J. Am. Chem. Soc.*, 2007, **129**, 10302–10303.
112 C. D. S. Brites, P. P. Lima, N. J. O. Silva, A. Millan, V. S. Amaral, F. Palacio and L. D. Carlos, *Nanoscale*, 2012, **4**, 4799–4829.
113 D. Jaque and F. Vetrone, *Nanoscale*, 2012, **4**, 4301–4326.
114 P. Michler, *Single semiconductor quantum dots*, Springer, Berlin, Heidelberg, 2009.
115 S. F. Wuister, C. de Mello Donegá and A. Meijerink, *J. Am. Chem. Soc.*, 2004, **126**, 10397–10402.
116 X. D. Wang, X. Chen, Z. X. Xie and X. R. Wang, *Angew. Chem., Int. Ed.*, 2008, **47**, 7450–7453.
117 R. Liang, R. Tian, W. Shi, Z. Liu, D. Yan, M. Wei, D. G. Evans and X. Duan, *Chem. Commun.*, 2013, **49**, 969–971.

118 T.-W. Sung and Y.-L. Lo, *Sens. Actuators, B*, 2012, **173**, 406–413.
119 P. A. S. Jorge, C. Maule, A. J. Silva, R. Benrashid, J. L. Santos and F. Farahi, *Anal. Chim. Acta*, 2008, **606**, 223–229.
120 Y. Zhao, C. Riemersma, F. Pietra, R. Koole, C. de Mello Donegá and A. Meijerink, *ACS Nano*, 2012, **6**, 9058–9067.
121 P. Haro-González, L. Martínez-Maestro, I. R. Martín, J. García-Solé and D. Jaque, *Small*, 2012, **8**, 2652–2658.
122 C.-H. Hsia, A. Wuttig and H. Yang, *ACS Nano*, 2011, **5**, 9511–9522.
123 E. J. McLaurin, V. A. Vlaskin and D. R. Gamelin, *J. Am. Chem. Soc.*, 2011, **133**, 14978–14980.
124 Y. Park, C. Koo, H.-Y. Chen, A. Han and D. H. Son, *Nanoscale*, 2013, **5**, 4944–4950.
125 L. M. Maestro, E. M. Rodriguez, F. S. Rodriguez, M. C. la Cruz, A. Juarranz, R. Naccache, F. Vetrone, D. Jaque, J. A. Capobianco and J. G. Sole, *Nano Lett.*, 2010, **10**, 5109–5115.
126 Y. Matsuda, T. Torimoto, T. Kameya, T. Kameyama, S. Kuwabata, H. Yamaguchi and T. Niimi, *Sens. Actuators, B*, 2013, **176**, 505–508.
127 V. Biju, Y. Makita, A. Sonoda, H. Yokoyama, Y. Baba and M. Ishikawa, *J. Phys. Chem. B*, 2005, **109**, 13899–13905.
128 H. D. Duong and J. Il Rhee, *Sens. Actuators, B*, 2008, **134**, 423–426.
129 D. Pugh-Thomas, B. M. Walsh and M. C. Gupta, *Nanotechnology*, 2011, **22**, 185503.
130 G. W. Walker, V. C. Sundar, C. M. Rudzinski, A. W. Wun, M. G. Bawendi and D. G. Nocera, *Appl. Phys. Lett.*, 2003, **83**, 3555–3557.
131 H. Sakaue, A. Aikawa and Y. Iijima, *Sens. Actuators, B*, 2010, **150**, 569–573.
132 H. Kawasaki, K. Hamaguchi, I. Osaka and R. Arakawa, *Adv. Funct. Mater.*, 2011, **21**, 3508–3515.
133 J. Xie, Y. Zheng and J. Y. Ying, *J. Am. Chem. Soc.*, 2009, **131**, 888–889.
134 C. I. Richards, S. Choi, J. C. Hsiang, Y. Antoku, T. Vosch, A. Bongiorno, Y. L. Tzeng and R. M. Dickson, *J. Am. Chem. Soc.*, 2008, **130**, 5038–5039.
135 H. Xu and K. S. Suslick, *Adv. Mater.*, 2010, **22**, 1078–1082.
136 Q.-M. Wang, Y.-A. Lee, O. Crespo, J. Deaton, C. Tang, H. J. Gysling, M. Concepción Gimeno, C. Larraz, M. D. Villacampa, A. Laguna and R. Eisenberg, *J. Am. Chem. Soc.*, 2004, **126**, 9488–9489.
137 F. Auzel, *C. R. Acad. Sci.*, 1966, **262**, 1016.
138 H. S. Mader, P. Kele, S. M. Saleh and O. S. Wolfbeis, *Curr. Opin. Chem. Biol.*, 2010, **14**, 582–596.
139 F. Auzel, *Chem. Rev.*, 2003, **104**, 139–174.
140 B. Dong, B. Cao, Y. He, Z. Liu, Z. Li and Z. Feng, *Adv. Mater.*, 2012, **24**, 1987–1993.
141 M. Quintanilla, E. Cantelar, F. Cussó, M. Villegas and A. C. Caballero, *Appl. Phys. Express*, 2011, **4**, 022601.
142 A. Sedlmeier, D. E. Achatz, L. H. Fischer, H. H. Gorris and O. S. Wolfbeis, *Nanoscale*, 2012, **4**, 7090–7096.
143 S. Zhou, K. Deng, X. Wei, G. Jiang, C. Duan, Y. Chen and M. Yin, *Opt. Commun.*, 2013, **291**, 138–142.
144 D. Wawrzynczyk, A. Bednarkiewicz, M. Nyk, W. Strek and M. Samoc, *Nanoscale*, 2012, **4**, 6959–6961.
145 N. N. Dong, M. Pedroni, F. Piccinelli, G. Conti, A. Sbarbati, J. E. Ramírez-Hernández, L. M. Maestro, M. C. Iglesias-de la Cruz, F. Sanz-Rodriguez and A. Juarranz, *ACS Nano*, 2011, **5**, 8665–8671.
146 E. Song, S. Ding, M. Wu, S. Ye, F. Xiao, G. Dong and Q. Zhang, *J. Mater. Chem. C*, 2013, DOI: 10.1039/c1033tc30450g.
147 F. Vetrone, R. Naccache, A. Zamarron, A. J. de la Fuente, F. Sanz-Rodriguez, L. M. Maestro, E. M. Rodriguez, D. Jaque, J. G. Sole and J. A. Capobianco, *ACS Nano*, 2010, **4**, 3254–3258.
148 R. Chen, V. D. Ta, F. Xiao, Q. Zhang and H. Sun, *Small*, 2013, **9**, 1052–1057.
149 B. S. Cao, Y. Y. He, Z. Q. Feng, Y. S. Li and B. Dong, *Sens. Actuators, B*, 2011, **159**, 8–11.
150 B. Dong, B. S. Cao, Z. Q. Feng, X. J. Wang and Y. Y. He, *Sens. Actuators, B*, 2012, **165**, 34–37.
151 S. W. Allison, G. T. Gillies, A. J. Rondinone and M. R. Cates, *Nanotechnology*, 2003, **14**, 859.
152 S. M. Borisov, T. Mayr, G. Mistlberger, K. Waich, K. Koren, P. Chojnacki and I. Klimant, *Talanta*, 2009, **79**, 1322–1330.
153 X.-d. Wang, R. J. Meier, M. Link and O. S. Wolfbeis, *Angew. Chem., Int. Ed.*, 2010, **49**, 4907–4909.
154 C. D. Brites, P. P. Lima, N. J. Silva, A. Millan, V. S. Amaral, F. Palacio and L. D. Carlos, *Adv. Mater.*, 2010, **22**, 4499–4504.
155 J. Feng, L. Xiong, S. Wang, S. Li, Y. Li and G. Yang, *Adv. Funct. Mater.*, 2013, **23**, 340–345.
156 Y. Shiraishi, R. Miyarnoto and T. Hirai, *Langmuir*, 2008, **24**, 4273–4279.
157 D. P. Wang, R. Miyamoto, Y. Shiraishi and T. Hirai, *Langmuir*, 2009, **25**, 13176–13182.
158 S. Uchiyama, Y. Matsumura, A. P. de Silva and K. Iwai, *Anal. Chem.*, 2003, **75**, 5926–5935.
159 C. Gota, S. Uchiyama, T. Yoshihara, S. Tobita and T. Ohwada, *J. Phys. Chem. B*, 2008, **112**, 2829–2836.
160 K. Okabe, N. Inada, C. Gota, Y. Harada, T. Funatsu and S. Uchiyama, *Nat. Commun.*, 2012, **3**, 705.
161 C. Gota, K. Okabe, T. Funatsu, Y. Harada and S. Uchiyama, *J. Am. Chem. Soc.*, 2009, **131**, 2766–2767.
162 S. Uchiyama, K. Kimura, C. Gota, K. Okabe, K. Kawamoto, N. Inada, T. Yoshihara and S. Tobita, *Chem.–Eur. J.*, 2012, **18**, 9552–9563.
163 C.-Y. Chen and C.-T. Chen, *Chem. Commun.*, 2011, **47**, 994–996.
164 K. Cui, D. D. Zhu, W. Cui, X. M. Lu and Q. H. Lu, *J. Phys. Chem. C*, 2012, **116**, 6077–6082.
165 W. T. Wu, J. Shen, P. Banerjee and S. Q. Zhou, *Biomaterials*, 2010, **31**, 7555–7566.
166 Y. Jiang, X. Yang, C. Ma, C. Wang, H. Li, F. Dong, X. Zhai, K. Yu, Q. Lin and B. Yang, *Small*, 2010, **6**, 2673–2677.
167 T. Pustelny, *Sens. Actuators, A*, 1995, **49**, 57–60.
168 R. A. Hansel, S. K. Desai, S. W. Allison, A. L. Heyes and D. G. Walker, *J. Appl. Phys.*, 2010, **107**, 16101.

169 L. L. Shi, H. J. Zhang, C. Y. Li and Q. Su, *RSC Adv.*, 2011, **1**, 298–304.
170 R. L. Vander Wal, P. A. Householder and T. W. Wright, *Appl. Spectrosc.*, 1999, **53**, 1251–1258.
171 J. Eldridge, T. Bencic, S. Allison and D. Beshears, *J. Therm. Spray Technol.*, 2004, **13**, 44–50.
172 Y. Cui, H. Xu, Y. Yue, Z. Guo, J. Yu, Z. Chen, J. Gao, Y. Yang, G. Qian and B. Chen, *J. Am. Chem. Soc.*, 2012, **134**, 3979–3982.
173 E. Maurice, S. A. Wade, S. F. Collins, G. Monnom and G. W. Baxter, *Appl. Opt.*, 1997, **36**, 8264–8269.
174 S. A. Wade, J. C. Muscat, S. F. Collins and G. W. Baxter, *Rev. Sci. Instrum.*, 1999, **70**, 4279–4282.
175 F. Sidiroglou, S. A. Wade, N. M. Dragomir, G. W. Baxter and S. F. Collins, *Rev. Sci. Instrum.*, 2003, **74**, 3524–3530.
176 V. K. Rai, *IEEE Sens. J.*, 2007, **7**, 1110–1111.
177 S. J. Skinner, J. P. Feist, I. J. E. Brooks, S. Seefeldt and A. L. Heyes, *Sens. Actuators, B*, 2009, **136**, 52–59.
178 R. Hansel, S. Allison and G. Walker, *J. Mater. Sci.*, 2010, **45**, 146–150.
179 S. M. Borisov, K. Gatterer, B. Bitschnau and I. Klimant, *J. Phys. Chem. C*, 2010, **114**, 9118–9124.
180 S. Borisov and I. Klimant, *Anal. Bioanal. Chem.*, 2012, **404**, 2797–2806.
181 S. F. León-Luis, U. R. Rodríguez-Mendoza, P. Haro-González, I. R. Martín and V. Lavín, *Sens. Actuators, B*, 2012, **174**, 176–186.
182 H. Berthou and C. K. Jorgensen, *Opt. Lett.*, 1990, **15**, 1100–1102.
183 L. Aigouy, G. Tessier, M. Mortier and B. Charlot, *Appl. Phys. Lett.*, 2005, **87**, 184105.
184 E. Saidi, B. Samson, L. Aigouy, S. Volz, P. Low, C. Bergaud and M. Mortier, *Nanotechnology*, 2009, **20**, 115703.
185 S. F. Leon-Luis, U. R. Rodriguez-Mendoza, E. Lalla and V. Lavin, *Sens. Actuators, B*, 2011, **158**, 208–213.
186 G. Tripathi, V. K. Rai and S. B. Rai, *Opt. Mater.*, 2007, **30**, 201–206.
187 C. R. Li, B. Dong, S. F. Li and C. H. Song, *Chem. Phys. Lett.*, 2007, **443**, 426–429.
188 P. V. dos Santos, M. T. de Araujo, A. S. Gouveia-Neto, J. A. M. Neto and A. S. B. Sombra, *Appl. Phys. Lett.*, 1999, **73**, 578–580.
189 B. Dong, X. S. Xu, X. J. Wang, T. Yang and Y. Y. He, *Appl. Phys. B: Lasers Opt.*, 2007, **89**, 281–284.
190 B. Dong, T. Yang and M. K. Lei, *Sens. Actuators, B*, 2007, **123**, 667–670.
191 B. Dong, Z. Q. Feng, J. F. Zu and L. Bai, *J. Sol-Gel Sci. Technol.*, 2008, **48**, 303–307.
192 B. Dong, X. J. Wang, C. R. Li and D. P. Liu, *IEEE Photonics Technol. Lett.*, 2008, **20**, 117–119.
193 L. Liu, Y. X. Wang, X. R. Zhang, K. Yang, Y. F. Bai, C. H. Huang and Y. L. Song, *Opt. Commun.*, 2011, **284**, 1876–1879.
194 D. Y. Li, Y. X. Wang, X. R. Zhang, K. Yang, L. Liu and Y. L. Song, *Opt. Commun.*, 2012, **285**, 1925–1928.
195 Z. P. Cai and H. Y. Xu, *Sens. Actuators, A*, 2003, **108**, 187–192.
196 E. Maurice, G. Monnom, B. Dussardier, A. Saïssy, D. B. Ostrowsky and G. W. Baxter, *Appl. Opt.*, 1995, **34**, 8019–8025.
197 S. K. Singh, K. Kumar and S. B. Rai, *Sens. Actuators, A*, 2009, **149**, 16–20.
198 O. Yarimaga, S. Lee, D. Y. Ham, J. M. Choi, S. G. Kwon, M. Im, S. Kim, J. M. Kim and Y. K. Choi, *Macromol. Chem. Phys.*, 2011, **212**, 1211–1220.
199 S. Ryu, I. Yoo, S. Song, B. Yoon and J. M. Kim, *J. Am. Chem. Soc.*, 2009, **131**, 3800–3801.
200 M. Obata, M. Morita, K. Nakase, K. Mitsuo, K. Asai, S. Hirohara and S. Yano, *J. Polym. Sci., Part A: Polym. Chem.*, 2007, **45**, 2876–2885.
201 K. Mitsuo, K. Asai, M. Hayasaka and M. Kameda, *J. Visualization*, 2003, **6**, 213–223.
202 T. Liu and S. Y. Liu, *Anal. Chem.*, 2011, **83**, 2775–2785.
203 S. Nagl and O. S. Wolfbeis, *Analyst*, 2007, **132**, 507–511.
204 M. I. J. Stich, L. H. Fischer and O. S. Wolfbeis, *Chem. Soc. Rev.*, 2010, **39**, 3102–3114.
205 G. J. Mohr, T. Werner, I. Oehme, C. Preininger, I. Klimant, B. Kovacs and O. S. Wolfbeis, *Adv. Mater.*, 1997, **9**, 1108–1113.
206 S. Pauly, *Permeability and Diffusion Data*, *Polymer Handbook*, John Wiley & Sons, New York, Chichester, Weinheim, Brisbane, Singapore, Toronto, 4th edn, 1999.
207 U. Resch-Genger, M. Grabolle, S. Cavaliere-Jaricot, R. Nitschke and T. Nann, *Nat. Methods*, 2008, **5**, 763–775.
208 R. K. P. Benninger, Y. Koc, O. Hofmann, J. Requejo-Isidro, M. A. A. Neil, P. M. W. French and A. J. deMello, *Anal. Chem.*, 2006, **78**, 2272–2278.
209 V. K. Natrajan and K. T. Christensen, *Meas. Sci. Technol.*, 2009, **20**, 015401.
210 G. L. Ke, C. M. Wang, Y. Ge, N. F. Zheng, Z. Zhu and C. J. Yang, *J. Am. Chem. Soc.*, 2012, **134**, 18908–18911.
211 J. M. Yang, H. Yang and L. W. Lin, *ACS Nano*, 2011, **5**, 5067–5071.
212 G. Marriott, R. M. Clegg, D. J. Arndt-Jovin and T. M. Jovin, *Biophys. J.*, 1991, **60**, 1374–1387.
213 D. Choudhury, D. Jaque, A. Rodenas, W. T. Ramsay, L. Paterson and A. K. Kar, *Lab Chip*, 2012, **12**, 2414–2420.
214 H. Huang, S. Delikanli, H. Zeng, D. M. Ferkey and A. Pralle, *Nat. Nanotechnol.*, 2010, **5**, 602–606.
215 O. S. Wolfbeis, *Fiber optic chemical sensors and biosensors*, CRC press, Boca Raton, Florida, 1991.
216 X. D. Wang and O. S. Wolfbeis, *Anal. Chem.*, 2013, **85**, 487–508.
217 B. Lee, *Opt. Fiber Technol.*, 2003, **9**, 57–79.
218 K. L. Brogan and D. R. Walt, *Curr. Opin. Chem. Biol.*, 2005, **9**, 494–500.
219 K. T. V. Grattan, A. W. Palmer and Z. Zhang, *Rev. Sci. Instrum.*, 1991, **62**, 1210–1213.
220 K. T. V. Grattan and T. Sun, *Sens. Actuators, A*, 2000, **82**, 40–61.
221 Y. Zhang, G. Keiser, C. Marzinsky, A. M. Schilowitz, L. Song and A. B. Herhold, *Sensors*, 2011 IEEE, 2011.
222 S. Grattan, S. Taylor, P. Basheer, T. Sun and K. Grattan, *Sensors*, 2009 IEEE, 2009.

223 K. A. Wickersheim and M. H. Sun, *J. Microwave Power*, 1987, **22**, 85–94.
224 K. A. Wickersheim and T. V. Samulski, *Med. Phys.*, 1986, **13**, 568.
225 R. V. Alves and K. A. Wickersheim, *Proc. Soc. Photo-Opt. Instrum. Eng.*, 1984, **403**, 146–152.
226 T. Samulski, *Temp.: Its Meas. Control Sci. Ind.*, 1992, **6**, 1185–1190.
227 S. S. Yin and P. Ruffin, *Fiber optic sensors*, John Wiley & Sons, Inc., 2006.
228 M. Farries, M. Fermann, R. Laming, S. Poole, D. Payne and A. Leach, *Electron. Lett.*, 1986, **22**, 418–419.
229 K. Wickersheim, M. Sun and A. Kamal, *J. Microwave Power*, 1990, **25**, 990.
230 C. Ovrén, M. Adolfsson and B. Hök, *Opt. Lasers Eng.*, 1984, **5**, 155–172.
231 J. Brübach, C. Pflitsch, A. Dreizler and B. Atakan, *Prog. Energy Combust. Sci.*, 2013, **39**, 37–60.
232 R. R. Sholes and J. G. Small, *Rev. Sci. Instrum.*, 1980, **51**, 882–884.
233 K. Grattan, R. Selli and A. Palmer, *Rev. Sci. Instrum.*, 1988, **59**, 1328–1335.
234 J. McCormack, *Electron. Lett.*, 1981, **17**, 630–631.
235 T. Bosselmann, A. Reule and J. Schroder, Proc. SPIE 0514, 2nd Intl Conf on Optical Fiber Sensors, 1984, 151–154.
236 K. T. V. Grattan and A. W. Palmer, *Rev. Sci. Instrum.*, 1985, **56**, 1784–1787.
237 K. T. V. Grattan, J. D. Manwell, S. M. L. Sim and C. A. Willson, *Opt. Commun.*, 1987, **62**, 104–107.
238 A. Augousti, K. Grattan and A. Palmer, *J. Lightwave Technol.*, 1987, **5**, 759–762.
239 A. T. Augousti, K. T. V. Grattan and A. W. Palmer, *IEEE Trans. Instrum. Meas.*, 1988, **37**, 470–472.
240 O. S. Wolfbeis, *Adv. Mater.*, 2008, **20**, 3759–3763.
241 T. Liu, *Pressure- and Temperature-Sensitive Paints*, Springer, Berlin, 2005.
242 C. Brites, P. Lima, N. Silva, A. Millán, V. Amaral, F. Palacio and L. Carlos, *J. Lumin.*, 2013, 230–232.
243 H. T. Lam, Y. Kostov, L. Tolosa, S. Falk and G. Rao, *Meas. Sci. Technol.*, 2012, **23**, 035104.
244 T. Liu, B. Campbell, S. Burns and J. Sullivan, *Appl. Mech. Rev.*, 1997, **50**, 227.
245 M. Gouterman, J. Callis, L. Dalton, G. Khalil, Y. Mebarki, K. R. Cooper and M. Grenier, *Meas. Sci. Technol.*, 2004, **15**, 1986–1994.
246 C. Klein, *Aerosp. Sci. Technol.*, 2000, **4**, 103–109.
247 J. W. Gregory, K. Asai, M. Kameda, T. Liu and J. P. Sullivan, *Proc. Inst. Mech. Eng., Part G*, 2008, **222**, 249–290.
248 J. J. Lee, J. C. Dutton and A. M. Jacobi, *J. Mech. Sci. Technol.*, 2007, **21**, 1253–1262.
249 V. Mosharov, A. Orlov and V. Radchenko, 20th International Congress on Instrumentation in Aerospace Simulation Facilities, 2003.
250 L. Goss, G. Jones, J. Crafton and S. Fonov, 43rd Aerospace Sciences Meeting and Exhibition, 2006.
251 M. E. Kose, A. Omar, C. A. Virgin, B. F. Carroll and K. S. Schanze, *Langmuir*, 2005, **21**, 9110–9120.
252 M. Gouterman, *J. Chem. Educ.*, 1997, **74**, 697.
253 L. Mannik, S. Brown and S. Campbell, *Appl. Opt.*, 1987, **26**, 4014–4017.
254 L. Aigouy, E. Saïdi, L. Lalouat, J. Labéguerie-Egéa, M. Mortier, P. Low and C. Bergaud, *J. Appl. Phys.*, 2009, **106**, 074301–074309.